Impact of Residential Prosumer Ownership of Plug-in Electric Vehicles on Voltage Quality and Transformer Aging: Modeling, Assessment and Planning

by

Yasser Assolami

A thesis
presented to the University of Waterloo
in fulfillment of the
thesis requirement for degree of
Doctor of Philosophy
in
Electrical and Computer Engineering

Waterloo, Ontario, Canada, 2021

Examining Committee Membership

The following served on the Examining Committee for this thesis. The decision of the Examining Committee is by majority vote.

External Examiner:	Bala Venkatesh, Professor, Dept. of Electrical and Computer Engineering, Ryerson University
Supervisor:	Ramadan El-Shatshat, Lecturer, Dept. of Electrical and Computer Engineering, University of Waterloo
Internal Member:	Kankar Bhattacharya, Professor, Dept. of Electrical and Computer Engineering, University of Waterloo
Internal Member:	Magdy Salama, Professor, Dept. of Electrical and Computer Engineering, University of Waterloo
Internal-External Member:	Ali Elkamel, Professor, Dept. of Chemical Engineering, University of Waterloo

Author's Declaration

I hereby declare that I am the sole author of this thesis. This is a true copy of the thesis, including any required final revisions, as accepted by my examiners.

I understand that my thesis may be made electronically available to the public.

Abstract

In the context of increasing concerns related to climate change, there has been a substantial change to both the transportation and residential sectors. While the transportation sector has previously been limited to conventional gasoline reliant vehicles, there has been a recent shift towards the use of plug-in electric vehicles (PEVs), powered by electricity. This shift will introduce new and different kinds of electric loads into the next generation of the electrical distribution systems (EDSs). The PEV charging load is seen as an additional load by EDSs; as such, an accurate and reliable model of these new loads is highly required. PEV loads are not modeled as an additional conventional load. They are stochastic in nature and impacted by the randomness of driver' behavior. There have also been significant deployment of using solar photovoltaic (PV) and energy storage system with residential premises, which has changed the role of residential customers from consumers to prosumers (i.e. power producers and consumers). Therefore, it is necessary for utility companies to accurately and realistically assess and quantify EDS asset conditions, with a consideration of different penetrations of PEV with residential prosumers, and develop future necessary infrastructure and policies in order to accommodate these and further changes.

This thesis focuses on developing a more realistic and accurate stochastic models of PEV loads and PV generation and investigate the addition of these elements into EDS assessment and planning. First, a new framework for modeling the stochastic nature of both PEV loads and PV generation while considering the effect of the spatial-temporal (SAT) characteristics of the driver' behavior, as well as solar irradiation and temperature, is proposed. A trip chain, based on the Markov Chain Monte Carlo process, is developed to properly model PEV daily driving activities and the PV uncertainty. Charging facilities are assumed available at home, work, and fast-charging stations, having charging levels of 3.7 kW, 6.6 kW, and 50 kW, respectively. The proposed framework is examined, considering the National Household Travel Survey global data, as well as the city of Buffalo and New York state datasets. The impact of varying the penetration levels of PEV and PV resources is also investigated. The present work strengthens the proposed models in the literature by integrating the SAT characteristics of PEV charging demand into PV stochastic models.

Second, a new framework is proposed for evaluating and enhancing voltage quality,

distribution transformer (DT) overload and aging, while considering residential prosumer ownership of PEVs. The proposed work develops a probabilistic power flow in order to investigate the impact of the stochastic nature of PEVs, PVs, and conventional load. In this work, the residential premises are modeled for supply through a detailed secondary distribution system which is integrated as a part of the EDS. This work enhances the existing research through the inclusion of PEV SAT charging activities into the assessment models of DT overload and aging, voltage imbalance, and voltage deviation. The proposed framework provides a more realistic life expectancy for DTs compared with a simplified model in the literature. The results indicate that the use of the proposed SAT-based approach has reduced DT lifetime to 6.30 years from 7.92 years for the same PEV penetration level.

Finally, a multi-year community battery energy storage system (CBESS) planning framework is proposed to accommodate a high PEV penetration level. A part from considering the conventional load (residential and commercial), the framework considers PEV charging demand based SAT approach, as well as PV options. Based on a back-propagation algorithm, a heuristic methodology is developed to determine the CBESS sites and sizes infrastructure plan while minimizing the total capital and operation costs. The proposed heuristic approach starts from the terminal year of the planning horizon, and propagate backward to the initial year, to determine the required CBESS sites a long with their corresponding sizes. The proposed CBESS planning framework is examined on the modified IEEE 123 primary distribution feeder and the effect of using the proposed PEV SAT-based approach versus simplified model in the literature is investigated. The results indicate that using the realistic proposed SAT-based approach increases the required total CBESS investment budget from M$6.3 to M$6.7.

The SAT model was coded using MATLAB software environment. For the proposed assessment framework, the three-phase power flow (PF) algorithm was programmed using OpenDSS and be integrated with MATLAB and Python software environments. The mathematical optimization model in the proposed planning framework was coded using MATLAB software.

Acknowledgements

First and foremost, I shall praise and thank "Allah" Almighty for giving me the strength, patience, knowledge, ability and opportunity to undertake this research journey and to persevere the successful completion of this thesis. This achievement would not be possible without his blessings.

Then, I would like to take this opportunity to express my sincere gratitude and appreciation to my supervisor, Prof. Ramadan El-shatshat, for his invaluable guidance, kindness, motivation, continual support, and encouragement throughout my PhD journey at the University of Waterloo. He provided me with a such great environment that made me go further than I had imagined.

I also extend my thanks and sincere gratitude to Prof. Ahmed Gaouda for his interest in my research and the fruitful discussion over the past two years.

My appreciation and thanks are also extended to Prof. Ali Elkamel, Prof. Kankar Bhattacharya, and Prof. Magdy Salama from the University of Waterloo, for serving on my doctoral Advisory Committee. Their constructive comments, suggestions, and feedback have significantly improved the quality of this thesis. I am also very thankful to Prof. Bala Venkatesh from Ryerson University, for serving as the external thesis examiner and for his careful reading, wise comments and insightful observations. Additionally, I would like to thank Prof. Svetlana Kaminskaia for chairing my thesis examination committee.

Special thanks to Taibah University in Saudi Arabia, for the financial support and scholarship to pursue my graduate studies at the University of Waterloo. I also would like to thank the Ministry of Education, Saudi Arabia, and the Saudi Arabian Cultural Bureau in Canada for their support.

I am truly indebted to my devoted father and mother for their endless love, care, support, encouragement, and sincere prayers during my academic journey. Their understanding and patient of being away of them pushed me to learn more and work harder. I also wish to express my deepest gratitude to my brothers and sisters for their love, encouragement, and taking care of my parent during the time of my absence.

Words fail me to express my deepest appreciation to my lovely wife, Entesar, for her endless love, patient, and support during all late night and early morning and both the ups and downs of my PhD studies. She tolerated the stressful times and shared with me the happiness and sadness moments. To my beloved sons, Hisham, Haitham, and Hattan, thank you very much for making my life enjoyable. Your endless love inspired me to work hard and achieve what I am proud of today. You all are the source of my inspiration and I shall always strive to make you happy and proud.

Finally, I would like to thank all my friends in Canada and Waterloo in particular, who supported me through my PhD journey. Your support and friendships made my stay memorable.

Thank you all!

Dedication

To my father, Obaidallah Assolami, for his unconditional support and blessed prayers.

To my mother, Salimah Alsulami, for her blessed prayers and late night DUA.

To my wife, Entesar Alsulami, for her scarifies, endless love ,and patient.

To my sons, Hisham, Haitham, and Hattan, for their love and support.

To all my brothers and sisters, for their encouragement and support.

Table of Contents

List of Tables

List of Figures

List of Abbreviations

BESS	battery energy storage system
PEV	plug-in electric vehicle
EV	electric vehicles
NHTS	National Household Travel Survey
MCMC	Markov Chain Monte Carlo
FCS	fast-charging stations
EDS	electrical distribution system
EDR	electric driving range
SE	specific energy
AMS	adjusted market share
AT	arrival time
TDM	driven distance
DDT	driving duration
PDT	parking duration
PL	parking location
MS	market share
CE	consumed energy
ER	energy required

DC	direct current
AC	alternating current
PDF	probability distribution function
BC	battery capacity
SOC	state of charge
PV	solar photovoltaic
RTS	Reliability Test System
CWEEDS	Canadian Weather Energy and Engineering Datasets
SSE	sum of the squares error
CDF	cumulative distribution function
MI	maximum iteration
POC	probability of occurrence
CD	charging duration
Pch	charging level
LDT	leaving destination time
ChP	charged power
HBES	home battery energy storage
US	United States
NY	New York
O&M	operation and maintenance cost
TCP	total charging profile
CS	cumulative sum
MA	moving average
SC	stopping criteria
PF	power flow

ECT	ending charging time
ESS	energy storage system
VI	voltage imbalance
ANSI	American National Standard Institute
DT	distribution transformer
LOL	loss of life
DG	distributed generation
US	United States
SDS	secondary distribution system
TOU	time-of-use
SAT	spatial-temporal
SDS	secondary distribution system
PDS	primary distribution system
UV	under voltage
OV	over voltage
SL	service line
SD	service drop
CBESS	community battery energy storage system
LDC	local distribution company
MINLP	Mixed Integer Non-linear Programming
HEV	Hybrid Electric Vehicle
OPF	Optimum Power Flow
PFA	Penalty Function Approach
EDN	electrical distribution network

Chapter 1

Introduction

1.1 Research Motivation

In an effort to address the concerns related to climate change, there has been a substantial change to both the transportation and residential sectors. While the transportation sector has previously been limited to conventional gasoline reliant vehicles, there has been a recent shift towards the use of electric vehicles (EVs), powered by electricity. EV is a general term that may or not include vehicles that primarily depend on recharging their batteries from the electrical grid, while plug-in electric vehicles (PEVs), which are a subgroup of EVs, are classified into vehicles that are recharged from the power grid [1]. Many governments have launched incentive programs for PEV buyers and, as such, the number of PEV sales has risen, with an increase from $199,826$ to $361,307$ in the United States (US) between 2017 and 2018 [2]. Globally, there has also been a dramatic increase in sales. In the period 2013 to 2018, sales gradually increased to exceed 5.1 million [3]. The continuous release of new generations of PEVs, taking into consideration customer's satisfaction, may lead to an even more rapid rise in the near future. As an example, launch of the Tesla model 3 on the July 2017, which affords 310 miles (498.897 km) electric driving range (EDR), has increased the sales of Tesla from 50,139 to 191,627, in 2017 and 2018, respectively [4]. This increase in the sale of PEVs will introduce new and different kinds of electric loads into the next generation

of the electrical distribution systems (EDSs). PEV charging is seen as an additional load by EDSs; as such, an accurate and reliable model of these new loads is highly required. PEV loads are not modeled as an additional conventional load. They are stochastic in nature and impacted by the randomness of driver' behavior. Determining the place (spatial characteristics) and time (temporal characteristics) for where and when PEV charging takes place constitutes a challenging task. The development of a realistic charging PEV demand profile requires a reliable estimate of many elements, such as driving behavior, travel patterns, and PEV manufacturing specifications. Based on these elements, other parameters are extracted, including departure time, arrival time (AT), driven distance (TDM), driving duration (DDT), parking duration (PDT), parking location (PL), PEV market share (MS), and available charging levels. For example, the TDM is used in computing the consumed energy (CE) for PEVs when driving from one location to another. The CE plays a vital role in estimating the remaining energy in a PEV battery. Improper modeling of the CE may result in underestimating the energy required (ER) from the grid. A more realistic representation of total PEV charging demand should reflect a PEV state of charge (SOC) model that depends on a previous state during the day. Oversimplifying all or some of the above elements may lead to underestimating the ER by PEVs from the EDSs and hence impact the accuracy of PEV demand. Furthermore, the structure of EDSs is changing in the type of loads and available energy resources. Solar photovoltaic (PVs) are deployed with a high penetration level in distribution systems at the end-users' premises. Therefore, a consideration of the stochastic nature of these distributed PV resources on the spatial-temporal (SAT) characteristics of PEV charging demand is essential for an accurate estimation of daily load profile.

For the residential sector in the US, a similar growth in solar photovoltaic (PV) panel installation saw PV capacity increase from $2,227$ to $2,800$ MW from 2017 to 2019 [5]. Further, there have also been significant advances in the development of home battery energy storage (HBES) technologies. As an example, Tesla has released a second generation of HBES that is double the size of the first generation [6]. The growth in HBES technology has led to an increase in the US residential energy storage system (ESS) market, from the second to the third quarter of 2019, and installation

observed a 32% increase [7]. The presence of a PV and HBES within residential premises has changed the role of residential customers from consumers to prosumers (i.e. power producers and consumers). This shift with charging PEV loads has altered the shape of the electrical distribution system (EDS) while evaluating EDS assets is becoming more complicated. Performing an assessment task becomes challenging, as increasing the penetration levels of PVs, PEVs, and HBESs will introduce new and different kinds of electric loads and generation into the current infrastructure of EDSs. Unfortunately, PEV loads are not modeled as additional conventional loads but are instead stochastic in nature and influenced by the randomness of a driver behavior. Similarly, PV generation and conventional load are also stochastic in nature, resulting from the variation in weather and residential consumption. In an existing EDS, the load model is changed towards prosumers while distribution transformers (DTs) are still installed taking conventional loads into consideration. These DTs step down the primary system voltage to service voltage in order to connect the single phase residential premises through the secondary distribution system (SDS). Different prosumers appeared in the secondary system and were modeled, during steady-state operation, as single phase loads and generators. Simplifying or ignoring the prosumer generation/demand model may lead to an inaccurate assessment and evaluation of the system operation condition. Implementing a simplified model for PEV charging at residential premises leads to underestimating PEV remaining SOC, and hence provides inaccurate PEV time-energy requirements that appear as an additional load on the DTs. The PEV energy requirement heavily relies on the statistical parameters of driver behavior. Lacking the representation of any of the driver statistical elements results in the development of an unrealistic impact of PEVs loads on the DT loading condition and quality of service. Therefore, a simplified PEV model will neither lead to accurate results of evaluating transformer aging conditions nor provide an estimate of voltage imbalance (VI) or of under and over voltage conditions for system studies and planning. So far, the impact of residential prosumer ownership of PEVs on DT aging, as well as voltage quality through a consideration of SAT characteristics of PEV driver behavior, has not been previously reported in the literature. Therefore, there is a need to address this missing component and develop an assessment framework for DT aging and voltage quality, while taking into

account PEV charging models based on SAT driver characteristics, as well as PV and conventional load uncertainty.

When a high number of PEV is deployed and added to the system, but not properly planned, a severe impact on EDS assets is likely to result. Recently, different ESS sizes and technology have been developed in order to add benefits and improvements to a future EDS grid [8]. The community battery energy storage systems (CBESSs) can provide loss reduction, peak shaving, and increased distributed generation (DG) integration. CBESS can help in the deferral of DT upgrade and improve service voltage quality and also can increase the electricity market competition. The CBESSs have been used intensively with PEV loads, but only a few studies have focused on the planning aspects. The few developed research in CBESS planning models while considering PEV demand did not consider the SAT characteristics of driver' behavior and VI, which may result in either over or under estimating the ESS power, energy, required number of sites, and capital and operation costs. However, it is very essential to include a PEV load-based SAT approach into the ESS planning models while considering DT's loss of life (LOL) and VI, which significantly affects the planning budged and timelines.

1.2 Literature Review

This section provides a comprehensive review for the relevant literature pertained to the topics and issues presented in this thesis. The section reviews the recent PEV and PV reported stochastic models, impact of residential prosumer ownership of PEV on DT aging and voltage quality, and the ESS planning models in a distribution grid.

1.2.1 PEV and PV Stochastic Models

A considerable number of studies have explored the development of PEV charging demand models.

Different examples are introduced in [9], and [10]; however, only trip to home is considered. The PEV models in these studies are developed with the assumption that

driving behavior follows the normal distribution curve. This assumption neglects the realistic nature of the driver' behavior and therefore the impact on PEV SOC and required energy from the grid becomes unrealistic. More deterministic models for PEV charging are reported in [11] and [12]. The authors in [11] assume that all vehicles are charged based on off-peak and on-peak times, while [12] assumes that all vehicles start charging at home before 6 P.M. However, these studies assume that the time to start charging PEV remains unchanged which neglects the diversity in the arrival time of PEVs. Other examples are developed by the authors in [13], [14] and [15] but the main focus is on modeling PEV charging at fast-charging stations (FCS). The authors do not consider the opportunity of charging either at home or work. These examples included the probability distribution functions (PDFs) of the arrival time and daily distance for FCS trip but they do not consider the sequence of trips per a day in their model which does not reflect the realistic representation of PEV SOC that depends on a previous state during the day. A another great examples are developed in [16–20] to model PEV charging demand at home. National Household Travel Survey (NHTS) survey data are used to extract the PDFs of the arrival and departure time and daily distance statistical parameters. These studies include a very important elements in PEV charging model but the authors consider PEV charging activities at home without including the daily complete chain of driver activities that take into account the cycles of other trips in a day. The authors in [21] assume all vehicle TDM ranges as varying from 10-40 miles, which may lead to an unclear conclusion regarding system performance with FCS charging demand. They fail to consider the statistical parameters of PEV driver' behavior using real data (i.e., NHTS). Study [21] focuses on PEVs arriving at the FCS without considering other possible trips in a day, which hence impacted the overall PEV daily charging demand. In [22], the authors strongly attempted to address the uncertainties of PEV TDM and AT . However, their assumption that arrival time is a uniformly distributed variable may not be realistic for some vehicles. The preceding studies [9, 22] do not consider multiple trips in a day and the main focus is on modeling the charging profile of PEVs while considering movement to only one location.

The researchers in [23–27] focus on investigating the implementation of PEV charging models at different locations. The studies presented in [23], [24] have developed a

methodology to investigate the impact of PEV charging at multiple locations. The authors have classified daily trips into home, work, and others. However, these studies do not investigate the possibility of having other trips during the day, which may have an essential impact on the PEV charging profile. Furthermore, the impact of distributed FCSs, which are expected to replace the current gas stations, on the PEV load profile is not considered. Study [23] also does not consider the actual PDFs of the TDM and DDT statistical variables, they assume both variables follow the Gaussian distribution curve, while the normal distribution curve is assumed by study [24] to represent PDT at each trip. Oversimplifying any of driver' behavior elements using typical distribution functions may lead to unrealistic driver' behavior and therefore estimating the total PEV charging demand becomes unreliable. Sun et al. [25] developed a methodology for modeling PEV charging that considers temporal characteristics. The study classified daily trips into home, work, and others, and used NHTS data to extract the arrival and departure times for each trip. However, the study does not address other spatial important elements such as PDT, TDM, DDT and driver randomness movement. Another research [26] has investigated the impact of six different locations, but the study is limited to use a fixed formula for determining the TDM and log-normal distribution for DDT. The authors in [26] do not consider either PEV market share or distributed FCSs. Because the trip travelled distance is a function in computing PEV SOC, simplifying TDM parameter may lead to inaccurate PEV SOC which may underestimate the ER by PEV from the grid. The work reported in [27] has also proposed a development for modeling PEV charging demand considering multiple trips. The authors investigated charging PEVs at six locations without considering charging at FCSs. Furthermore, it is assumed that fast and low charging levels are available at all locations, which is not a realistic assumption since the available rated power at homes is different compared to either work or FCSs. Moreover, considering this assumption would ignore the temporal and spatial characteristics. Study [27] also does not consider the PDF of the TDM using NHTS real data and uses DDT and average PEV speed to quantify its value. Al thought the previous reported models [23–27] have studied the development of PEV charging demand while taking into account multiple trips in a day, several important factors, such as PEV market share, PDT, TDM, and DDT, are either largely ignored or oversimplified.

The research in [28] and [29] has explored the impact of installing PVs and the results conclude that installing PVs may defer upgrading EDS assets. Several researchers have made recently noteworthy attempts to develop PEV stochastic models while considering the stochastic nature of PV generation [30], [31], [32]. These studies conclude that increasing PV penetration levels would improve the total system load profile. However, none of these studies considers the impact of PV uncertainty with the inclusion of PEV SAT characteristics.

Table 1.1: Summary of the literature review of the stochastic models of PEV charging loads with solar energy resources

Ref. No.	PEV stochastic Models											PV Energy Resources
	Charging locations			Dependency on previous charging activities	PEV market share	Trips per day	Spatial rating power levels at each location	SVDB				Uncertainty
	Home	Workplace	FCS					AT	PDT	TDM	DDT	
[9, 10]	C	NC	NC	NC	NC	1	NC	TD	NC	NC	NC	NC
[11], [12]	C	NC	NC	NC	NC	1	NC	F	NC	NC	NC	NC
[13–15]	NC	NC	C	NC	C	1	NC	RD	NC	NC	NC	NC
[23, 24]	C	C	C	C	NC	3	C	TD	TD	TD	TD	NC
[25]	C	NC	C	NC	NC	2	C	TD	TD	NC	NC	NC
[26]	C	C	C	C	NC	6	C	TD	TD	TD	TD	NC
[27]	C	C	NC	C	NC	6	NC	RD	RD	TD	TD	NC
[30–32]	C	NC	NC	NC	NC	NC	NC	RD	NC	NC	NC	C
Proposed work	C	C	C	C	C	6	C	RD	RD	RD	RD	C

F: Fixed, NC: Not considered, C: Considered, SVDB: Statistical variables of driver behaviour, TD: Typical distribution

Table 1.1 presents an overview of the literature on the developed models regarding stochastic PEV charging loads with solar energy resources. Al thought most of the previous research has studied the development of PEV charging demand while taking into account the realistic dynamic behavior of drivers, it can be observed that very little attention has been paid to the assessment of SAT driver' behavior characteristics on PEV charging demand. In the few developed studies, PEV market share, PDT, TDM, and DDT elements are either largely ignored or oversimplified. Modeling these factors without relying on realistic data generates a PEV charging profile that does not reflect the natural habits of drivers.

It should be noted that, none of the above works attempted to integrate the PDT, TDM, and DDT elements using NHTS real data within the PEV driver SAT characteristics, while considering the inherited uncertainty of PVs. The integration of these components provides

an enhanced and improved model in comparison to the existing stochastic models, which calls for in-depth research on this subject .

1.2.2 Impact of Residential Prosumer Ownership of PEVs on Transformer Overload and Aging, and Voltage Quality

A growing body of literature is devoted to assessing the integration of residential prosumer ownership of PEVs into an EDS. The reported research includes the assessment of transformer overload and voltage quality in [32–41], and transformer aging in [30, 31, 42–46].

1.2.2.1 Impact of Residential Prosumer Ownership of PEVs on Transformer Overload and Voltage Quality

Specifically, the studies [32–36] report assessments while taking into account residential PEVs and PVs. The researchers in [32] studied the feasibility of charging PEVs through PV panels. The authors in this study proposed a probabilistic power flow (PF) to evaluate the impact on DT overload, energy losses, and under and over voltage. Study [32] used the NHTS survey data to construct the PDFs of the arrival time and daily distance and only trip to home was considered. The assumption, considering one trip in a day, neglects the realistic pattern of PEV daily driving cycles and hence impacted PEV ER from grid which may lead to underestimate the DT overload and voltage quality evaluation. This study focused on investigating the impact on DT overload without estimating the DT lifetime and degradation. In [34] and [35], the VI together with voltage drop and rise were also evaluated, and both studies focused on maintaining voltage quality indices within normal limits, by controlling the residential single-phase PEV loads and PV generators. These studies do not consider the uncertainty of PEV and PV and hence neglecting these models may lead to inaccurate evaluation. They also failed to consider the assessment of DT overload and aging even though their normal limits could be violated due to the high penetration levels of charging PEV. The authors in [36] evaluated and mitigated the voltage rise caused by

PV generation, while the researchers in [33] proposed a distributed control strategy to reduce the grid power exchange by controlling PEV battery charging/discharging. However, these studies focused on regulating the voltage and power and do not include the inherited uncertainty of PV and PEV.

Moreover, having ESSs with PEVs and PVs is also discussed by the researchers in [37–41, 47]. Study [37] proposed a methodology to avoid the transformer overload caused by PEVs, wherein the coordination of an ESS with PV units was developed in order to discharge power to the grid in instances when the power measured at the transformer is higher than that of the rating. The proposed solution in [37] does not include the assessment of DT aging, as well as the inherited uncertainties of PV generation and PEV loads. Moreover, an assessment framework was proposed in [38] in order to evaluate voltage profile, feeder loading, and active and reactive power losses, while considering ESSs with different penetration levels of PVs and PEVs. The results from this study show that an ESS can be used as a means to alleviate the negative impact of PEVs and PVs on under and over voltages, respectively. In study [38], only trip to home was considered and DT lifetime was not investigated. The study also assumed that PEV arrival at home follows a normal distribution curve, with 6 P.M. and 2 hours for mean and variance, respectively. Modeling PEV arrival time using typical distributions without relying on realistic data generates a PEV charging profile that does not reflect the natural habits of drivers, which may affect the evaluation of DT overload and voltage quality. Further, in [39], ESS sizing was proposed in order to maintain over and under voltage within acceptable limits. The study concluded that increasing PEV penetration level reduces ESS capacity. The author in [39] assumed fixed profiles for PV generation and PEV demand which neglects the inherited uncertainty. The study also considered one trip in a day and focused on investigating the voltage quality without including DT aging estimation. Additionally, Yang et al. [40] developed a methodology to shape fluctuated PV output power into a relatively flat power using an ESS. Interestingly, the proposed approach supported the system at peak load and reduced the line losses. Another examples are developed by the authors in [41, 47] for implementing ESS units in the residential distribution networks. An ESS location, power, and energy are determined and used in conjunction with PV profile, to alleviate DT overload [41], VI and under/over voltage violations [47], while taking into account

the uncertainties inherent in PV generation and PEV demand. These studies used the NHTS data to construct the PDFs of PEV arrival time and daily distance parameters, and only trip to home was considered. The PEV model, used in [41, 47], neglects the realistic pattern of PEV daily driving cycles and hence the ER from the grid will be affected which impacted the assessment and evaluation of DT overload, VI, and under and over voltage. The study also focused on DT overload without including the assessment of its aging.

However, none of the preceding studies involved taking into account DT aging nor the stochastic models of PEV driver behavior and travel patterns that considered SAT travel pattern characteristics.

1.2.2.2 Impact of Residential Prosumer Ownership of PEVs on Transformer Aging

Some researchers have considered evaluating the impact of residential prosumer ownership of PEVs on transformer aging [30, 31, 42–46]

Such impact of PEVs and PVs on transformer aging is assessed in [30, 31, 42–44, 48]. The authors in [31, 48] developed a probabilistic methodology to investigate the impact of stochastic models using different PEV and PV penetration levels on DT overload and aging, with the conclusion that DT replacement can be deferred by four years when PV generation is used. It was also determined that 10% PV is capable of alleviating the DT overload between 10 A.M. and 5 P.M. In this study, only trip to home was considered and NHTS survey data was used to extract the important statistical parameters (i.e., arrival time and daily distance). However, this study focuses on investigating the impact on DT aging, but the authors do not include realistic pattern of PEV daily driving cycles which may lead to inaccurate estimation for DT lifetime. The authors of [30] focused on quantifying main substation transformer aging, while the researchers in [42] investigated the DT aging when a PEV is charged following time-of-use (TOU) pricing. The study in [30] concluded that DT LOL is improved by 75% when 100% penetration level of PV is used, while the authors of [42] observed that PEV charging during TOU negatively affects DT aging. Both research works consider one trip in a day and neglect the complete PEV daily driving cycles, which results in affecting the accuracy of estimating DT remaining

lifetime. Further, the proposal of a deterministic and stochastic assessment for DT aging was presented in [43], which found that increasing LOL due to PEV charging can be compensated by PV generation. However, this study does not consider the complete daily driving cycles of PEV stochastic model, as well as PV uncertainty. Neglecting these factors may lead to different LOL evaluation results. An excellent example was also introduced in [44], which investigated the impact of solar-powered EVs on DT aging and annual vehicle energy usage, with the conclusion that using solar-powered EVs contribute to an overall reduction in annual vehicle energy usage, in comparison to regular PEVs. In study [44], the authors developed a methodology to extract the statistical quantities of arrival and departure times and daily distance, but the realistic pattern of the complete daily driving cycles was neglected, which may lead to inappropriate estimation.

Research in [45] and [46] focused on studying the impact of implementing ESSs with PEVs and PVs. Particularly, the study reported in [45] displayed how the impact on DT aging could be mitigated through the use of residential HBESs. The authors proposed that HBES charging occurs during the time in which PV is available and discharges during the night when PEV charging occurs. The study found that HBES reduces LOL to normal limits value from 55% in the case of a scenario with 100% PEV and 100 PV penetration level. Finally, the work presented in [46] proposed a coordination strategy between ESS, PV, and PEV in an attempt to extend DT lifetime and minimize energy consumption costs, with results indicating that DT life can be retained. The developed PEV model in studies [45] and [46] considered only trip to home and NHTS were used to extract the statistical distributions of arrival time and daily distance parameters. However, neglecting other important variables such as

The research studies introduced above in [30, 31, 42–46] focus primarily on evaluating DT aging when prosumer (i.e., PV and ESS) ownership of PEVs is considered. However, there is a gap in this research, as none of these studies takes into consideration the statistical SAT characteristics of PEV driver behavior.

Several researchers have recently made noteworthy attempts to develop the statistical SAT accurate models of PEV driver behavior [23,27,49–52]. Although these studies discuss the statistical SAT accurate models of PEV driver behavior with some simplifications, they do not consider the assessment of either DT overload and aging or voltage quality (i.e.,

VI, and under and over voltage). In addition, PV generation and residential demand are stochastic in nature, which has not been fully considered in these recent studies. However, the inclusion of PV generation and residential demand uncertainty, as well as PEV SAT-based approach models into DT aging and overload, and voltage quality assessment, was not considered in any of the previously discussed works. The existing developed models on the impact of integrating residential prosumer ownership of PEVs on DT aging [45] and voltage quality [32] were limited to the employment of the simplified models of PEV driver behavior. Modeling PEV drivers in these examples only considered one trip per day and represented driver behavior by only two parameters (i.e., destination arrival time and daily distance), while realistic driving and travel law include a sequence of trips per day and involve SAT travel information. Specifically, the temporal characteristics of driver behavior includes driving and parking time, while travel distance and destination location are spatial characteristics. SAT travel parameters are significant in estimating PEV charging location, time, and SOC. For instance, travel distance is used to calculate PEV energy consumption while driving and, therefore, modeling the distance that drivers travel in an entire day by a single PDF leads to unrealistic estimations of PEV energy consumption, and further results in inaccurate PEV remaining SOC and required energy. Consequently, the impact of residential prosumer ownership of PEVs on DT aging, as well as voltage quality through a consideration of SAT characteristics of PEV driver behavior, has not been previously reported in the literature. Therefore, there is a need to address this missing component and develop an assessment framework for DT aging and voltage quality, while taking into account PEV charging models based on SAT driver characteristics, as well as PV and conventional load uncertainty.

1.2.3 Planning of Energy Storage Systems in an Electrical Distribution Grid

There is a large body of literature towards the use of ESSs in an EDS to assist the utility in resolving overload and voltage violation issues and managing grid operations.

Several researchers have discussed the ESS planning models in a distribution system while considering DGs [53–61]. In study [53], a multi-objective optimization was used

to develop a planning model for sitting DGs and ESSs in a distribution grid. Studies [54, 55] proposed an optimal planning approach for determining ESS energy, power, and location, that are required to alleviate the effect of uncertainties inherent in DGs. A meta-heuristic genetic algorithm based planning framework was developed in [56] to optimally size and site ESSs in an EDS in order to minimize total system losses, defer system upgrade, and maximize the overall profit. The research in [57] proposed an operational planning framework by developing a coordination between ESSs and wind farms in order to mitigate the effect of wind forecast errors. The study also proposed a reduction to the frequent charge / discharge operations in order to extend the expected lifetime of ESS battery. A stochastic optimal planning model is proposed by the authors in [58], which focused on developing a decomposition technique to optimally determine the ESS sizes and year of installation. Two stages were proposed, including several iterations, to ensure that the overall budget is allocated effectively over the planning horizon. Another research for ESS sizing model was proposed in [59] to optimally select ESS power, energy, and number of units, that are required to be in place, to minimize total operation and unserved energy costs. In study [60], a planning model was proposed for sitting and sizing ESSs while considering smart residential loads. This research included more details of ESS battery degradation into the planning horizon model and provided a comprehensive comparison for the proposed approach versus the fixed degradation. An optimal plan for transmission line expansion and ESS deployment was proposed in [61] using multi-stage approach. In [62], an optimal planning model was proposed for sizing ESSs considering the usage of EV re-purposed batteries. However, none of the above works have considered PEV loads nor the assessment of DT aging or VI.

Some researchers have considered the integration of PEV loads with ESS operation [63–66] and planning [67]. Study [63] proposed an optimal operation strategy for maintaining feeder' loading and voltage limit within standards. The research in [64, 65] proposed an optimization model for energy management system considering HBES, PV, and PEV. The proposed framework in these studies was developed to address the conflict between utility and residential customers while ensuring that DT LOL, VI, and under and over voltage within standards. Agüero et al. in [66] utilized CBESS to mitigate the negative impact of integrating PEV and PV in an EDS. The research in [66] improves system power loss and

voltage deviation, but the authors did not consider PEV uncertainty.

El-Khattam et al. [68] developed the first research on distribution system multi-year planning using the backward propagation approach. The authors in [68] proposed an excellent heuristic approach to alleviate the use of binary variables in the optimization model for sitting DG units over the planning horizon, but they did not consider PEV demand and ESS resources. Recently, Bin Humayd et al. [69] developed a planning model using the same heuristic approach while considering PEV loads and diesel DG units. This example discussed PEV stochastic nature model, but they assumed that charging activities happens only at home and ESS was not considered. A multi-year planning approach was proposed in [67] for sizing CBESSs while considering PVs and PEVs, to maximize the Net Present Value (NPV) of profit from the energy storage arbitrage. A particle swarm optimization was developed in this study to solve the planning model and the results found that the CBESS can benefit an EDS by reducing power loss, improving DT LOLs and voltage profile, and providing energy arbitrage. It is noted that most of the works, which pertain to the ESS integration with PEV, have focused on studying the operation of the electrical distribution system while only study [67] focused on planning.

It can be noticed from the above discussion that the recent attempt in [67] did not consider the VI as a part of the planning model and the developed stochastic nature model of PEV considered only trip to home. NHTS data were used to extract the statistical quantities of arrival time and daily distance without including other statistical important parameters, namely PDT, TDM, PL, DDT, and driver movement. Neglecting these important elements ignores the SAT characteristics of driver' behavior and affects the ESS planning decisions, which may result in either over or under estimating the ESS power, energy, required number of sites, and captial and operation costs. Therefore, there is a dire need to include PEV demand using SAT-based approach into the ESS planning models while considering DT LOLs and VI, which significantly impacts the investment timelines and budget.

1.3 Research Objectives

The main objectives of the research presented in this thesis focus on modeling PEV demand based-SAT approach and the integration of these models into the EDS assessment and planning. The research objectives are listed below:

- The development of a generalized statistical spatial-temporal (SAT) distribution model that addresses the realistic pattern of PEV daily driving cycles for any type of driving behavior data. The US NHTS datasets are used to establish the PDFs of the required parameters in the SAT model, namely PDT, TDM, DDT, and transition probability matrix for different trips in a day.

- The uncertainty of PV generation (i.e., temperature and irradiation) and conventional loads is modeled and integrated with SAT models of PEV charging load. The integration of these components provides an enhanced and improved model in comparison to the existing stochastic models.

- The above models are used to develop a new assessment framework to estimate the distribution transformer (DT) overload and aging, voltage imbalance (VI), and under and over voltage considering a complete and more realistic EDS model. The remaining lifetime of the DTs considering SAT models of PEV charging with residential prosumers at different scenarios is quantified, in addition to VI, and under and over voltage.

- A control strategy utilizing different generations of home battery energy storage (HBES) is proposed in order to avoid DT overload, and to enhance and extend DT lifetime.

- A multi-year planning framework is proposed to size and site the CBESSs while considering a PEV demand-based SAT approach as well as PV options. A backward propagation approach is developed in order to determine the CBESS sizes and sites over the planning horizon while considering transformer' LOL and VI aspects.

1.4 Thesis Outlines

The rest of the thesis is organized as follows:

Chapter-2 presents a brief background on an EV charging characteristics and its types, the concept of trip chain and its formulations, followed by a detailed discussion on three-phase distribution system models and PF solution, and PV and energy storage systems.

Chapter-3 presents a comprehensive statistical analysis model for SAT characteristics of PEV driver' behavior, and evaluate their effect on conventional loads while considering the uncertainty of PVs.

Chapter-4 presents the proposed assessment and enhancement framework for DT overload and aging, VI, and voltage deviation while considering residential prosumer ownership of PEV.

Chapter-5 presents a multi-year planning framework for sizing and sitting CBESS to accommodate a high PEV penetration levels.

In Chapter-6, the summary and conclusions of the thesis are presented, and directions for future work are outlined.

Chapter 2

Background Review

This chapter presents a brief review of the necessary definitions and main concepts related to the subject of the research presented in this thesis. A detailed discussion of EV basic definitions and required mathematical equations are presented, followed by an overview of trip chain definition and its applications. An overview of three-phase electrical distribution system models, components, and PF solution are explained and briefly discussed. Finally, a review of the fundamental aspects and mathematical models of PV and energy storage system are presented.

2.1 Electric Vehicles

The history of EVs technology started in the late 1800s when Dr. Ferdinand Porsche and his team developed the first hybrid vehicle [70]. The first vehicle that could be plugged into an electrical wall outlet was first developed by General Motors (GM) during the late 1960s, when the concept of EVs was initiated. Now, in the 21st century, when great attention is focused on global warming issues, EVs have been introduced as a solution toward more fuel efficient vehicles. In the current market, the following types of PEVs, as specified by [70], are described below:

- Hybrid Electric Vehicles (HEVs): These vehicles are operated by combining an ICE with an electric motor and battery. HEVs cannot be plugged into an electricity supply, but charge their batteries through regenerative braking.

- Plug-in Electric Vehicles (PEVs): PEVs are classified into Plug-in Hybrid Electric Vehicles (PHEVs) and Plug-in Battery Electric Vehicles (PBEVs). PHEVs have the same characteristics as conventional cars, but they are powered by an ICE and an additional battery energy system that can be recharged by plugging into an external electricity supply. In contrast, PBEVs rely solely on electricity by recharging their batteries from an external supply.

- All-electric vehicles (EVs) or battery-electric vehicles (BEVs): Rather than using an ICE, these vehicles use batteries as a storage system to supply the electric motor in the car.

Since PEVs are defined as the vehicles that recharged their batteries from the grid, these types of vehicles are only considered in the work presented in this thesis, as they are expected to have an impact on the electrical distribution grid.

2.1.1 PEV demand Characteristics

From the perspective of the EDS, PEV demand is a significant additional load which must be considered in the assessment and planning process. To correctly estimate the PEV charging demand, there are several definitions of some parameters that need to be well defined and discussed [71]:

- Charging Characteristics:

  These characteristics determine the amount of the additional PEV load, and charging duration. The main required parameters to obtain these quantities are battery capacity (BC), battery SOC, EDR, specific energy (SE), and charging efficiency (η), wherein their definitions are listed below:

1) BC, which is expressed in kWh, represents the maximum amount of energy to which vehicles can be charged.

2) Battery SOC, which represents the remaining amount of energy that can still be used by a vehicle, is expressed as a percentage (%). The SOC can be estimated using the driven distance (TDM) by the vehicle in miles. For example, assuming that the BC of vehicle is 100 kWh, having an SOC of 5 % implies that the battery has only 5 kWh for use.

3) EDR, which is expressed in miles, is defined by how much distance a PEV, using battery energy, is capable of achieving during the day, until the minimum acceptable battery SOC is reached.

4) SE, which is expressed in kWh/mile, represents how much energy the vehicle consumes to travel for one mile.

Estimating the energy required (ER) by recharging PEVs from the grid depends on the SOC and BC. When the consumed energy (CE) is determined using (2.1) by multiplying the TDM in SE, the remaining PEV SOC is calculated using (2.2) assuming the initial SOC was 100%. Thus, ER is obtained using (2.3) and η is assumed as 90% [72].

$$\mathrm{CE} = \mathrm{SE} \cdot \mathrm{TDM} \tag{2.1}$$

$$\mathrm{SOC} = \frac{\mathrm{BC} - \mathrm{CE}}{\mathrm{BC}} \tag{2.2}$$

$$\mathrm{ER} = \frac{(1 - \mathrm{SOC}) \cdot \mathrm{BC})}{\eta} \tag{2.3}$$

For determining the chronological charging profiles of PEVs and charging duration (CD), two quantities are needed in addition to ER: the time of start charging and the charging level (power rating) which are discussed next in more details.

- The time of start charging:

  Determining the time of PEV to start charging is very challenging and important. It always depend on the user' preference and which charging scheme is applied. In the literature, three charging schemes were reported [73, 74], namely uncontrolled,

indirect controlled, and controlled. A more detailed discussion is introduced in the following:

Uncontrolled charging (UC): The owners of PEVs, in this type of charging scheme, select the time to start charging their vehicles with no restrictions. Several studies in the literature have shown that UC widely used wherein some owners prefer to charge their vehicles at predefined time (always overnight) due to the very low electricity price rates. This assumption does not reflect the realistic behavior of drivers, which does not give the possibility of plug and charge at any time of the day. Other researchers have developed a probabilistic representation for the time of start charging, using NHTS available data, which simulates the driving law during the day and hence each PEV starts charging based on the arrival times.

Indirect controlled charging (ICC): This charging scheme is similar to UC, as PEV owners are capable to charge their vehicles whenever they wish. However, the incentives that were set by utility may create a certain level of control over time. For example, although some of PEV owners arrive home at on-peak and mid-peak hours, they response to the TOU electricity pricing by waiting for off-peak hours and start charging their vehicles. This way of control benefits the utility by shifting the on-peak and mid-peak demand to the off-peak period while PEV owners are helped by reducing the costs of their electricity bills.

Controlled charging (CC): In this scenario, PEV owners are not able to choose the time of start charging their vehicles. The utility companies or any service providers have the privilege to fully control and manage PEV loads. For determining the time to start charging each PEV, the service providers tend to maximize the benefits while satisfying all associate parties including PEV users and system operating conditions. The context of CC is then extended to what is known as "smart charging", which paves the way toward smart grid paradigm as a two-way communication infrastructure is required. Having smart charging infrastructure implemented enables bidirectional power flow between PEV and an EDS grid, which creates an opportunity for V2G technology and ESS provision at the residential premises.

For the scope of this work, UC type was only considered, as it simulates the realistic pattern of PEV drivers.

- Charging level:

  There are three available charging levels for PEV charging loads, as proposed by the Society of Automotive Engineers (SAE) [72] in North America. These sets are known as the J1772 standard. An overview of these levels is listed in Table 2.1 as specified by the J1772 standard and the report in [75].

Table 2.1: PEV Charging Levels.

Type	Voltage (V)	Current (A)	Power (kW)	Location
AC Level 1	120	12 to 16	1.3 to 1.9	On-board 1-phase
AC Level 2	208 or 240	Up to 80	Up to 19.2	On-board 1
DC Level 3 (Fast Charging)	208 to 600	Up to 200	50 to 150	Off-board 3-phase

When the ER, charging level, and time to start charging PEV are determined, ER is divided by charging level to obtain the duration of PEV charging event. The start time of PEV charging, along with charging duration time helps to allocate the new PEV profile on the top of the 24 original load curve.

2.2 Trip Chain

The concept of the trip chain is well explained and discussed in [76]. A trip chain has become widely developed in transportation sector planning [77], but is rarely used in power system analysis. Trip chain methodology simulates a sequence of trips, starting at home, where two or more visits may be involved, and ending at home. It is used to model activities in space and time by linking all daily trips. The mathematical representation of the trip chain is taken from [23], and modified and developed for each individual driver, as follows:

$$(T^s, d, DD, PD, L^s, L^e) = (T_1^s, T_2^s, \cdots, T_n^s; d_1, d_2, \cdots, d_n; DD_1, DD_2, \cdots, DD_n; PD_1, PD_2, \cdots, PD_n; L_1^s, L_2^s, , \cdots, L_n^s; L_1^e, L_2^e, \cdots, L_n^e)$$

$$\text{Subject to} \quad L^s_{j+1} = L^e_j \tag{2.5}$$

$$T^e_j = T^s_j + DD_j \tag{2.6}$$

$$T^s_{j+1} = T^e_j + PD_j \tag{2.7}$$

where T^s_j is the start time, T^e_j is end time, d_j is the distance in miles, DD_j is driving duration, PD_j is parking duration at destination, L^s_j is start location, L^e_j is end location, j denotes j^{th} trip, and n is the number of daily trips involved.

The developed model considers complete daily driving cycles and models each individual trip as a function of the previous trip. Because our developed approach focuses on modelling the movements of drivers from one location to another, the Markov chain process was necessary in order to determine the current location for the drivers as a function of the previous location using the transition probability matrix. Combining the different PDFs with transition probability matrix formed the Markov Chain Monte Carlo (MCMC) simulation. As an example, the start time of the next trip is calculated using (2.7), and equals the summation of the end time and parking time at the previous trip destination. Also, in (2.5), the start location of the next trip is the same as the end location of the previous trip. Since the driver travel pattern is different from day to day and from location to location, the trip chain variables mentioned in (2.4)-(2.7) are represented by corresponding probabilities extracted from the NHTS, the details of which will be discussed in Section 3.1 of Chapter 3.

2.3 Unbalanced Three Phase Distribution System Modeling

The EDS typically begins from the distribution substation that is fed by one or more sub-transmission lines and ends at the consumer meters [78]. A typical EDS is illustrated in Fig. 2.1 [78] including a primary distribution system (PDS) with main and lateral feeders. The main feeders are usually three-phase while the laterals, which can be either single or three phase, are usually tapped from the main feeders. The system mainly includes primary and secondary networks. The primary distribution system (PDS) generally starts from the

distribution substation and ends at the distribution transformers. The voltage levels of

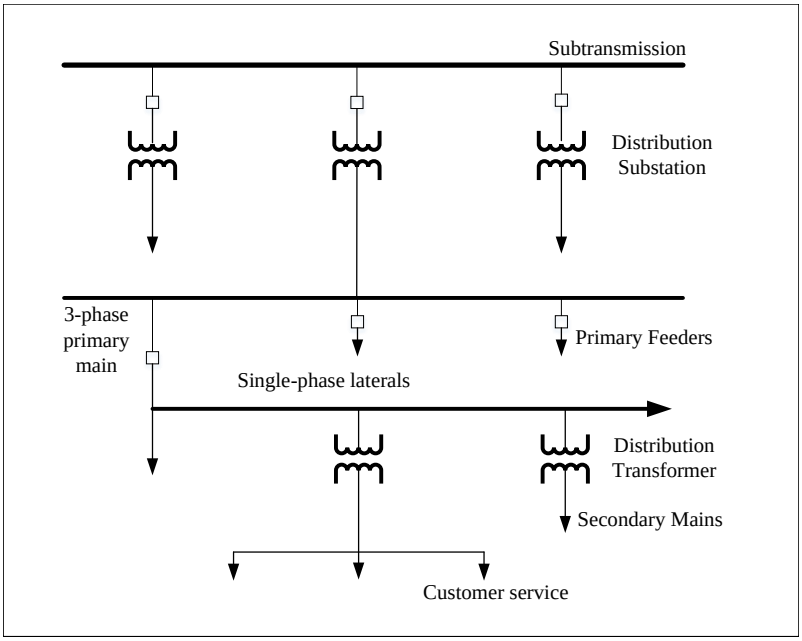

Figure 2.1: Typical EDS single line diagram

a PDS range from 4.16 to 35 kV, while a SDS starts from the distribution transformers, including service lines (SLs) and service drops (SDs), and ends at the consumer's level. Through a center tapped transformer, an SDS connects the primary voltages to the 120/240 voltage level, which is more suitable for a consumer's equipment.

2.3.1 Power Flow Approach for Unbalanced Radial an EDS

Evaluation of the impact of PEV stochastic loads on voltage quality and DT aging in the electrical distribution network (EDNs) requires the development of proper models involving all the components. PF is then used to thoroughly investigate the inclusion of the uncertainty associated with the introduction of PEV charging. Because, by nature, the EDNs have single-phase loads, higher resistance to reactance (R/X) ratio, and radial configuration, the Newton-Raphson method that was commonly used in the bulk generation-transmission system may not be applicable in a distribution system. A robust

iterative technique, known as the forward/backward method, is used. This method is based on the ladder network theory as developed in [78]. The approach relies on representing the components of EDNs, such as feeders, transformers, and regulators by a set of transfer matrices named as A, B, C, and D, which are used in forward/backward PF solutions, as shown in Fig. 2.2. Further detail of how these matrices are developed is provided in [78]. The first step of the approach starts by assuming zero load currents and

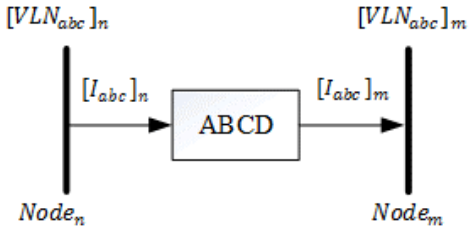

Figure 2.2: Ladder network theory

computes the voltages at each node moving from the substation down to the terminal nodes (forward sweep), as given in (2.8):

$$[VLN_{abc}]_m = [A].[VLN_{abc}]_n - [B].[I_{abc}]_n \tag{2.8}$$

The second step will solve for currents based on the obtained voltages from the first step by moving backward from the terminal nodes up to the substation, as given in (2.9):

$$[I_{abc}]_n = [C] \cdot [VLN_{abc}]_m - [D] \cdot [I_{abc}]_m \tag{2.9}$$

The currents obtained from (2.9) are then used to calculate the node voltage in the next iteration using (2.8) and so on, and the backward/forward sweeps are repeated until the stopping criteria given in (2.11) is satisfied, for all system buses.

$$[Error]_i = \frac{\parallel V_{new,i} \parallel - \parallel V_{old,i} \parallel}{V_{nominal,i}} \quad \forall i = 1, 2, 3, ...N \tag{2.10}$$

$$Max[Error] <= Tolerance \tag{2.11}$$

where the voltage at bus i is denoted as V_i , $V_{nominal,i}$ is the nominal voltage, and N is

the numbers of buses. A flowchart explains all the steps for performing backward/forward sweep power flow is illustrated in Fig. 2.3.

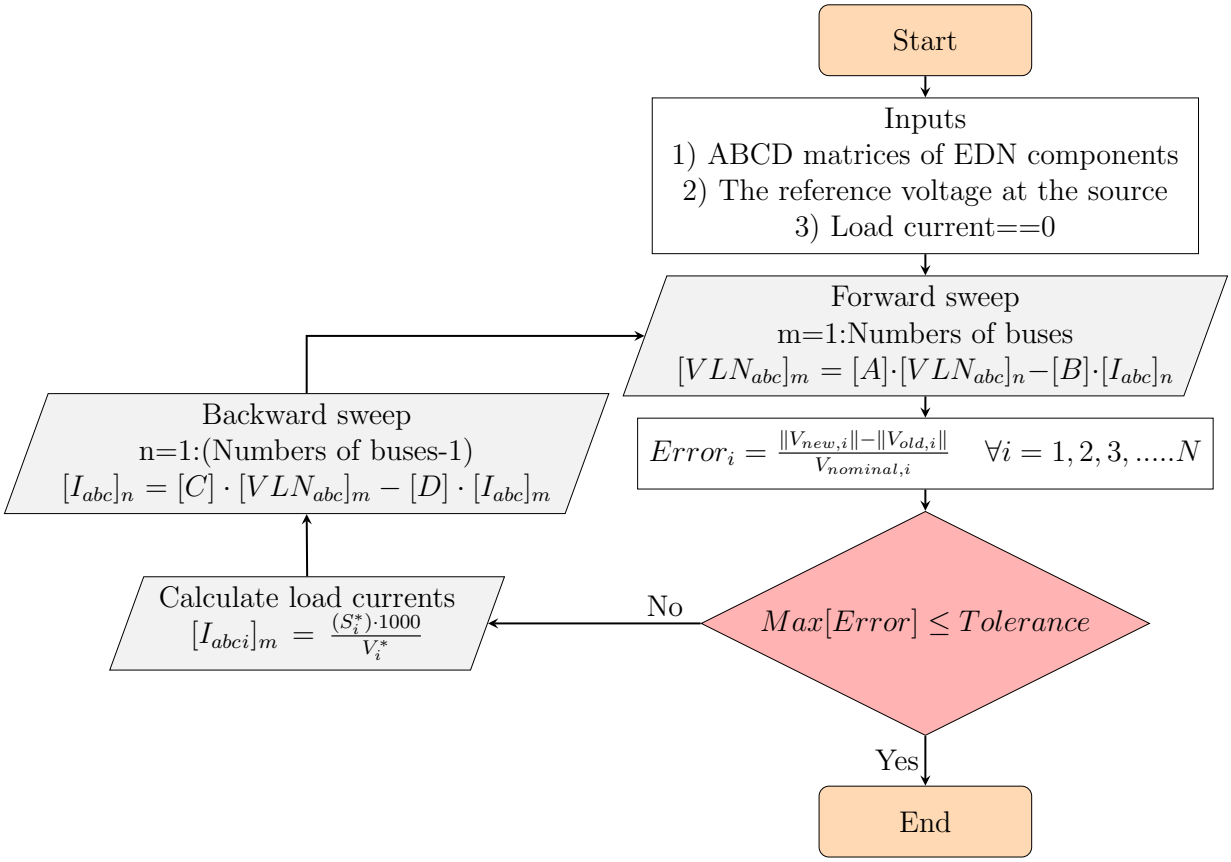

Figure 2.3: Steps needed to perform backward/forward power flow.

2.4 PV Generation

In the past, PV was used as stand-alone system to supply electricity for the rural areas and suburbs which lack availability of other energy resources. Recently, PV has received a noticeable shift toward using the PV-grid connected system due to improve its technology and increase the concerns related to global warming issues. According to [79], PVs are classified, based on their power ratings, into the following three categories:

- A Small PV system ranges between 0 kW and 10 kW.
- A medium PV system ranges between 10 kW and 500 kW.
- A large PV system ranges between 500 kW and above.

The first and second categories are more common to be installed at the electrical distribution network level. For small buildings, PV with ranges between 0 and 10 kW are used, while the medium and large buildings use PV with ranges between 10 kW and 500 kW. At the transmission or sub-transmission levels, the third category, ranging between 500 kW and above, is used.

For the type of PV interconnection, the International Energy Agency (IEA) [3] has classified PV into four types, namely off-grid domestic, off-grid non-domestic, grid-connected distributed, and grid-connected centralized. The research presented in this thesis considers the grid-connected distributed residential PVs with small ranges (i.e., 0 - 10 kW).

2.4.1 Main Components of PV Generation Systems

The key elements that need to be available in the grid-connected distributed PV systems are discussed in the following:

i) The sun: The sunlight irradiance is defined as the instantaneous solar power that received on a unit surface area, and is measured in watts per square meter (W/m^2). The sun releases amount of energy, which travels for more than 150 million km in order to reach the terrestrial orbit of the earth. As reported in [80], 9% is scattered by air molecules and 17% and 7% are reflected back to the space by clouds and earth's surface, respectively. It was reported that the quantity of light that reaches the ground level is around $1,000\ W/m^2$.

ii) PV array: It represents the most expansive component in the PV system. The cells that form the solar arrays are made of different types of materials; for instance, polycrystalline and monocrystalline silicons are globally used with 54.5% and 29.36%

of the world market share [81]. A PV module is formed by connecting the solar cells in series and these formed modules of PV are then connected together in series to form a string. Finally, the strings are connected in parallel in order to form the final design of PV arrays.

iii) Power conditioning unit (PCU): PCU integrates the grid-connected PV system into the alternating current (AC) electrical grid. Two main functions are performed by PCU which involve controlling the output current or voltage of PV arrays, and converting the direct current (DC) output power of PV into AC power. By controlling either the voltage or current, the maximum power of PV at certain irradiance and temperature is extracted. The second function is used then to prepare the output of PV array for AC grid integration by converting PV DC power to AC power.

The temperature and solar irradiation are important factors in constructing PV generation profiles, as will be discussed in Section 3.1.1.3 of Chapter 3.

Having PV installed at the residential premises contributes to change the role of residential consumers to be more prsomuers. Since PV output is associated with a high degree of variability and its peak does coincide with PEV or system peak demand, it became necessary to install the ESS units at the residential premises to fully utilize PV energy and participate with utility companies to solve any overload or voltage issues.

2.5 Energy Storage Systems

The deployment of energy storage technology increases the potential of integrating more renewable energy resources and providing some level of controllability in the system. Different technologies of an ESS are available in the market, each of which provides its own characteristics and features. In general, any type of an ESS includes energy reservoir and power conversion. Based on an ESS type, the power conversion can be determined, either a DC-AC converter or motor-generator module. The superconducting magnetic energy storage (SMES) and battery energy storage systems (BESSs) have the DC-AC

converters while the pumped hydro, compressed air energy storage (CAES), and flywheels have the motor-generator set [82, 83].

There are various applications for an ESS in power system, which can be divided into three categories, namely bridging power, energy management, and power quality [84]. For the energy management applications, the ESSs units reduce the stress on the grid by using the stored energy during off-peak times at the times of high demand. In this thesis, the BESS type is selected among all available ESS technologies in the market. The reason is due to its ability to coordinate with the PV generation over the day horizon in order to improve the overload and voltage issues in the EDS networks.

The BESS can be installed at the distribution system level, or at the transmission level. The CBESS and HBES are considered as one of the BESSs that most commonly used in small-scale, at the SDS of an EDS [85]. CBESSs are connected at the secondary of the DTs and fully operated and managed by the utility while HBESs are owned and managed by the residential owners. In 2009, it was proposed to build a Lithium-Ion based facility of 25/50 (kW/kWh) for 20 CBESS units in Detroit, Michigan, USA, due to the expected introduction of PEV load [86].

The BESS operation is modeled using the following mathematical equations [87]:

BESS Energy Balance Constraint: Constraint (2.12) is used to ensure that battery SOC at the current hour is equal to the SOC of the previous hour plus or minus either the charged or discharged power from/to battery at that hour.

$$SOC_{k+1} = SOC_k + \eta^{CH} P_k^{CH} - \frac{P_k^{DCH}}{\eta^{DCH}} \quad \forall k \tag{2.12}$$

The physical capacity of BESS sets a limit on its SOC, as in (2.13), assuming 20% of the maximum allowable SOC.

$$0.2.C^E \leq SOC_k \leq C^E \tag{2.13}$$

BESS charging and discharging limits: The imported and exported power from/to

BESS are limited to BESS rated power, as follows:

$$P_k^{CH} \leq P_{Rate}^{BESS} \quad \forall k \tag{2.14}$$

$$P_k^{DCH} \leq P_{Rate}^{BESS} \quad \forall k \tag{2.15}$$

Also, a constraint (2.16) is used to ensure that the initial and final SOC are equal to 50% of BESS battery capacity.

$$SOC_k = 0.5.C^E \quad \forall k = 1 \,\&\, k = 24 \tag{2.16}$$

2.6 Summary

In this chapter, a general description of the topics related to the research in this thesis was presented. The concepts of EV and trip chain, along with their mathematical representations were discussed. A brief discussion of three-phase electrical distribution system models, components, and PF solution were briefly explained. Finally, PV and energy storage system definition and models were presented.

Chapter 3

A New Framework for Plug-In Electric Vehicle Charging Models Supported by Solar Photovoltaic Energy Resources[1]

This chapter discusses the development of modeling the stochastic nature of both PEV loads and PV generation while considering the effect of the temporal-spatial characteristics of the driver' behavior, as well as solar irradiation and temperature. A trip chain, based on the Markov Chain Monte Carlo process, is developed to properly model PEV daily driving activities and the PV uncertainty. Charging facilities are assumed available at home, work, and fast-charging stations, having charging levels of 3.7 kW, 6.6 kW, and 50 kW, respectively. The proposed framework is examined, considering the National Household Travel Survey global data, as well as the city of Buffalo and New York state. The impact of varying the penetration levels of PEV and PV resources is also investigated.

[1]This chapter has been published as:
Y. O. Assolami, A. Gaouda and R. El-Shatshat, "A New Framework for Plug-In Electric Vehicle Charging Models Supported by Solar Photovoltaic Energy Resources," in *IEEE Canadian Journal of Electrical and Computer Engineering*, vol. 44, no. 2, pp. 118-129, Spring 2021.

3.1 Proposed Framework: Input data, Mathematical Models and Treatment

This section discusses NHTS data extraction and treatment for obtaining SAT variables, followed by presenting an overview of PEV manufacture and available rated power infrastructure data. The rest of the section discusses using k-mean clustering on the annual data of PV and conventional load and the detailed steps of simulating SAT approach.

3.1.1 Required Input Data for the Proposed Framework

3.1.1.1 NHTS Data Analysis for Extracting the Important Statistical Variables of Driving Habits

In this analysis, the updated NHTS survey has been used because the data that simulate the driver behavior of PEVs are either scarce or not available. Al thought this data is based on the gasoline vehicles, the proposed procedure in this thesis is generic and can be applicable to any form of driving behavior data if existed. The NHTS provides a large size of data, including $1,0485,765$ trips, for all regions in the US. Since data size is a very important factor in giving a clear pattern of driver behavior, different partitions of the NHTS data were considered. NHTS global data are compared with the city of Buffalo and New York (NY) State datasets, respectively. To filter out data relevant to the city of Buffalo and New York (NY) state, the codebook in [88] was followed. Once the dataset for each partition was extracted, the first step was to preprocess the data by removing the outlier and negative data. For the scope of this work, daily trips are classified into six different locations: home, work, FCSs, shopping, entertainment, and buying a meal. For the FCS trip data, it is assumed that the patterns of arrival time to the gas station are similar to the FCSs. Because PEV drivers have access for a home charging facility, which is not the case for gasoline vehicle drivers, it is assumed that PEVs will recharge to 60% as a maximum at the FCSs. Following the codebook in [88], the PDFs for the significant statistical variables in the proposed framework are obtained. The first important variable

is the start time of the daily trip chain, denoted as $T_{s_{ch}}$. The related data to the start time of the trip chains are extracted for each dataset. Based on the frequency of occurrence, the PDF is generated as seen in Fig. 3.1. In the case of both NHTS global and NY state datasets, the $T_{s_{ch}}$ has similar behavior and the majority of drivers start their daily activities at around 7 A.M. For the Buffalo dataset, the pattern is shifted by three hours; the majority of drivers start at 4 A.M. instead of 7 A.M.

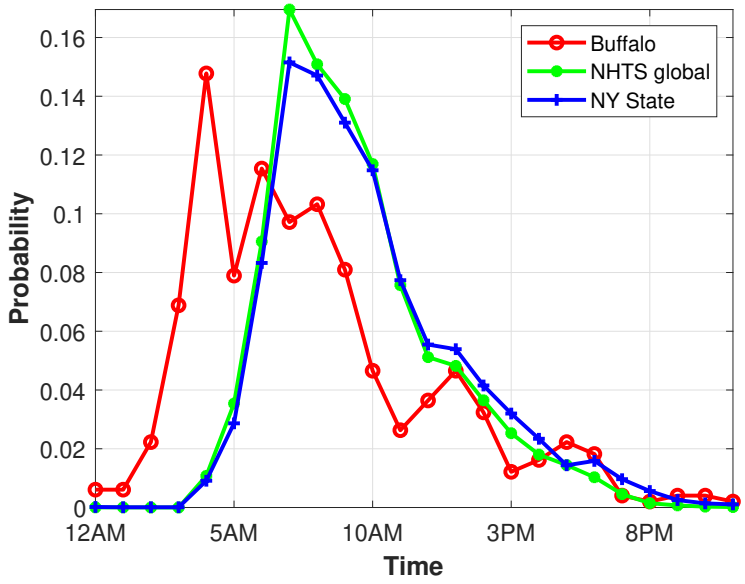

Figure 3.1: PDF of the start time of the trip chain.

3.1.1.1.1 Driver Movement Activities

To model driver movement among the six different locations, namely: home, work, FCSs, shopping, entertainment, and buying a meal, the Markov chain process is used. Let the arrival time T^e be discretized to $t_1, t_2, t_3, t_4, \ldots\ldots.., t_k$ with a specific time step, where k is the number of time intervals. The conditional probability of moving from location i to location j can be formulated as:

$$P\Big(\text{location}_j \,\Big|\, \text{location}_i, T_{AT}\Big) = P_{ij} \tag{3.1}$$

P_{ij} is known as the transition probability from location i to location j. Equation (3.1) is used for each location. Having location=$\{1, 2, \cdots, Q\}$, $Q \times Q$, a matrix can be formulated. The obtained matrix is known as the transition probability matrix and can be written as:

$$TransitionMatrix = \begin{bmatrix} P_{ii} & P_{ij} & \dots & P_{1Q} \\ P_{ji} & P_{jj} & \dots & P_{jQ} \\ \vdots & \vdots & \ddots & \vdots \\ P_{Qi} & P_{Qj} & \dots & P_{QQ} \end{bmatrix} \tag{3.2}$$

Each row of (3.2) relates to the current location, while each column represents the next possible location, and the summation of each row equals one. The probabilities pertaining to moving to the next location consider the time (temporal characteristics) and current location (spatial characteristics) extracted from the NHTS.

Equation (3.2) has been extracted for k time slots for each dataset. For the sake of clarification, two time slots of daily activities, considering the NHTS global dataset, were selected, namely 7 A.M. and 6 P.M., respectively. At 7 A.M., the majority of drivers move toward work, as depicted in Fig. 3.2(a), while during the evening at 6 P.M., as shown in Fig. 3.2(b), most drivers move toward home.

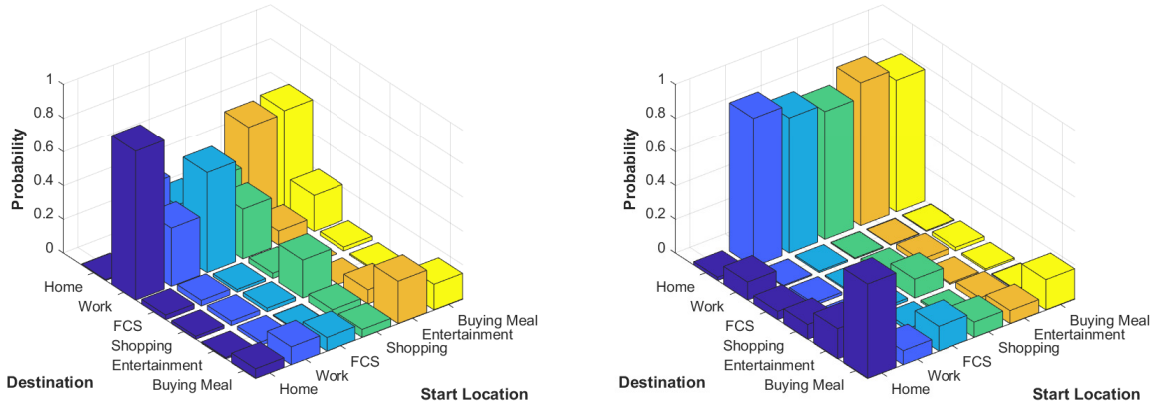

(a) Driver movements at 7 A.M.

(b) Driver movements at 6 P.M.

Figure 3.2: Driver movements based on the transition probability matrix.

3.1.1.1.2 Parking Duration (PDT)

PDT at the destination of each trip is considered an important factor in determining the start time of the next trip. For the six locations of a daily trip, the related data to the PDT (minutes) at each location is extracted from each dataset. The PDFs for all locations are generated and considered, but due to the limited number of pages, only the PDFs of PDT at home, work, and FCSs are illustrated in Fig. 3.3. It can be inferred that the patterns of PDFs are almost the same for both the NHTS global and NY state datasets, while there is a slight difference when considering the Buffalo dataset. It is noted that drivers spend most of the time at home, followed by work and FCSs, respectively. The majority of drivers spent approximately eight hours at the workplace, which is realistic for full-time employees in North America, as reported in [89]. The highest probability for home indicates that the majority spend 50 minutes, which means that most drivers have multiple trips to home without staying permanently. Most of the trips reveal that drivers arrive home and leave within an hour of returning from work or shopping. However, there is 0.02 probability of drivers arriving home and staying longer than eight hours.

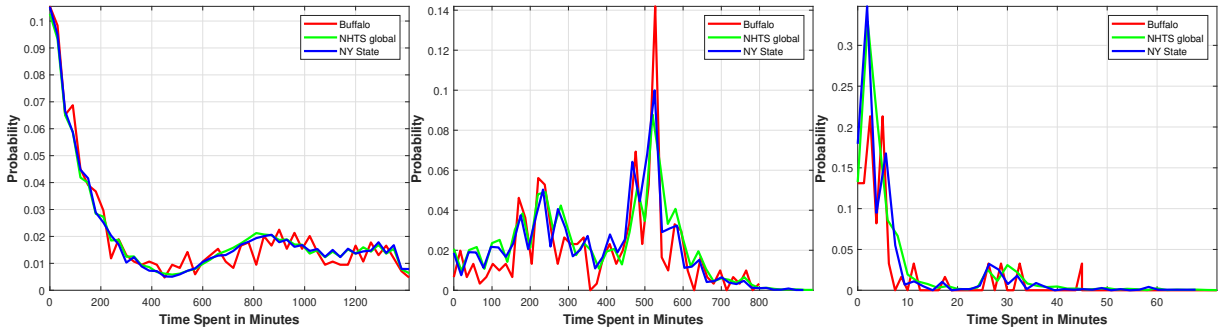

(a) Home. (b) Workplace. (c) FCS.

Figure 3.3: PDFs of PDT at home, work, and FCSs.

3.1.1.1.3 Travelled Distance (DDM) and Driving Duration (DDT)

The relevant data to the TDM and DDT variables are extracted from each considered dataset. The PDFs are then generated to cover all combinations of the six different

locations. This has generated 30 PDFs of TDM and DDT using the NHTS and NY state datasets. In the case of using the Buffalo dataset, only 20 PDFs are generated, as considering a small portion of the NHTS dataset limits the number of trips. For example, based on the Buffalo dataset, the drivers only arrive at the entertainment trip destination from either FCS or home; the other three locations (i.e, buying a meal, work, and shopping) are not linked to the entertainment destination. Only one example for the PDFs of TDM and DDT, namely from work to home, is illustrated in Fig. 3.4. It can be seen that the distance in the case of the NHTS and NY state datasets is longer than the case of Buffalo. The same is repeated for all other combinations.

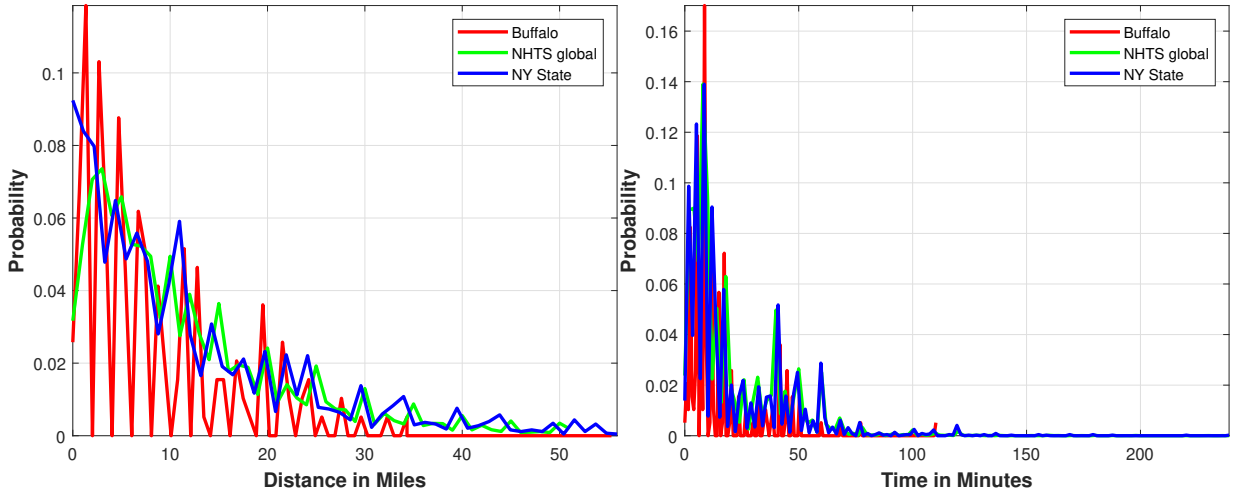

(a) TDM from work to home.

(b) DDT from work to home.

Figure 3.4: PDFs of the work to home for both TDM and DDT.

3.1.1.2 PEV Characteristics Data and Available Rated Power Infrastructure

The used charging levels (rated power) are AC charging levels of 3.7 kW and 6.6 kW for home and work, and 50 kW DC charging level in the case of FCSs. These values and charging source types are selected based on SAEJ1772 standard [72]. However, the AC to DC conversion process and models are not part of the scope of this work. For PEV manufacturing data, three PEV types are considered, representing the most popular PEVs

sold in the Canadian market from January 2011 until June 2019 [90], and as listed in Table 3.1. Sales of the Chevy Volt, Tesla Model S, and Nissan Leaf have reached 15,926, 7,463, and 7,927 vehicles, respectively, which represents more than 45% of all PEVs in the Canadian market. The vehicle corresponding data, such as BC, EDR, and specific energy, along with their adjusted MS, are also listed in Table 3.1 [91]. From the PEV data, the Tesla Model S has the largest BC and the least specific energy.

Table 3.1: PEV DATA

PEV Type	BC (kW)	EDR (mi)	Specific Energy (kWh/mi)	Market Share (%)	Adjusted Market Share (%)
Chevy Volt	16	53	0.302	23.2	50.8
Tesla Model S	100	335	0.298	10.9	23.9
Nissan Leaf	32	107	0.299	11.53	25.3

3.1.1.3 Conventional loads and solar photovoltaic (PV) models

The data pertaining to the irradiation in W/m^2 and temperature in degree Celsius are extracted from the Canadian Weather Energy and Engineering Datasets (CWEEDS) [92]. The CWEEDS includes solar irradiation and temperature data from 1998 to 2014 for different provinces in Canada. The dataset related to the city of Toronto for 2014 are selected. These sets are initially processed to exclude missing data or anomalies. The size of the data for the entire year is (364×24), representing irradiation and temperature, respectively. For conventional loads, the Reliability Test System (RTS) is used. The RTS data are given in [93] on an hourly basis as a percentage of the annual peak demand. To overcome the complexity in increasing the computation time due to incorporating the 364 profiles into the MCMC, an unsupervised machine learning approach using k-mean [94] is developed. Since all three data types (irradiation, temperature, and conventional load profiles) are co-dependent, a new group of a combined dataset is generated. The K-mean is then applied to the new dataset $(364 \times 72\ )$ and the sum of the squares error (SSE) in (3.3) is used to classify the days for each group into a single cluster.

$$\text{SSE} = \sum_{i=1}^{N} \sqrt{\sum_{p \in C_i} (d_i - p)^2} \tag{3.3}$$

where N is the maximum number of clusters, p is the data points belonging to cluster C_i, and d_i is the representative point for cluster C_i. In order to find the most suitable number of clusters representing the dataset, the described approach [95] based on the knee point of the SSE curve is implemented. Table 3.2 shows the representation of each cluster with the corresponding number of days and the probability of occurrence. The power generated

Table 3.2: Representative Profiles

Cluster number	Number of corresponding days	Probability of occurrence
1	101	0.2775
2	48	0.1319
3	61	0.1676
4	32	0.0879
5	16	0.0440
6	35	0.0962
7	47	0.1291
8	24	0.0659

from the PV array depends on the irradiation, the rating of the array, and the temperature corresponding factor, as in (3.4) [96].

$$P_{PV,array} = P_{PV,Rated} \cdot I_{rad} \cdot F_T(T) \tag{3.4}$$

where $P_{PV,Rated}$ is the array rated power in kW, I_{rad} is the solar irradiation in kW/m^2, and $F_T(T)$ is linearly interpolated for the temperature from Table 3.3. Because the output of the PV is a DC power, there must be an inverter with efficiency (η) to form the applicable AC power at the grid side. Table 3.4 shows the inverter efficiency taken from [96], which is mainly dependent on $P_{PV,PU}$, and can be computed from (3.5). Based on $P_{PV,PU}$, the efficiency can be interpolated or extrapolated from the table and the AC outpower is then estimated using (3.6).

$$P_{PV,PU} = \frac{P_{PV,array}}{P_{PV,Rated}} \tag{3.5}$$

$$P_{PV,Out} = P_{PV,array} \cdot F_{Inverter}(P_{PV,PU}) \tag{3.6}$$

Table 3.3: Temperature Factor

$T°(C)$	$F_T(T)$
0	1.2
25	1
75	0.8
100	0.6

Table 3.4: Inverter Efficiency

$P_{PV,PU}$	$F_{Inverter}(P_{PV,PU})$
0.1	0.86
0.2	0.9
0.4	0.93
1	0.97

3.1.1.4 Number of PEVs and PVs

Determining the numbers of PEVs and PVs is an important preliminary step that needs to be taken prior to developing the MCMC. For performing this task, the formula for computing the number of PEVs in terms of different parameters is given in (3.7) :

$$N_{PEV} = X_P \cdot N_h \cdot n_c \tag{3.7}$$

where N_{PEVs} is the penetration level, expressed as a percentage of PEVs with respect to the total number of vehicles, N_h is the number of houses, and n_c is the average number of vehicles per household, assumed to be 1.9, as estimated by NHTS 2009 [97]. Estimation of N_h can be performed by dividing the total system residential demand (P_r) by the average load of each house (P_h), which was estimated to be 2.08 kW by the IEEE committee in [93]. For the number of PV units, Equation (3.8) can be used where X_{PVs} is the penetration

level of PV and N_h is the number of houses. Once the number of PV units is determined, the total generated power from the PV is computed using (3.9).

$$N_{PVs} = X_{PVs} \cdot N_h \tag{3.8}$$

$$\mathrm{PV}_{Total,kW} = P_{PV,Out} \cdot N_{PVs} \tag{3.9}$$

3.1.2 Simulation Model of PEV Charging demand based SAT-approach with PV

In this work, several locations are considered, but it is assumed that home, 10% of all workplaces, and FCSs have charging facility infrastructure. The inclusion of shopping, entertainment, and buying a meal trip locations only contribute to the time when PEVs arrive at the charging facility. The proposed stochastic model framework is outlined in Fig. 3.5, and in the following detailed steps procedures:

Step 1: From Section 3.1.1: a) Read all NHTS PDFs and transform all to cumulative distribution functions (CDFs); i.e., PDTs, DDT, TDM, transition matrix, the start time of the daily trip chain ($T_{s_{ch}}$); b) Read each location's available charging level and PEV specification; i.e., BC, SE, EDR, and adjusted market share (AMS); c) Read the conventional load and PV probability of occurrence (POC); d) Read the N_{PVs}, N_{PEV}, and maximum iteration (MI).

Step 2: Start the simulation with iteration k of MCMC.

Step 3: Begin to select the PV and conventional load profiles for iteration k.

Step 4: Generate a uniform random variable between 0 and 1, interpreted as a probability.

Step 5: Equate the random variable value with the POC in order to estimate the profile cluster number of PV and conventional load at iteration k.

Step 6: Multiply the obtained profile by total system residential demand (P_r) in order to determine the daily conventional load profile. Use (3.4), (3.5), (3.6), (3.8), and (3.9) to find the daily generated PV power in kW.

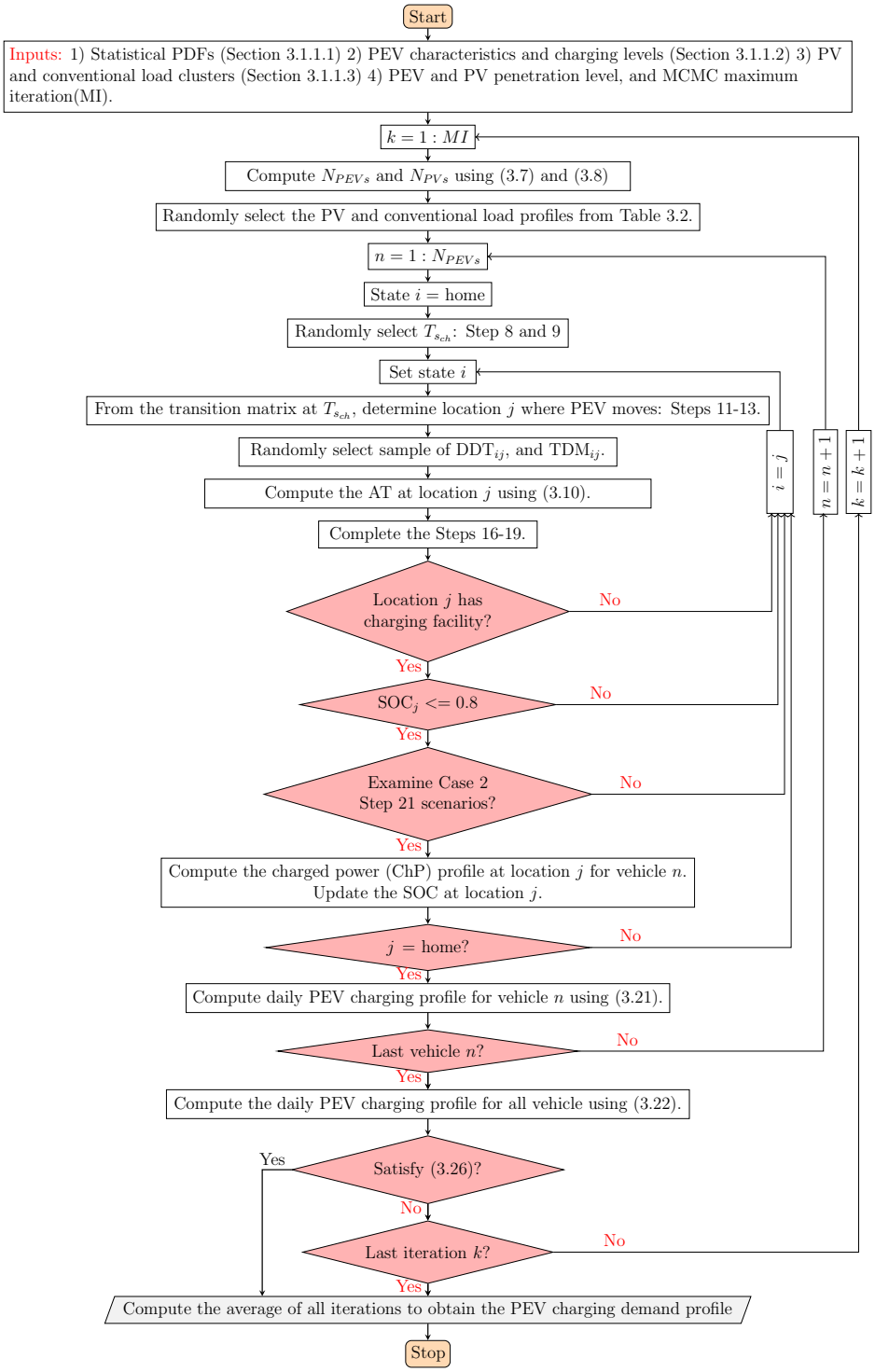

Figure 3.5: The procedures required to generate the proposed framework.

Step 7: Start to simulate the daily charging profile for the first PEV vehicle n of the total N_{PEV}. The initial SOC_i is assumed to be normally distributed with 0.7 mean and 0.1 standard deviation.

Step 8: Generate another uniform random variable between 0 and 1, interpreted as a probability.

Step 9: Equate the random variable value from Step 8 with the inverse CDF of $T_{s_{ch}}$ in order to estimate the start time of the daily trip chain.

Step 10: Set the current location.

Step 11: Go to the transition matrix at time $T_{s_{ch}}$.

Step 12: Generate another uniform random variable between 0 and 1, interpreted as a probability.

Step 13: Equate the random variable value from Step 12 with the transition matrix row corresponding to the current location i and determine the next location j.

Step 14: Take another random sample from the DDT and TDM inverse CDFs moving from i to j.

Step 15: Calculate the AT at the next location j using (3.10)

$$\text{AT}_j = T_{s_{ch}} + \text{DDT}_{ij} \tag{3.10}$$

Step 16: Calculate the CE from location i to j

$$\text{CE}_{ij} = \text{SE} \cdot \text{TDM}_{ij} \tag{3.11}$$

Step 17: Calculate the current SOC at location j

$$\text{SOC}_j = \frac{(\text{SOC}_i \cdot \text{BC}) - \text{CE}_{ij})}{\text{BC}} \tag{3.12}$$

Step 18: Calculate the ER in kWh

$$\text{ER}_j = (0.9 - \text{SOC}_j) \cdot \text{BC}) \tag{3.13}$$

Step 19: Take a random sample again, but from the PDT_j inverse CDF.

Step 20: Based on the charging level (Pch) and ER, compute the CD and the leaving destination time (LDT) for location j using (3.14) and (3.15).

$$\mathrm{CD}_j = \frac{\mathrm{ER}_j \cdot 60}{\mathrm{Pch}_j} \tag{3.14}$$

$$\mathrm{LDT}_j = \mathrm{AT}_j + \mathrm{PDT}_j \tag{3.15}$$

Step 21: Case 1: If j equals to location with no charging facility or $\mathrm{SOC}_j >= 0.8$, set the current location = location j, update $T_{s_{ch}}$ following (3.16), and go to Step 10.

$$T_{s_{ch\,i+1}} = \mathrm{LDT}_j \tag{3.16}$$

Case 2: If j equals to location with charging facility, the following scenarios are applied :

a) j = home and SOC<= 0.8: If $\mathrm{CD}_j <= \mathrm{PDT}_j$, the PEV plugs in for CD_j time, the ending charging time (ECT) is calculated using (3.17). If $\mathrm{CD}_j >= \mathrm{PDT}_j$, the PEV is charged for the PDT_j time and ECT_j is calculated based on (3.18).

$$\mathrm{ECT}_j = \mathrm{AT}_j + \mathrm{CD}_j, \mathrm{CD}_j <= \mathrm{PDT}_j \tag{3.17}$$

$$\mathrm{ECT}_j = \mathrm{LDT}_j, \mathrm{CD}_j >= \mathrm{PDT}_j \tag{3.18}$$

b) j = work: If SOC>= 0.5 and $n >= 0.1 \times N_{\mathrm{PEV}}$, go to case 1, otherwise the PEV plugs in and ECT_j is calculated following either (3.17) or (3.18).

c) j = FCS: If SOC>= 0.3, go to case 1, otherwise plug in and recharge until 60 % of the PEV BC. The ER is changed following (3.19), then the ECT_j is calculated based on (3.17) and let $\mathrm{LDT}_j = \mathrm{ECT}_j$.

$$\mathrm{ER}_j = (0.6 - \mathrm{SOC}_j) \cdot \mathrm{BC}) \tag{3.19}$$

Step 22: Vehicle n ChP_j profile at location j is based on Pch_j and computed using (3.20).

$$\mathrm{ChP}_{n,j}(T) = \mathrm{Pch}_j, T = \mathrm{AT}_j, ..., \mathrm{ECT}_j - 1 \tag{3.20}$$

Step 23: Update the SOC at j and equate it to the SOC at location $i + 1$.

Step 24: Go to Step 10 where $T_{s_{ch}} = \mathrm{LDT}_j$ if j is not at home.

Step 25: If j is at home, calculate the daily PEV charging profile (PEV profile) for vehicle n by making a summation of charging activities occurring at all locations during the day.

$$\text{PEV profile}_n \;=\; \sum_j \mathrm{ChP}_{n,j}(T), T \;=\; T_{s_{ch}}, \cdots\cdots\cdots\cdots \mathrm{LDT}_j, \forall j \tag{3.21}$$

where $T_{s_{ch}}$ is the same value obtained from Step 9. If $n <= N_{PEV}$, go to Step 7, otherwise continue to Step 26.

Step 26: Compute the daily total charging profile (TCP) at iteration k by following (3.22).

$$\mathrm{TCP}_k = \sum_{n=1}^{N_{PEV}} \text{PEV profile}_n \tag{3.22}$$

Step 27: The convergence stopping criteria is based on the change in the moving average (MA) of the cumulative sum (CS) of the TCP. If $k > 1$, compute the CS of the TCP for iteration k using (3.23), otherwise $\mathrm{CS}_k = \mathrm{TCP}_k$

$$\mathrm{CS}_k = \sum_{k=1}^{k} \mathrm{TCP}_k \tag{3.23}$$

The MA is then calculated, as stated in (3.24).

$$\mathrm{MA}_k = \mathrm{CS}_k / k \tag{3.24}$$

The stopping criteria (SC) of the MCMC is determined based on the difference

between the MA for iteration k and $k-1$, as stated in (3.25).

$$Deviation_k = \mathrm{MA}_k - \mathrm{MA}_{k-1} \tag{3.25}$$

$$Deviation_k <= 1 \times 10^{-}5 \tag{3.26}$$

Step 28: If $k <$ MI, check (3.26). If it is not satisfied, go to Step 2. If $k >=$ MI or the condition in (3.26) is satisfied, terminate the simulation and report PEV profiles.

3.1.3 Analysis and Results

The effects of three PEV penetration levels (i.e., 0%, 30%, and 50%), three PV penetration levels (i.e., 0%, 30%, and 50%), and three different dataests (i.e., Buffalo, NHTS global, and NY state) are investigated in this work. The impact of PEV battery specification on charging profiles at work, FCS, and home is also studied. The IEEE 123 node distribution system primary feeder [98] is used as a benchmark system in this work. It is assumed that all system demand, 3490 kW, is residential. The number of houses (N_h) is determined by dividing 3490 kW by the average load of each house (P_h) and then estimating the N_{PEVs} and N_{PVs} using (3.7) and (3.8).

3.1.3.1 The Impact of PEV Battery Specification on Charging Activities

Since Tesla S has the largest BC among the top three PEV vehicles sold in Canada, its impact versus the PEV market share is studied. Fig. 3.6(a) and 3.6(b) show samples of the impact of home, work, and FCS charging facilities on overall daily PEV charging activities. The results are generated based on 50% PEV penetration level. It can be observed from Fig. 3.6(a) that charging at work is concentrated during the interval between 7 A.M. and 3 P.M. while, at home, the charging starts at 7 P.M. when the drivers return home, and starts decreasing early in the morning. The peak for the overall PEV charging demand occurs at home at midnight, while the FCSs and work peak demand represent 19% and 16%, respectively, of total peak demand. Charging at the FCSs happens when the remaining

energy in the battery has reached low (30% or below). When there is not enough energy to reach home, drivers visit the FCSs to recharge their batteries. Based on the Tesla S model, as depicted in Fig. 3.6(a), it can be noticed that only a small group of drivers need to recharge their vehicles at the FCSs when they leave work to go home. This is due to the very large BC used in the case of the Tesla model S, 100 kWh, that can support long distances without the need to visit an FCS. In contrast, more drivers recharge their vehicles at the FCS when the PEV market share is considered, as shown in Fig. 3.6(b). The figure shows a considerable number of drivers visit the FCS while leaving work, returning home or going to work in the morning. As stated in Table 3.1, if the PEV market share is considered, there will be a diversity in the battery. The BC of the Chevy Volt and the Nissan Leaf is 16 kWh and 32 kWh, respectively, which is very low compared to the Tesla S. The time when PEV charging takes place at each location is repeated again in Fig. 3.6(b), which confirms the same observation that was noted in Fig. 3.6(a).

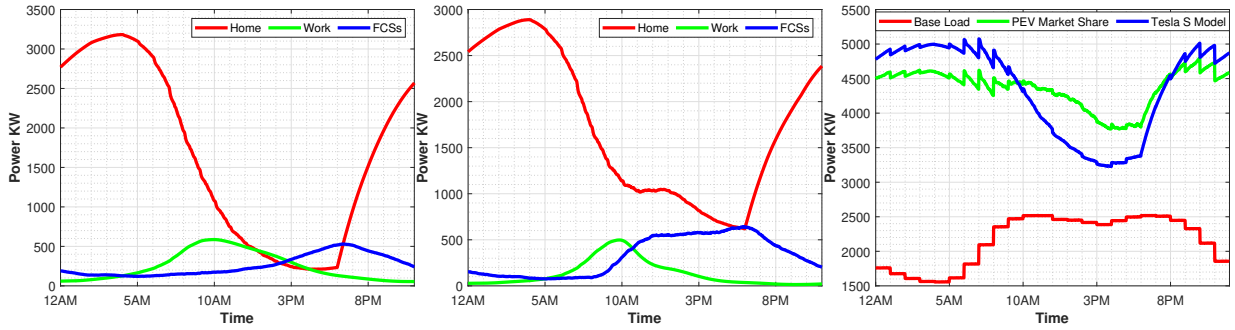

(a) Impact of Tesla S model. (b) Impact of PEV market share. (c) PEV market share versus the Tesla S on total demand.

Figure 3.6: Impact of PEV battery specification on overall PEV charging activities.

The impact of the PEV market share versus the Tesla S on the total demand of PEV charging is illustrated in Fig. 3.6(c). It is noticed that considering the PEV market share provides more contribution to the base load during the interval between 10 A.M. and 6 P.M. compared to the Tesla S. When the PEV market share is considered, some vehicles with a low BC were not able to complete the trip and needed to visit the FCS during the day to recharge their batteries before completing the remainder of the trip. It can also be observed from Fig. 3.6(c) that the total energy required by charging the Tesla S is $3,143.5$

MWh compared to 3,166 MWh when considering market share data. In this scenario, when the BCs are diversified, the charging activities at the FCS are increased. Due to the high rated power at the FCS, assumed to be 50 kW, there was no significant reduction in the total energy required.

3.1.4 The Impact of Different PV and PEV Penetration Levels on the Base Load

The impact of charging PEVs with different penetration levels is presented in Fig. 3.7(a). It can be noticed from the figure that there is a significant increase on the load profile. Compared with 0% PEV, the load at 10 P.M. was significantly increased by almost double in the case of 50% PEV penetration level and increased by 70% in the case of 30% PEV penetration level. It can also be observed that, although the conventional load in the interval between 10 A.M. and 3 P.M. was very high, the effect on demand when PEV is added was not significant. This is due to the effect of charging at workplaces and FCS compared to home.

When PV integration into the system is considered, as shown in Fig. 3.7(b), the load profile becomes a combination of conventional and PEV loads, as well as PV generation. It can be noticed from Fig. 3.7(b) that there was a reduction in the total load profile, especially during the daytime when there is a high amount of solar irradiation. The increase in PEV charging, as seen in Fig. 3.7(b), has been decreased to small values, less than the conventional load, during the interval from 10 A.M. to 5 P.M. Charging with 50% penetration level of PEV, and having 30% PV penetration level, can reduce the demand at 1 P.M. by almost 65%. However, the loading conditions during the night and early morning are not eliminated. For 50% penetration level of PV, there will be extra generated power of 800 kW at 1 PM, while the 30% penetration level is only capable of reducing the total demand without injecting any extra power. It has been observed from Fig. 3.7(b) that the load becomes highly negative at that instance. This is because the widespread usage of the rooftop PV that generates an excessive amount of power.

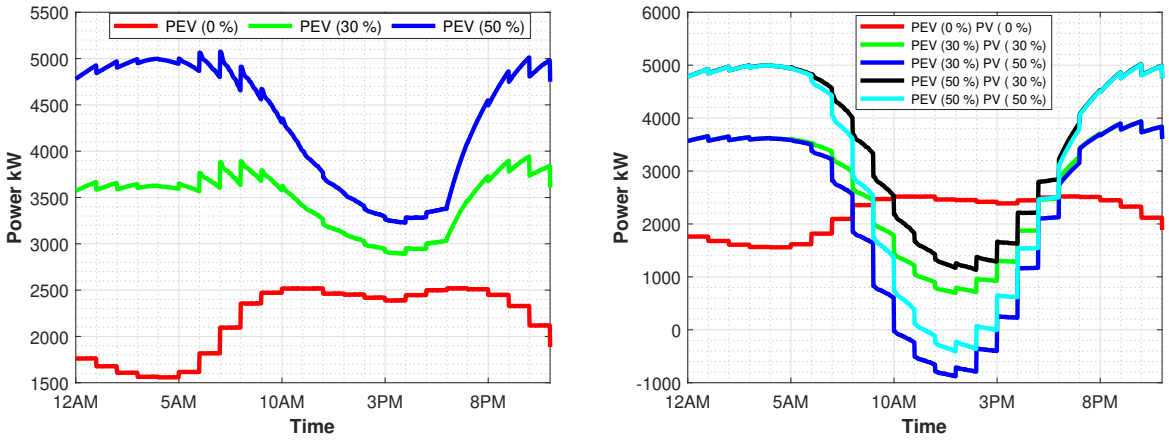

(a) Different PEV penetration levels. (b) Different PEV and PV penetration levels .

Figure 3.7: Impact of PEV and PV different penetration levels on the base load using Tesla S model.

3.1.5 The Impact of Using Different Partitions of NHTS Data on the PEV Charging Demand

The impact of using the Buffalo and NY state datasets versus the NHTS global data on PEV charging demand is illustrated in Fig. 4.3. It is noted that the pattern of charging activities is the same but, in the case of the Buffalo dataset, there is a significant reduction in the charging energy between 5 A.M. and 6 P.M. compared to the NHTS global or NY State datasets. When the Buffalo dataset is used, the distance miles and driving duration are less compared to when a large scale of data is considered. Due to the short TDM in the case of the Buffalo dataset, the majority of PEV drivers did not need to recharge their batteries during the day (5 A.M. - 6 P.M.), especially when returning from work to home after 3 PM. It can be noticed from Fig. 4.3 that the drivers prefer to wait until they arrive home before recharging their vehicles. This explains why the demand increased in the case of the Buffalo dataset between midnight and 5 A.M..

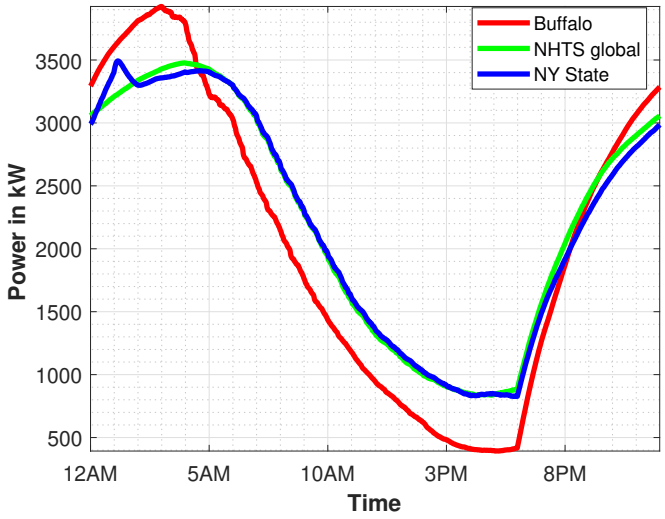

Figure 3.8: Impact of different datasets on the total PEV charging load profile using the Tesla S with 50% penetration level..

3.1.6 The Impact of PEV Charging Loads on the Main Substation

To investigate the impact of additional PEV loads on the main substation, a PF analysis is performed. The IEEE 123 primary feeder, that includes single and three-phase loads ,is used. The three-phase load nodes (47, 48, 49, and 65) are modeled for the vehicles recharged at the FCS, the single-phase load nodes (64, and 66) for work, and all other single-phase load nodes assigned for homes. From the spot load at each node, the number of PEVs is calculated following (3.7), as discussed in Section 3.1.1.4. Fig. 3.9(a) shows the impact of PEV charging on the main substation, where it can be noticed that the substation transformer is overloaded when 50% PEV penetration level is considered, while in the cases of 20% and 30% penetration levels there is no overload. The transformer lasts 14 hours under overload conditions and it can be inferred that charging PEVs at home is the main factor contributing to this overload. Even though the conventional load profile at midnight and early morning is not considered high, PEV charging under 50% penetration level can cause overloading to the transformer.

In the case of using different datasets, it can be noted from Fig. 3.9(b) that using the Buffalo dataset overloads the transformer by 133% at 3 AM, while both the NY State and NHTS global overload the transformer by 127% and 124% , respectively, at 1 AM.

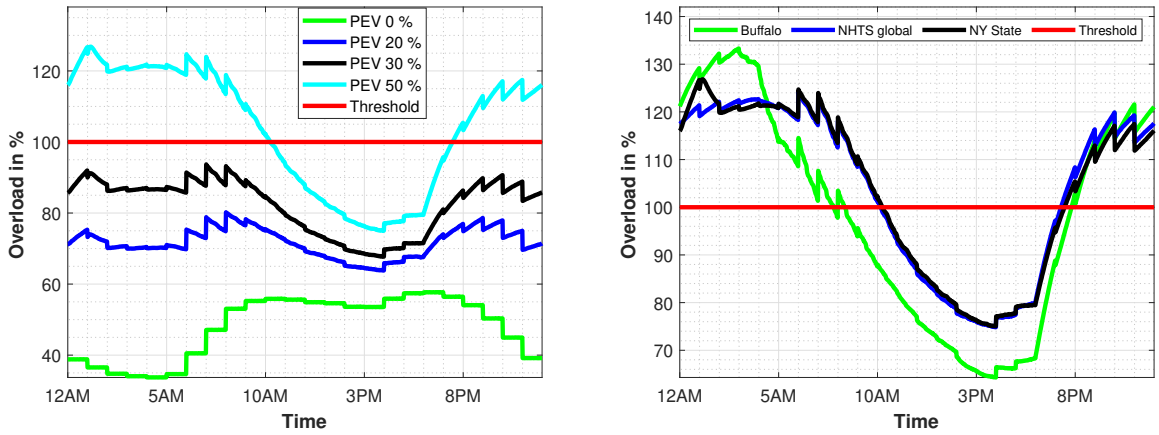

(a) Impact of different PEV penetration levels. (b) Impact of different NHTS datasets at 50% PEV.

Figure 3.9: Impact on the main substation loading % using Tesla S model.

3.1.7 MCMC Convergence and Accuracy

MCMC approaches estimate the load profile of PEV charging demand using simulations of the actual process. A few samples (iterations) are always desirable, but the accuracy of the estimation cannot be guaranteed. In contrast, the accuracy is increased by increasing the number of samples, but the computational time definitely increases. Thus, the MCMC is generally associated with convergence stopping criteria that identify the required number of iterations to ensure a high level of confidence. The termination of the MCMC mainly relies on the moving average, which is the average of the cumulative sum as discussed in (3.22)-(3.25) of Section 3.1.2. The maximum number of iterations was set at 3,000. For each trial, the average of the cumulative sum of the total demand is computed and compared with the previous. If there is no major change, the MCMC is terminated. As depicted in Fig. 3.10(b), at 30% PEV with 0% PV around the 1,000 trial mark, the

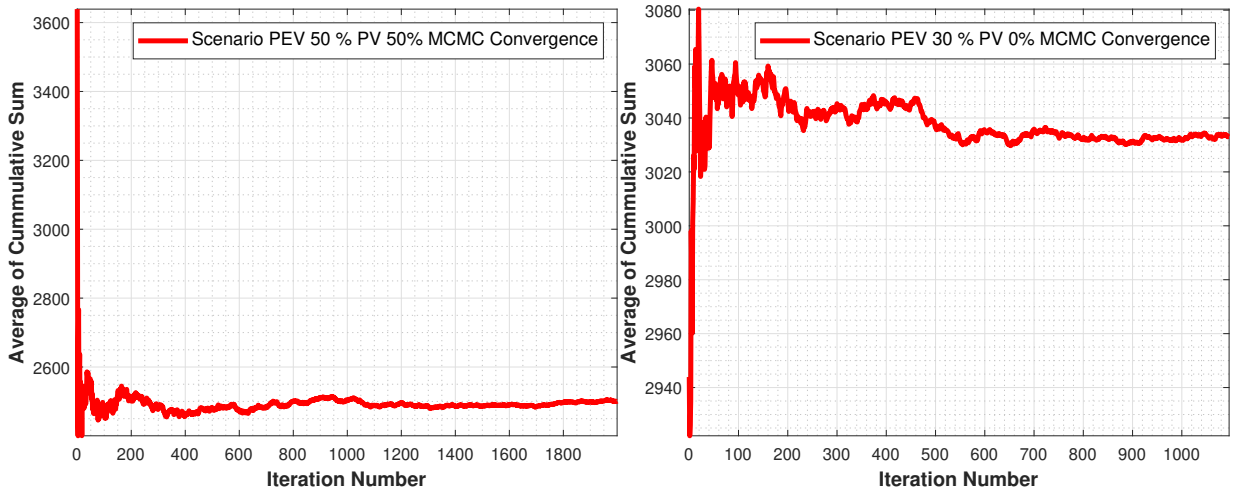

Figure 3.10: MCMC convergence for different scenarios.

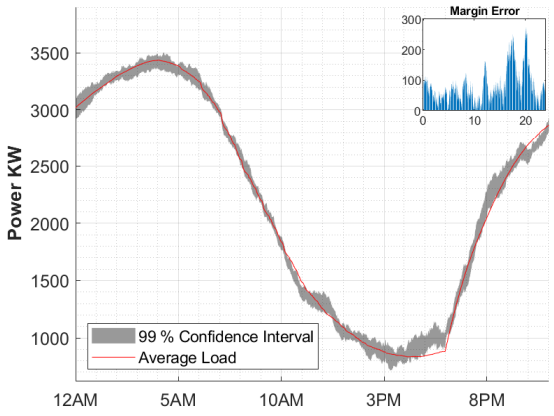

(a) Small sample of iterations.

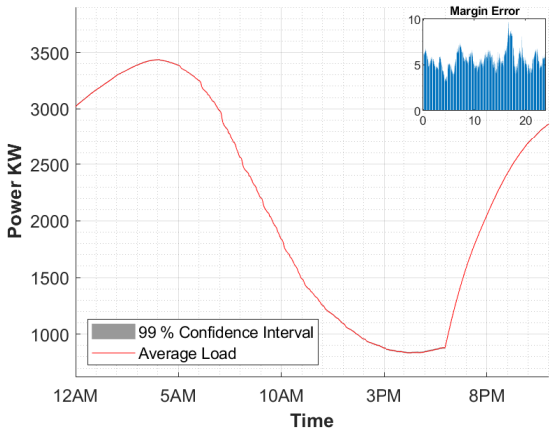

(b) PEV charging average demand for $2,000$ iterations compared with the measured 99% confidence interval for $1,800$ iterations.

Figure 3.11: Average PEV charging demand and their 99% confidence interval: 50% PEV and 50% PV scenario.

average is not subjected to any change, while in the case of 50% PEV with 50% PV, the convergence is only satisfied after 1,800 iterations. The accuracy of the MCMC proposed model is assessed using 99% confidence interval, from Fig. 3.11(a) and Fig. 3.11(b), it can be observed that using a small sample of iteration leads to a high margin error compared to the case of $1,800$ iterations. When the simulation was converged at iteration 1,800 as depicted in Fig. 3.10(a), the average of the demand of higher iterations (e.g., 2,000 iterations) is still within the 99% confidence intervals, as shown in Fig. 3.11(b).

3.2 Summary

In this chapter, a comprehensive statistical analysis is developed considering different datasets (i.e., NHTS global, NY State, and city of Buffalo data) based on an updated version of NHTS. The aim is to study the behavior of PEV SAT characteristics and evaluate their effect on the conventional load when PVs are included. The MCMC in conjunction with a trip chain methodology is used to probabilistically estimate the uncertainty with a PEV charging load profile (e.g, home, work, and FCSs), conventional loads, and PV generation. Charging levels of 3.7, 6.6, and 50 kW are used as available sources of power at home, work, and FCSs, respectively. The impact of the location of each charging facility on the time taken to recharge is studied while considering different PEV battery specifications. The results reveal that the majority of charging activities take place at home, followed by at FCSs and work. Drivers tend to visit the FCSs when they leave work by 3 PM and when the remaining energy of the battery does not support the remaining daily activities. With respect to PEV battery specification, it is observed that the diversity of batteries leads to an increase in the number of vehicles being charged at the FCSs. Different penetration levels of PVs and PEVs are studied and the results show that 50% PEV penetration level doubles the demand, while 30% PEV penetration level increases the demand by only 75%. In contrast, the 30% PV penetration level would reduce demand during the interval between 10 AM and 5 PM, while the 50% penetration level contributes to extra power during the day time. However, the profile of the home charging load during the night and early morning is still not eliminated. Using different datasets shows that the impact of NHTS global data and NY state datasets provides a

similar pattern, while there is a considerable difference in the case of using the Buffalo dataset. At the main substation level, the results show that only 50% PEV penetration level causes overloading to the substation transformer and lasts for almost 14 hours, while there is no overloading in the case of both 20% and 30% PEV penetration levels.

Chapter 4

Impact on Voltage Quality and Transformer Aging of Residential Prosumer Ownership of Plug-in Electric Vehicles: Assessment and Solutions [1]

Chapter 3 discussed the detailed proposed framework for modeling the SAT characteristics of PEV driver behavior and PV uncertainty. This chapter, on the other hand, provides a comprehensive assessment for the EDS assets (i.e., DT overload and aging, VI, and under and over voltage) when SAT models with PV are integrated. Thereafter, a control strategy using different generations of HBES in conjunction with PV generation is also proposed as a solution to alleviate the DT overload that results from charging PEVs using a SAT-based approach.

[1] This chapter has been accepted for publication in:
Y. O. Assolami, A. Gaouda and R. El-shatshat, "Impact on Voltage Quality and Transformer Aging of Residential Prosumer Ownership of Plug-in Electric Vehicles: Assessment and Solutions," *IEEE Transactions on Transportation Electrification*, (available in IEEE Xplore Early Access).

4.1 Proposed Assessment and Enhancement Framework: Methodology and Components models

Fig. 4.1 presents a layout of the proposed framework that provides an evaluation and solution for DT aging and voltage quality considering the integration of SAT models with residential prosumer ownership of PEV. The framework comprises four main stages. Stage 1 is an essential preliminary step for preparing the required input data to the proposed framework, the uncertainty of PEV and conventional load and PV generation is modelled correctly, and all needed information of EDS elements are collected. For PEV, the NHTS survey datasets are used to construct the PDFs of the required parameters (i.e., $T_{s_{ch}}$, PDT, TDM, DDT, and transition matrix) in the proposed-SAT model (discussed in Section 3.1.1.1). For treating the uncertainty of PV generation and conventional load, an unsupervised machine learning approach using k-mean is developed to the yearly data to obtain the representative clusters with a certain probability (discussed in Section 3.1.1.3). Theses representative clusters with the PDFs of SAT model and EDS information are used as inputs to Stage-II. In Stage II, the obtained PDFs of SAT parameters and probability of clusters are used to generate random samples of PEV profiles, PV generation, and conventional loads, which are employed to develop a probabilistic PF based on MCMC. The convergence of Stage-II is determined based on the change of the moving average of the cumulative sum of the DT apparent power at each sample [99]. When such convergence is achieved, the average of PF results is computed. These averaged values obtained from Stage-II are used in Stage-III to calculate DT overload and aging, VI, and under and over voltage. In the final stage, a control strategy utilizing the HBES is developed to avoid DT overload (discussed in Section 4.1.2). The locations and measured apparent power of DTs that reported an overload from Stage-III are used as input in this stage. At each overloaded DT, the connected HBES units to that particular DT are determined, and the profile of individual HBES is generated. Having the HBES profiles distributed over the EDS network, a deterministic PF is performed. Hence, the evaluation in Stage-III is repeated to see the

added value of implementing the HBES control strategy.

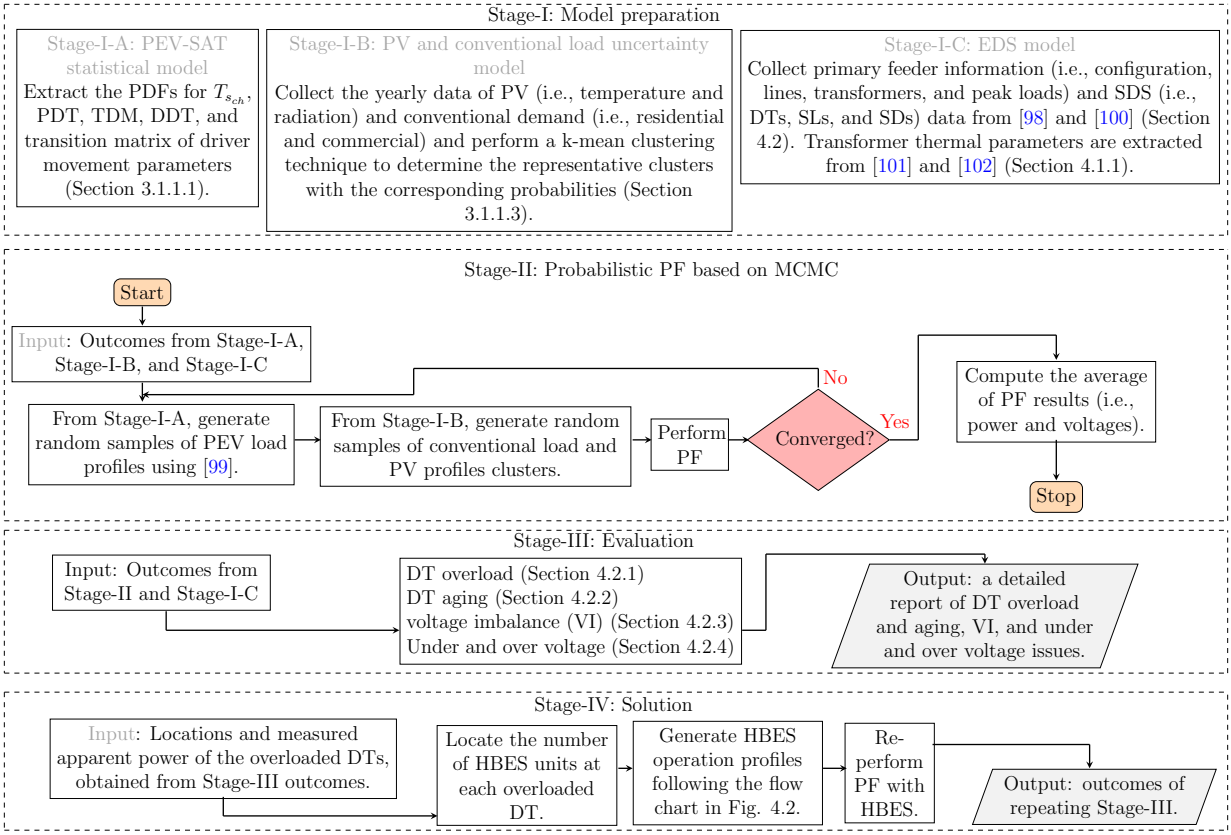

Figure 4.1: Flow chart of the proposed framework.

4.1.1 Transformer Aging Estimation

The transformer lifetime is estimated based on IEEE C57.91-2011 [4]. The mineral-oil-immersed transformer types were considered in the standard as they are more commonly used in Europe and middle east regions. Since this thesis focuses on estimating the aging of DTs and their types in North America are either pole-mount or pad-mount transformers, the standard only was used to obtain the mathematical models and required procedures to compute the transformer loss of life ($LOL\%$) per day. The typical thermal parameters in

calculating the LOL for 25 kVA, 50 kVA, and 75 kVA DTs are taken from [101] and [102] in order to incorporate the actual effect of these transformers with equations mentioned in the standard.

As identified in the standard, the main factor contributing to transformer insulation degradation is transformer winding hottest-spot temperature (θ_H), computed using (4.1). The components making the θ_H are ambient temperature (θ_A), the top-oil rise over ambient temperature ($\Delta\theta_{TO}$), and the winding hottest-spot rise over top-oil temperature ($\Delta\theta_H$).

$$\theta_H = \Delta\theta_{TO} + \Delta\theta_H + \theta_A \tag{4.1}$$

The $\Delta\theta_{TO}$ is computed using (4.2) and depends on the ultimate top-oil rise over ambient temperature ($\Delta\theta_{TO,U}$), the initial top-oil rise over ambient temperature ($\Delta\theta_{TO,i}$), and the oil thermal constant for rated load ($\tau_{TO,R}$).

$$\Delta\theta_{TO} = (\Delta\theta_{TO,U} - \Delta\theta_{TO,i})[1 - e^{-t/_{TO,R}}] + \Delta\theta_{TO,i} \tag{4.2}$$

The $\Delta\theta_{TO,U}$ and $\Delta\theta_{TO,i}$ are computed using the top-oil rise over ambient temperature at rated load ($\Delta\theta_{TO,R}$) following (4.3) and (4.4).

$$\Delta\theta_{TO,U} = \Delta\theta_{TO,R}\left[\frac{K_U^2 R + 1}{(R+1)}\right]^n \tag{4.3}$$

$$\Delta\theta_{TO,i} = \Delta\theta_{TO,R}\left[\frac{K_i^2 R + 1}{(R+1)}\right]^n \tag{4.4}$$

where R is the ratio of load loss at rated load to no-load loss, n is the exponent of loss function vs. top-oil rise, K_U is the ratio of ultimate load to rated load in per-unit, and K_i is the ratio of initial load to rated load in per-unit. For calculating the $\Delta\theta_H$, the ultimate winding hottest-spot rise over top-oil temperature ($\Delta\theta_{H,U}$), the initial winding hottest-spot rise over top-oil temperature ($\Delta\theta_{H,i}$), and the winding time constant at hottest-spot location (τ_w) are used as explained in (4.5). Using the hottest-spot conductor rise over top-oil temperature, at rated load ($\Delta\theta_{H,RS}$), the $\Delta\theta_{H,U}$ and $\Delta\theta_{H,i}$ can be computed using

(4.6) and (4.7) where m is the exponent of load squared vs. winding gradient.

$$\Delta\theta_H = (\Delta\theta_{H,U} - \Delta\theta_{H,i})[1 - e^{-t/w}] + \Delta\theta_{H,i} \tag{4.5}$$

$$\Delta\theta_{H,U} = \Delta\theta_{H,RS}.K_U^{2.m} \tag{4.6}$$

$$\Delta\theta_{H,i} = \Delta\theta_{H,RS}.K_i^{2.m} \tag{4.7}$$

When the θ_H is calculated using (4.1), the transformer aging acceleration factor (F_{AA}) can be computed based on (4.8). The F_{AA} is then aggregated over all time steps Δt_j to find the equivalent accelerated aging factor (F_{EQA}) as explained in (4.9).

$$F_{AA} = e^{\left[\frac{15000}{110+273} - \frac{15000}{\theta_H+273}\right]} \tag{4.8}$$

$$F_{EQA} = \frac{\sum_{j=1}^{J} F_{AA,j}.\Delta t_j}{\sum_{j=1}^{J} \Delta t_j}, j = 1, 2, ...J \tag{4.9}$$

where J is the total time period considered and Δt_j is the time interval. The transformer normal insulation life in years ($TNIL_y$) is assumed to be 20.5 years, as reported in [4], and used to calculate the transformer lifetime in years (TLT_y) following (4.10) [103]. For transformer LOL per day considering a 1-minute resolution, Equation (4.11) can be used, where T is 1440 and transformer normal insulation life in minutes ($TNIL_m$) is $10,800,000$. $TNIL_m$ was converted to minutes from the transformer normal insulation life in hours ($180,000$), as reported in [4].

$$TLT_y = \frac{\sum_{j=1}^{J} F_{AA,j}.\Delta t_j}{TNIL, y} \tag{4.10}$$

$$LOL_d\% = \frac{F_{EQA} \cdot T \cdot 100}{TNIL_m} \tag{4.11}$$

Equation (4.11) can be simply multiplied by 365 in order to find the transformer LOL on a yearly basis (LOL_y), as explained in (4.12). The typical necessary parameters in calculating the LOL for considered transformers are given in Table 4.1 according to [101] and [102]. As reported in the standard, 0.0131% and 5% are the normal values limits for

Table 4.1: Transformer Thermal Parameters.

Parameters	25 kVA transformer value	50/75 kVA transformer value	5,000 kVA substation transformer value
$\Delta\theta_{H,RS}$	20.3C	27C	35C
$\Delta\theta_{TO,R}$	38.8C	53C	55C
θ_A	30C	30C	30C
R	5.65	4.87	3.20
$\tau_{TO,R}$	150 minutes	411.6 minutes	180 minutes
τ_w	4.8 minutes	4.8 minutes	4.8 minutes
n	0.8	0.8	0.8
m	0.8	0.8	0.8

$LOL_d\%$ and $LOL_y\%$, respectively. For calculating transformer LOL in years ($TLOL_y$) , Equation (4.13) can be used with respect to TLT_y and $TNIL_y$. Equation (4.14) is used to compute total transformer LOL in years ($TTLOL_y$) when there is a group of transformers in the system under study.

$$LOL_y\% = LOL_d\% \cdot 365 \tag{4.12}$$

$$TLOL_y = TNIL_y - TLT_y \tag{4.13}$$

$$TTLOL_y = \sum_{DTN=1}^{TT} TLOL_{y,DTN}, DTN = 1, 2, ..TT \tag{4.14}$$

where TT denotes the total number of transformers and DTN is the transformer number.

4.1.2 Energy Storage System

An ESS has three modes of operation: charging, discharging, and idle. The energy storage element acts as a load in the case of charging, as a generator in the case of discharging, and does not supply or absorb any power in the case of idle mode. Different ESS sizes and

technology have recently been developed in order to add benefits and improvements to a future EDS grid [8]. For the scope of this chapter, three different types of HBES, in terms of generation and battery capacity and power, are considered, as shown in Table 4.2 [6].

Table 4.2: HBES manufacture data

Make/Model	Generation	Battery capacity (kWh)	Power (kW)
Tesla/Powerwall 2	Second	13.5	5
Tesla/Powerwall 1	First	7	2
LG/RESU6.5	First	6.5	2.2

The ESS operation mathematical formulations are taken from [104], and explained in the following equations:

$$-P_B^R \leq P_{B_t} \leq P_B^R \tag{4.15}$$

where P_B^R is the ESS rated power in kW and P_{B_t} is the supplied or consumed power by the ESS at time t of day. The SOC of the HBES, which represents the remaining energy at time t, is computed using (4.16) considering the storage efficiency (η_{HBES}) . The P_{B_t} is either a negative $P_{B_{Charg,t}}$ when an HBES is charged, a positive $P_{B_{Disch,t}}$ at discharging mode, or zero at idling mode. Equation (4.17) is used to set the $\text{SOC}_t^{\text{HBES}}$ limits where $\text{SOC}_{t,min}^{\text{HBES}}$ denotes the minimum energy reserve in the battery and $\text{SOC}_{t,max}^{\text{HBES}}$ denotes the maximum BC of the HBES.

$$\text{SOC}_t^{\text{HBES}} = \text{SOC}_{t-1}^{\text{HBES}} - (P_{B_{Charg,t}} \cdot \Delta t \cdot \eta_{\text{HBES}}) + (\frac{P_{B_{Disch,t}}}{\eta_{\text{HBES}}} \cdot \Delta t) \tag{4.16}$$

$$\text{SOC}_{min}^{\text{HBES}} \leq \text{SOC}_t^{\text{HBES}} \leq \text{SOC}_{max}^{\text{HBES}} \tag{4.17}$$

To ensure that the initial ESS energy stored is always fixed at any given day, Equation (4.18) is used to equate the HBES initial energy stored ($\text{SOC}_{ini}^{\text{HBES}}$) to the energy stored at the last time of day ($\text{SOC}_T^{\text{HBES}}$).

$$\text{SOC}_0^{\text{HBES}} = \text{SOC}_{ini}^{\text{HBES}} = \text{SOC}_T^{\text{HBES}} \tag{4.18}$$

$$DEF = P_{DTk,t} - \text{DT}_{k,rating} \tag{4.19}$$

In this work, a controlled strategy for HBES units at residential premises is proposed. It is assumed that customers have been engaged in mutual agreement with the utility company via an incentive program. The financial payout to customers participating in this program is out of the scope of this study and will not be discussed in this paper. With respect to ESS operation models (4.15) to (4.18), the proposed control strategy of HBES is utilized with emphasis on the DT overloading condition. It is proposed that HBES is discharged when DT power loading is higher than its rating, and charged when PV is available and DT loading is less than DT rating. The HBES profile models are outlined in Fig. 4.2 and in the following step-wise procedures:

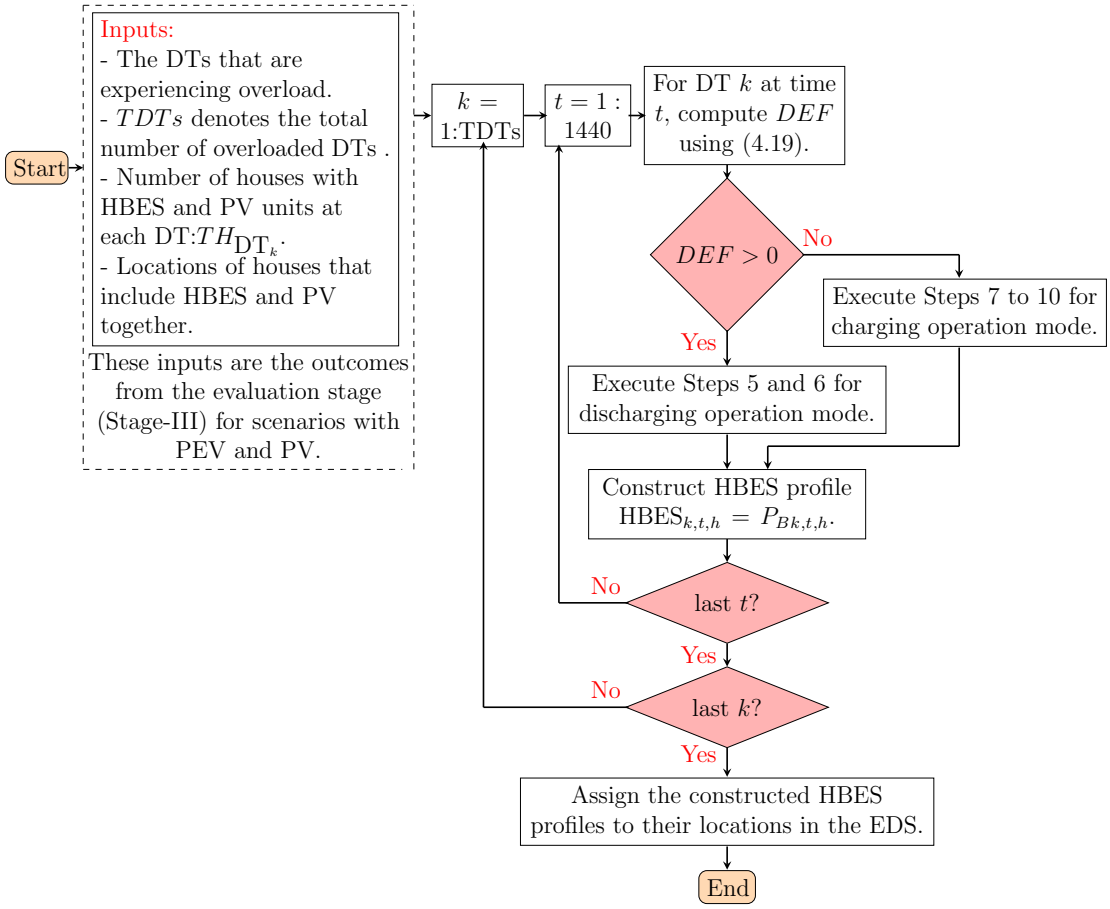

Figure 4.2: Flow chart of proposed HBES control strategy.

Step 1: Read only the DTs data that reported an overload from Stage-III outcomes (i.e., number of DTs ($TDTs$), DTs apparent power (P_{DT^k}), number of houses with HBES-PV at each DT (TH_{DT^k}) and their locations, and PV profiles at each house).

Step 2: Start the simulation with the first overloaded transformer, denotes as DT_k, over the day. The process starts with $t = 1$ and ends at $t = 1440$.

Step 3: Begin to generate charging/discharging power for HBES units that are connected to DT_k at t.

Step 4: Use (4.19) to compute the difference between P_{DT} and rating for DT_k at t. If the difference ($DEF_{k,t}$) is less than 0, go to Step 7, otherwise continue to Step 5.

Step 5: Compute the required discharging power ($P_{BDisch,k,t}$) that is needed to alleviate the resulted overload for DT_k at t. $P_{BDisch,k,t}$ is determined by dividing the $DEF_{k,t}$ by the number of connected houses with HBES-PV at DT_k (TH_{DT^k}). To ensure the HBES charging/discharging power with acceptable limits, substitute P_{Bt} by $P_{BDisch,k,t}$ and check the condition in (4.15). If this condition is satisfied, then make the variable P_{Bt} equal to $P_{BDisch,k,t}$ and continue to the next step. Otherwise, P_{Bt} must equal to P_B^R and continue to the next step as well.

Step 6: Begin to assign P_{Bt} value for discharging each HBES that belongs to house h in TH_{DT^k} group. First, calculate the SOC of each HBES using (4.16) and check constraint (4.17). If the condition in (4.17) is satisfied, make $P_{B,k,,t,h}$ equals to P_{Bt}; otherwise, $P_{B,k,,t,h}$ must equal 0. Then, continue to Step 11.

Step 7: Compute the charging power (P_{BCharg}) by dividing the $DEF_{k,t}$ by TH_{DT^k} which guarantees that charging HBES units will not overload the connected DT_k. Replace P_{Bt} by P_{BCharg} and go to (4.15) and check for the limits. If this condition is satisfied, make P_{Bt} equals to P_{BCharg}; otherwise, P_{B_t} has to equal $-P_B^R$. When P_{Bt} is finalized, move to the next step.

Step 8: Begin to assign P_{B_t} value for charging each HBES that belongs to house h in TH_{DT_k} group. Check the PV profile for each house h connected to DT_k at time

t. If PV output power is greater than zero, continue to the next step; otherwise, make $P_{B_{k,t,h}}$ equals 0 and go to Step 11.

Step 9: Compare the obtained PV power from Step 8 with the absolute value of P_{B_t}. If PV >= $|P_{B_t}|$, go to Step 10; otherwise, P_{B_t} must equal to the negative value of PV power and then continue to Step 10.

Step 10: Calculate the SOC using (4.16) and check the constraint in (4.17). If this constraint is not satisfied, make $P_{B_{k,,t,h}}$ equals 0; otherwise, $P_{B_{k,t,h}} = P_{B_t}$. After either case 1 or 2, continue to the next step.

Step 11: Construct the energy profile for each HBES using (4.20).

$$\text{HBES}_{k,t,h} = P_{Bk,t,h} \tag{4.20}$$

where k is the DT number, t denotes the time of the day, and h is the house number where HBES unit is connected. If t does not reach the end, go back to Step 3 and select another time; otherwise go to Step 2 to start with new k of DTs. When k reaches the $TDTs$ and t reaches the end, simulating the HBES profiles will stop and all their corresponding profiles are distributed over their locations in the EDS networks.

4.1.3 Voltage Imbalance Evaluation

Due to the single-phase loads or generators in the EDS, some buses may experience VI, which is evaluated using either the deviation in voltage between the three phases or voltage symmetrical components. In this work, the line-to-neutral voltage deviation index is used and explained in (4.20) and (4.21).

$$\%\text{VI}_{L-N,i,t} = \frac{max[V - \text{VI}_{L-N,AVG,i,t}]}{\text{VI}_{L-N,AVG,i,t}} \cdot 100 \tag{4.21}$$

$$\text{VI}_{L-N,AVG,i,t} = \frac{|V_{A-N,i,t}| + |V_{B-N,i,t}| + |V_{C-N,i,t}|}{m} \tag{4.22}$$

where $\text{VI}_{L-N,AVG}$ is the line-to-neutral average voltage, i is the bus at which the voltage is evaluated, t denotes the time of day, and m is the number of phases at buses. The

V_{A-N}, V_{B-N}, and V_{C-N} are the line-to-neutral voltage magnitude of phases a, b, and c, respectively. The American National Standard Institute (ANSI) C84.1 [105] standard recommends that the $\%\text{VI}_{L-Ni,t}$ does not exceed 3%.

4.2 Analysis and Results

The impact of different PEV and PV penetration levels, along with different generations of HBES on DT overload and aging, VI, and under and over voltage, is quantified in this work. The different scenarios and case studies are constructed based on the change in various elements, as shown in Table 4.3. The scenarios consider different PEV and PV penetration levels, HBES type, PEV drivers' model, and data representative clusters. Scenario 1 is

Table 4.3: Studied Scenarios.

<table>
<tr><th rowspan="2">Scenarios</th><th colspan="2">Penetration levels</th><th rowspan="2">HBES make/model</th><th rowspan="2">PEV driver behavior model</th><th rowspan="2">PV and load representative clusters</th></tr>
<tr><th>PEVs</th><th>PVs</th></tr>
<tr><td>1</td><td>0</td><td rowspan="5">0</td><td rowspan="9">-</td><td>-</td><td rowspan="16">All</td></tr>
<tr><td>2</td><td>60</td><td rowspan="3">Proposed SAT approach</td></tr>
<tr><td>3</td><td>70</td></tr>
<tr><td>4</td><td rowspan="2">80</td></tr>
<tr><td>5</td><td>A simplified ATDD model</td></tr>
<tr><td>6</td><td>60</td><td rowspan="8">80</td><td rowspan="3">Proposed SAT approach</td></tr>
<tr><td>7</td><td>70</td></tr>
<tr><td>8</td><td rowspan="2">80</td></tr>
<tr><td>9</td><td>A simplified ATDD model</td></tr>
<tr><td>10</td><td>60</td><td rowspan="4">Tesla/Power-wall 2</td><td rowspan="3">Proposed SAT approach</td></tr>
<tr><td>11</td><td>70</td></tr>
<tr><td>12</td><td rowspan="2">80</td></tr>
<tr><td>13</td><td>A simplified ATDD model</td></tr>
<tr><td>14</td><td>0</td><td>100</td><td>-</td><td>-</td></tr>
<tr><td>15</td><td rowspan="4">80</td><td rowspan="4">80</td><td>Tesla/Powerwall 1</td><td rowspan="4">Proposed SAT approach</td></tr>
<tr><td>16</td><td>LG/RESU6.5</td></tr>
<tr><td>17</td><td rowspan="2">-</td><td>Cluster-1</td></tr>
<tr><td>18</td><td>Cluster-5</td></tr>
</table>

ATDD: Considered destination arrival time and daily distance parameters.
Proposed SAT: Considered daily driving cycles parameters (i.e., PDT, TDM, DDT, and driver movement).

used to represent the base case. The scenarios from 2 to 4 studied the impact of using the proposed SAT approach of the PEV driver model with different PEV penetration levels. In contrast, Scenario 5 is used to examine using the simplified ATDD approach of PEV driver model with 80% PEV penetration level. The impact of using 80% PV with different PEV driver models and PEV penetration levels is studied in Scenarios 6 to 9. Scenarios 10 to 13 investigated the effect of using HBES with 80% PV considering different PEV penetration levels and PEV driver models. Scenarios 15 and 16 are also created to examine the impact of using new sizing and generations of HBES at fixed PEV and PV penetration level, PEV driver model, and representative cluster. The effect of the representative clusters of PV and conventional load yearly data is considered in Scenarios 17 and 18. As illustrated in Section 3.1.1.3, k-mean was applied to the annual data, and eight clusters were obtained. Cluster-1 represents the highest number of corresponding days, while there were only sixteen days in the case of cluster-5. Using the random selection of any of the eight clusters, as denoted by Scenario 8, is compared with Scenario 17 (cluster-1) and Scenario 18 (cluster-5). Scenario 14 is also considered to study the impact of 100% PV penetration level with 0% PEV. In Scenario 14, because the PEV was not considered, the result was not significant for evaluating DT overload and aging, and VI. The result was only included in the under and over-voltage evaluation section to check the over voltage (OV) violation when 100% PV with 0% PEV is used. The IEEE 123 node PDS feeder [98] is modified, as depicted in Fig. 4.3, and used as a testbed system to evaluate the proposed framework in this work. The system is a primary feeder with 4.16 kV voltage level and includes single and three-phase loads. The apparent power of the existing single-phase loads in the system is either 44.72 kVA, 22.36 kVA, or 82.76 kVA. These loads are replaced by SDSs (i.e., center tape DTs, SLs, and SDs). The SDS archetypes were selected from [100], feeding six or twelve houses, with triplex cable 4/0 AA SLs and 1/0 AA SDs, as shown in Fig. 4.4. The size of the DTs is selected based on the apparent power of loads: 50 kVA DT rating replaced 44.72 kVA loads serving twelve houses, 25 kVA DT rating replaced 22.36 kVA loads serving six houses, and 75 kVA DT rating replaced 82.76 kVA loads serving a small commercial office. The number of added DTs is 47 with 50 kVA, 31 with 25 kVA, and 2 with 75 kVA, respectively. Multiplying each DT by the number of connected houses at particular DT gives 750 residential houses in the system. The pattern of the daily load

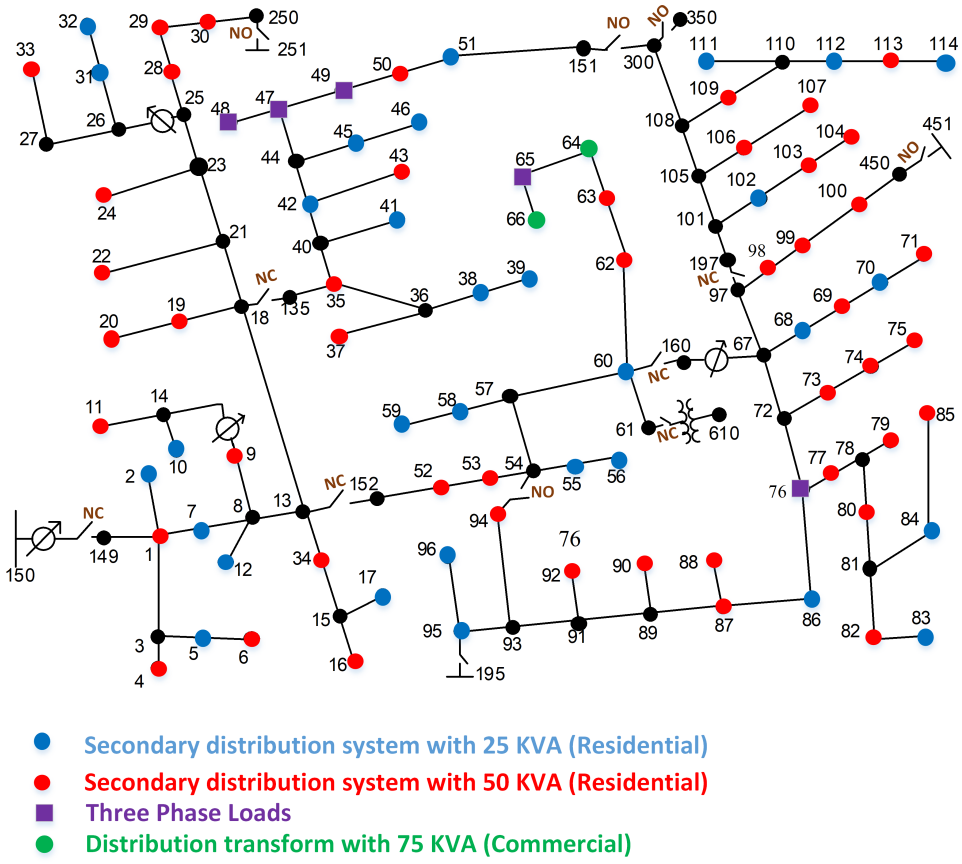

Figure 4.3: Modified 123 PDS test feeder.

profile for each house is modeled using the RTS. The RTS data are given in [106] on an hourly basis as a percentage of annual peak demand. The category of all houses is assumed to be residential dwellings with gas heating and without an electric water heater with median annual maximum demand of 4.93 kVA [107]. Determining the number of PEVs and PVs available in the system is an important preliminary step that needs to be taken prior to developing the probabilistic PF-based MCMC. To perform this task, the formula for computing the number of PEVs in terms of different parameters is given in (4.23) :

$$N_{PEV} = X_P \cdot N_h \cdot n_c \tag{4.23}$$

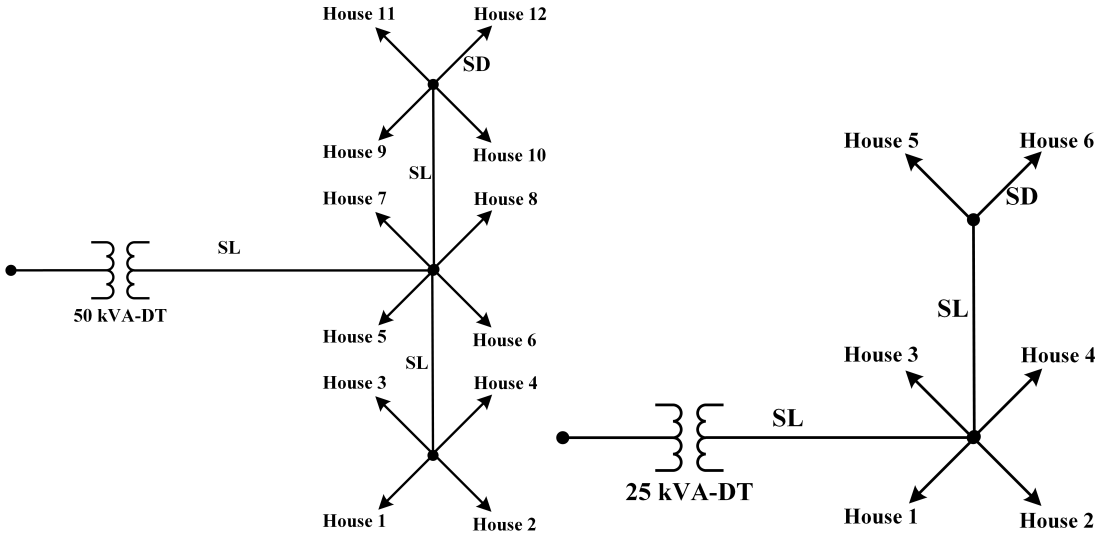

(a) SDS archetype with 50 kVA DT feeding 12 houses .

(b) SDS archetype with 25 kVA DT feeding 6 houses .

Figure 4.4: SDS archetypes for 50 and 25 kVA DTs.

where N_{PEVs} is the penetration level, expressed as a percentage of PEVs with respect to the total number of vehicles, N_h is the number of houses, and n_c is the average number of vehicles per household, assumed to be 1.9, as estimated by NHTS 2009 [77]. For the number of PV units, Equation (4.24) can be used where X_{PVs} is the penetration level and N_h is the number of houses.

$$N_{PVs} = X_{PVs} \cdot N_h \tag{4.24}$$

4.2.1 Impact on Transformer Overload

Because the considered case study includes a large number of transformers (i.e., 80 DTs and a one-substation transformer), investigating the daily measured overload for each individual DT is more complicated. For the system level, the percentage of transformers experiencing overload over a day is discussed and investigated for different scenarios in this work. The impact of different scenarios considering PEVs, PVs, and HBESs as a percentage of transformer overload is shown in Fig. 4.5. As depicted in Fig. 4.5(a), there is no observed overload in the case of Scenario 1 (no PEV), while the percentage of DTs

experiencing overload increases when PEV penetration levels are increased. In the case of Scenario 3 (70% PEV) and Scenario 4 (80% PEV), DTs are overloaded between 11 A.M. and 11 P.M., whereas in the case of Scenario 2 (60% PEV) there was only an overload between 1 P.M. till 10 P.M. The number of hours the transformers are overloaded is reduced when PEV penetration levels are decreased. For example, in the case of Scenario 4 (80% PEV), 95% of DTs are overloaded between 12 P.M. and 11 P.M., while in the case of Scenario 2 (60% PEV), DTs are overloaded with 95% only between 4 P.M. and 10 P.M., resulting in a five-hour difference between both scenarios. Further, the proposed SAT PEV driver behavior model impacted more on the percentage of DT overload compared to the PEV driver simplified model. In the case of using the proposed SAT in Scenario 4, 95% of DTs are overloaded for 11 hours compared to only seven hours in the case of Scenario 5.

Interestingly, using PV contributes to a decreased percentage of DT overload, although this decrease is only observed between 11 A.M. and 4 P.M. when PV is available, as illustrated in Fig. 4.5(b). It is noted that, in the case of Scenario 9, which is based on a simplified PEV driver model, PV with 80% penetration level was unable to mitigate the overload between 4 P.M. and 5 P.M. while it was fully alleviated in the case of Scenario 8. Although the use of the proposed SAT PEV driver behavior model resulted in a negative impact on DT overload, the simplified model, in contrast, increases the load between 4 P.M. and 5 P.M. as it inaccurately assumes that drivers take only one trip per day.

Further, the impact of using an HBES control strategy with different penetration levels of PEVs and PVs is depicted in Fig. 4.5(c). It is assumed that the HBES units are available when there is PV at the house, which makes the total number of PV units in the system equal to the HBES units. It can be observed that the proposed control strategy of HBES was, to an extent, able to successfully mitigate the DT overload issue over the day. However, it is observed that two hours of overloading occurred between 10 P.M. and midnight. In fact, using HBES with 80% PEV and 80% PV penetration levels led to an increase in the percentage of DTs experiencing overload during the period 11 P.M. until midnight and, as such, there was no observed overloading issue in the case of Scenarios 8 and 9 while the percentage of DTs with overload was 95% in the case of Scenarios 12 and 13. This increase occurred as a result of charging HBES before the end of the day,

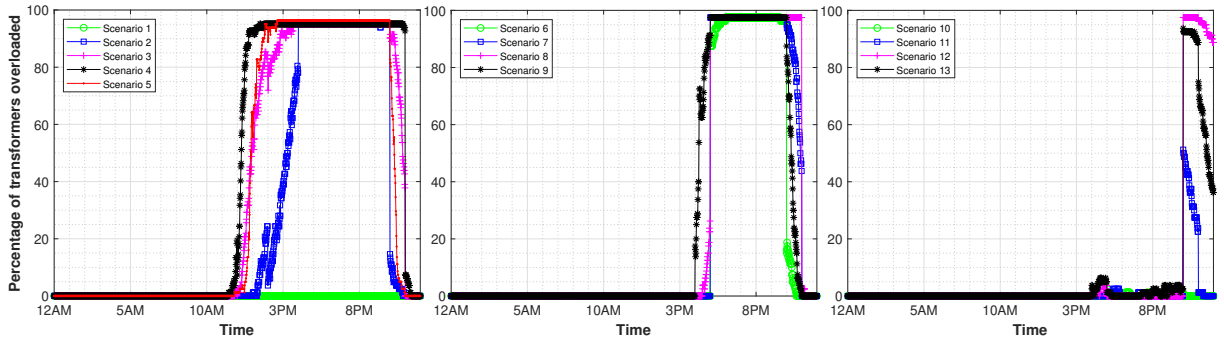

(a) (b) (c)

Figure 4.5: Number of distribution transformers experiencing overload in different scenarios. (a) Only PEV. (b) PEV and PV. (c) PEV and PV with HBES.

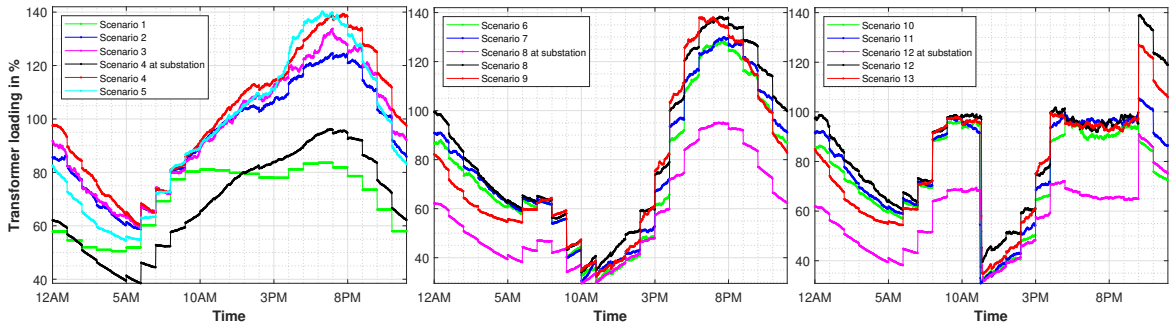

(a) (b) (c)

Figure 4.6: Impact on main substation and worst case of distribution transformer daily loading. (a) Only PEV. (b) PEV and PV. (c) Effect of HBES control strategy considering PEV and PV.

in order to return the HBES SOC back to the same state at the beginning of the day. To illustrate the impact of different components (i.e., PEVs, PVs, and HBESs) on the daily measured overload, the DT with the highest peak (e.g., at bus 103) and substation main transformer are selected. As observed in Fig. 4.6(a), Scenario 1 (no PEV) did not cause any overload over the day. The results show that increasing PEV penetration levels leads to more overload for DTs, but no overload was found at the main substation transformer. In the case of Scenarios 2, 3, and 4, it is noted that DTs are overloaded between 12 noon until midnight and that DT overload increases with increasing PEV penetration levels. In the case of Scenario 4 (80% PEV) and Scenario 2 (60% PEV), the peak occurred at 8 P.M., with 138% and 125% loading, respectively. It was also observed that using the proposed SAT PEV model, as labeled by Scenario 4, provided more loading on the DT, between 12 midnight and 6 A.M., and 8 P.M. and midnight, compared to using the PEV driver simplified model in Scenario 5.

Additionally, the impact of using PV generation with different penetration levels of PEV loads on daily DT overload is illustrated in Fig. 4.6(b). It can be inferred that using 80% PV penetration level with different PEV penetration levels can reduce DT loading less than 100% during afternoons when PV generation is high, while in the case of after 5 P.M. when no PV is available, the DT still overloaded. An HBES control strategy was proposed in order to alleviate the DT overloading after 5 P.M., as shown in Fig. 4.6(c). The results reveal that HBES is charged from PV between 7 A.M. and 11 A.M., and discharged when the DT is overloaded between 4 P.M. and 9 P.M. Further, although the DT was overloaded between 10 P.M. and midnight, the HBES operated in charging mode in order to charge the HBES battery, reaching 50% SOC, which was assumed at the beginning of the day.

4.2.2 Impact on Transformer Aging

Using the transformer thermal models discussed in Section 4.1.1, the transformer LOLs are estimated when the different scenarios in Table 4.1 are considered. The case study in this work includes 47, 31, and 2 DTs with 50, 25, and 75 kVA ratings, respectively. The primary distribution feeder is supplied by a main substation with a $5,000$ kVA transformer. The effect of different scenarios on the transformer yearly LOLs is illustrated using the boxplot

in Fig. 4.7. The figure was used to represent the distribution of the group of transformers LOL values at each scenario. The boxplot describes any data by the minimum, maximum, 25^{th} and 75^{th} percentiles, and the median. The red horizontal line inside the blue box is used to mark the median, while the upper and bottom of the same box represent 75^{th} and 25^{th} percentiles. There are also two horizontal lines outside of the blue box that

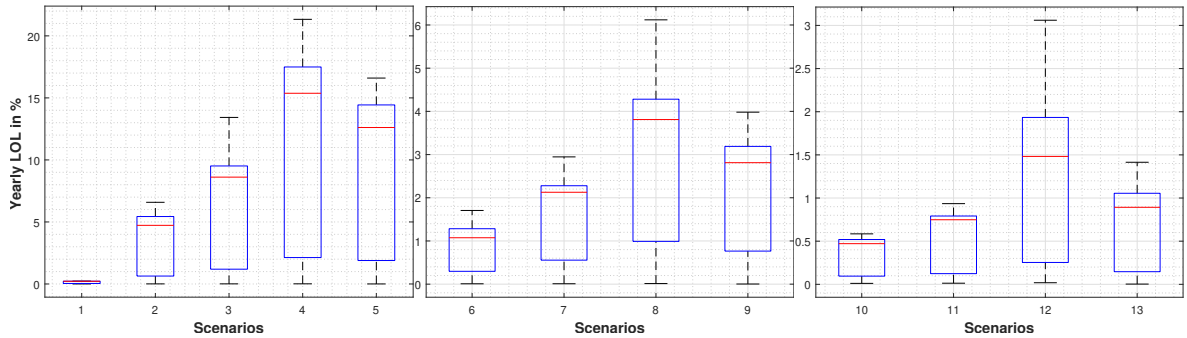

(a) (b) (c)

Figure 4.7: Impact of different scenarios on transformer yearly LOL. (a) Only PEV. (b) PEV and PV. (c) Effect of HBES control strategy considering PEV and PV.

represent the maximum and minimum of the data. The 25^{th} percentile, located at the bottom of the blue box, indicates the middle value between the median and minimum. The 75^{th} percentile, located at the upper of the blue box, marks the middle value between the median and maximum. As an example, if the 25^{th} percentile is corresponded to 5% LOL, this means that 25% of transformer LOLs is below the normal limit (i.e., 5%), and 75% of transformer LOLs is higher than the normal limit (i.e., 5%). It can be noted from Fig. 4.7(a) that increasing PEV penetration levels impacts more on the yearly LOLs for all transformers. When Scenario 1 (no PEV) is considered, yearly DT LOLs are within the normal limit (i.e., 5%) while in the case of scenarios with 60%, 70%, and 80% PEV penetration levels, the LOLs are increased beyond the normal limit. The median of DT LOLs in the case of Scenario 2 (60% PEV) was 4.8% while it was increased to 8.5% and 15.4% in the case of Scenario 3 (70% PEV) and Scenario 4 (80% PEV), respectively. This increase in LOL medians has impacted DT remaining life, and was reduced to 11.6 and 6.5 years in the case of Scenario 3 (70% PEV) and Scenario 4 (80% PEV), respectively. The

impact of using SAT PEV driver behavior versus the simplified models on LOL has been highlighted in Scenarios 4 and 5. The results show that using the proposed SAT model (Scenario 4) brings the LOLs higher than the case of using a simplified PEV driver models (Scenario 5). Using Scenario 5 brings the LOL median to 12.6% while it was increased to 15.4% in the case of Scenario 4, which degraded the transformer lifetime to 6.30 from 7.92 years.

Fig. 4.7(b) shows the effect of using PV when considering different PEV penetration levels on DT LOLs. It can be observed that using 80% PV has improved overall DT aging and significantly reduced the DT yearly LOLs. In the case of Scenario 6 (80% PV and 60% PEV), all DT LOLs have been brought within the LOL normal limit, while there was 25% of DTs beyond the normal limit in the case of Scenario 2 (60% PEV). Further, the impact of adding 80% PV to Scenario 4 (80% PEV) is highlighted in Scenario 8, which has reduced the median of DT yearly LOLs to 3.8% from 15.4%. This significant reduction results in the extension of the DT remaining life from 6.5 years to normal insulation lifetime (20.5 years). The results also show that using the proposed SAT (Scenario 8) impacted more on DT LOLs compared to simplified models (Scenario 9). Using 80% PV with 80% PEV when considering the proposed SAT PEV driver behavior has led to approximately 12.5% of DTs above the LOL normal limit (i.e., 5) while in the case of the simplified PEV model no violation was reported.

The impact of HBES control strategy while considering different PEV and PV penetration levels on DT LOL is illustrated in Fig. 4.7(c). It can be noticed that the proposed HBES control strategy has successfully maintained all DT LOLs within the normal limit. For example, in the case of Scenario 8 (80% PV with 80% PEV), there was 12.5% of DTs above 5% while in the case of using the implemented HBES control strategy, all DT LOLs were brought to normal values. Because the given $\Delta\theta_{H,RS}$ and $\Delta\theta_{TO,R}$ values in Table 4.1 for 50 kVA DTs are higher than 25 kVA DTs, it was noted that 50 kVA DTs insulation lifetime at different PEV penetration levels degrades faster than 25 kVA DTs. At different PEV penetration levels (i.e., Scenarios 2, 3, and 4), 25 kVA DT LOLs were always within normal limits while in the case of 50 kVA, the yearly LOL gradually rose above the accepted LOL limit when PEV penetration levels are increased. Table 4.4 shows the yearly LOLs for the main substation and 75 kVA DTs at

different PEV penetration levels. As depicted in the table, all LOL values are less than 5% and, as such, their lifetime does not degrade for any of the scenarios considered in this study.

Table 4.4: Main substation and 75 kVA transformers yearly LOLs.

Transformer name	Scenarios			
	Scenario 1	Scenario 2	Scenario 3	Scenario 4
5,000 kVA substation	0.04	0.3927	0.6529	1.0941
75 kVA T1	0.0031	0.0085	0.0095	0.0132
75 kVA T2	0.0035	0.0074	0.0119	0.0121

4.2.3 Impact on Voltage Imbalance

This section investigates the effect of different scenarios considering PEVs, PVs, and HBESs on VI. Equation (4.23) of Section 4.1.3 is used to compute VI% index for each bus at time t. When bus VI% index is above 3%, the voltage at the typical bus is imbalanced. Fig. 4.8 shows a summary of buses experiencing VI in a typical day when different scenarios are considered. It can be noticed from Fig. 4.8(a) that using different PEV penetration levels increases the percentage of buses experiencing VI between 10 A.M. and midnight compared to the case of no PEV. It is observed that 90% of buses suffered VI between 4 P.M. and 10 P.M. in the case of Scenario 4 (80% PEV), and that impact gradually decreased for the cases of Scenario 3 (70% PEV) and Scenario 2 (60% PEV). It can be noted that 70% of buses violated VI index at 12 midnight when Scenario 4 (80% PEV) is considered while the percentage decreased to 55% and 12% in the case of Scenario 3 (70% PEV) and Scenario 2 (60% PEV), respectively. Scenarios 4 and 5 in Fig. 4.8(a) highlight the effect of using different PEV driver behavior models on VI, where it was found that the percentage of buses experiencing VI between 11 P.M. and 2 A.M. in the case of the proposed SAT models (Scenario 4) is higher than Scenario 5 when PEV driver simplified models are considered.

Using PV as illustrated in Fig. 4.8(b) has mitigated the violation in VI for all buses between 11 A.M. and 3 P.M., but the violation still exists after 3 P.M. when PV

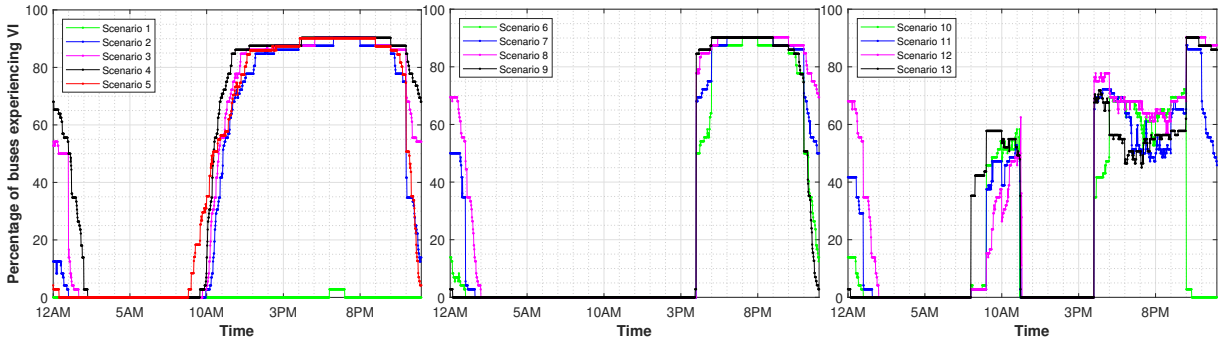

(a) (b) (c)

Figure 4.8: Impact of different scenarios on the percentage of buses experiencing VI. (a) Different PEV penetration levels. (b) Different PEV penetration levels with 80% PV. (c) HBES with 80% PV and different penetration levels of PEV.

generation is either decreased or unavailable. Using 80% PV for scenarios with 60%, 70%, and 80% PEV penetration levels introduced single phase PV generators that were capable of compensating the VI caused by the PEV single phase loads.

The impact of HBES control strategy while considering PV and PEV on VI is depicted in Fig. 4.8(c). The results show that charging HBES increases the percentage of buses experiencing VI while the percentage is decreased when HBES discharges power to the grid. It is observed that charging HBES occurs between 8 A.M. and 11 A.M. when PV generation reaches the peak while discharging HBES occurs between 4 P.M. and 10 P.M. when DTs are overloaded. As depicted in Fig. 4.8(c), charging HBES between 8 A.M. and 11 A.M. impacts more on the VI when fewer PEV penetration levels are considered. The HBES is charged/discharged based on the DT power loading, while the amount of either charging or discharging HBES power is determined by comparing measured DT power to its rating. For example, at 10 A.M., Scenario 10 (60% PEV with 80% PV) has led to VI of 55% of buses but only 25% of buses in the case of Scenario 12 (80% PEV with 80% PV). Having fewer PEV penetration levels leads to lower DT loading and, as a result, increases the difference between DT loading and rating. This difference determines the amount of charging HBES power, which provides an explanation as to why VI in the case of Scenario 10 is higher than Scenario 12. The HBES also contributes to an overall decrease in VI

between 4 P.M. and 10 P.M., as it is observed that, at 8 P.M., the percentage of buses experiencing VI reduced from 90% to 65% in the case of Scenarios 8 and 12, respectively. HBES is discharged between 4 P.M. and 10 P.M. in order to reduce the DT overload caused by charging PEV loads, which then improves the VI issue. After 10 P.M., the HBES was capable of reducing the VI when Scenario 10 (60% PEV with 80% PV) is considered while in the case of Scenario 11 (70% PEV with 80% PV) and Scenario 12 (80% PEV with 80% PV) the VI was not alleviated. Although DTs were overloaded after 11 P.M., HBES turned to operate in charging mode in the case of both Scenarios 12 and 13, in order to bring the HBES SOC equal to the same amount at the beginning of the day. In the case of other scenarios, DT overload during the day was not as extremely high and, as such, HBES SOC was not reduced to values less than those observed at the beginning of the day, which did not require HBES to charge any power from the grid.

4.2.4 Under and Over Voltage Evaluation

The under or over voltages are assessed based on ANSI C84.1 standards. The ANSI C84.1 document allows deviation in the voltage within ±10% of nominal voltage, respectively. The impact of different scenarios (i.e., PEVs, PVs, and HBESs) on under and over voltage violating limits for PDS and SDS nodes is listed in Table 4.5. For each scenario, voltage magnitude data are collected at each node for time t. The generated data formed a matrix with the number of nodes as rows and time steps as columns. The matrix is then transformed to a vector including the system voltage data. Hence, the probability of violating the under voltage (UV) limit (i.e., 0.9 PU) or the OV limit (i.e., 1.1 PU) is computed. The scenarios from 2 to 5 in Table 4.5 reported some nodes

Table 4.5: Probability of violating limits - under and over voltage.

Scenarios		1	2	3	4	5	6	7	8	9	10	11	12	13	14
At PDS	UV	0	0.0011	0.0034	0.0098	0.0075	0.001	0.003	0.008	0.0045	0	0	0.0014	0.0002	0
	OV	0	0	0	0	0	0	0	0	0	0	0	0	0	0
At SDS	UV	0	0.048	0.073	0.101	0.080	0.033	0.049	0.066	0.054	0.0008	0.0037	0.0205	0.0098	0
	OV	0	0	0	0	0	0	0	0	0	0	0	0	0	0

experiencing an under voltage (i.e., below 0.9 PU) when different PEV penetration levels are considered. It was observed that increasing PEV penetration levels increases the

probability of violating the UV limit. Additionally, focusing on PDS, Scenario 1 (0% PEV) shows that there was no UV violation, without PEV inclusion while, in the case of Scenario 2 (60% PEV), Scenario 3 (70% PEV), and Scenario 4 (80% PEV), the probabilities of violating the UV limit were 0.0011, 0.0034, and 0.0098, respectively. Furthermore, it was found that using the proposed SAT driver model leads to more UV violation, wherein the probability of violating the UV limit was observed to increase from 0.0075 to 0.0098, in the case of Scenarios 5 and 4, respectively. Results show that SDS nodes experience more UV compared to PDS nodes, and that the probability of violating UV for Scenario 4 increased from 0.0098 in the case of PDS to 0.101 in the case of SDS. This increase is due to the integration of PEV charging loads at the SDS, which does not have installed voltage regulation devices, as is the case for PDS. In addition, it is observed that there is still violation in UV limits for both PDS and SDS when PV generation is added with PEV charging loads, as reported in Scenarios 6 to 9. The results reveal that the probability of violating the UV limit for SDS is reduced to 0.066 (Scenario 8) from 0.101 (Scenario 4) when 80% PV penetration level is used with 80% PEV. The impact of adding HBES with PV and PEV on UV and OV is also listed in Scenarios 10 to 13, and the results show that using HBES improves UV violation at both PDS and SDS. For example, using HBES for Scenario 6 (60% PEV with 80% PEV) and Scenario 7 (70% PEV with 80% PV) has led to no UV violation at any PDS nodes while in the case of Scenario 8 (80% PEV with 80% PV), the probability was improved to 0.0014 from 0.008. For violating OV, Scenario 14 with 100% PV and no PEV was selected, and results show that there was no violation at either PDS or SDS nodes.

4.2.5 Impact of HBES Size

This section provides a comprehensive assessment for DT overload and aging, and VI when different HBES sizes are considered, as depicted in Fig. 4.9. Three HBES types were used considering various power and battery capacity (BC). Scenarios 12, 15, and 16 are considered using Tesla/Powerwall 2, Tesla/Powerwall 1, and LG/RESU6.5 HBES types. The BC and power data of these types are 13.5 kWh and 5 kW, 7 kWh and 2 kW, and 6.5 kWh and 2.2 kW, respectively. The impact of different HBES sizes at the same

PEV and PV penetration level (i.e., 80%) on DT daily measured overload is shown in Fig. 4.9(a), the DT with the highest peak (e.g., at bus 103) is selected. The results show

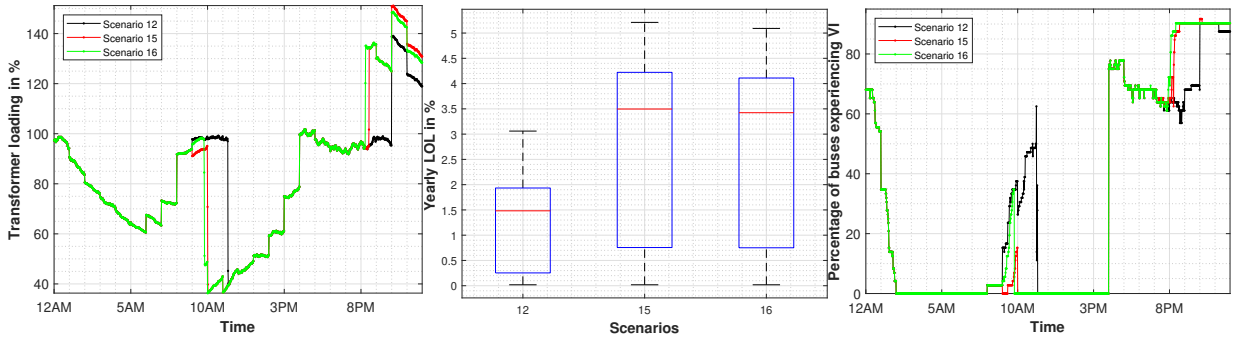

(a) (b) (c)

Figure 4.9: Impact of different HBES size on DT overload and aging, and VI. (a) DT daily overload. (b) DT aging. (c) Percentage of buses experiencing VI.

that Tesla/Powerwall 2, as labelled by Scenario 12, was able to mitigate DT overload between 8:30 P.M. and 10 P.M. while in the case of using both Tesla/Powerwall 1 and LG/RESU6.5 types, DT still overloaded. It is also observed that the impact of Tesla/Powerwall 1 (Scenario 15) and LG/RESU6.5 (Scenario 16) types is almost the same because there was no significant difference between their power and BC parameters values. Because the BC parameters of Tesla/Powerwall 1 and LG/RESU6.5 are less than Tesla/Powerwall 2, it is noted that they provided more loading on the DT between 10 P.M. and midnight. This increase occurred due to charging both Tesla/Powerwall 1 and LG/RESU6.5 HBESs with higher power compared to Tesla/Powerwall 2, although their rating power parameters are lower. Having lower BC in Tesla/Powerwall 1 and LG/RESU6.5 types led to depleting HBES SOC significantly to very low values. This reduction required HBES to charge with a higher power, between 10 P.M. and midnight, to bring SOC to those observed at the beginning of the day, which explains why the overload during this time in the case of Tesla/Powerwall 1 and LG/RESU6.5 is higher than Tesla/Powerwall 2.

For evaluating DT aging, the impact of different HBES types is illustrated using the boxplot in Fig 4.9(b). The results show that the medians of LOLs for all scenarios are

within the normal limit (i.e., 5%). It is noted that the median of DT LOLs is 1.5% in case of using Tesla/Powerwall 2 type, as labelled by Scenario 12, and increased to 3.5% in the case of using Tesla/Powerwall 1 and LG/RESU6.5. The overall results have shown that using Tesla/Powerwall 2 has maintained all DT yearly LOL values within normal limit (i.e., 5%) while in the case of using the Tesla/Powerwall 1 and LG/RESU6.5, a small portion of DT LOLs was above the normal limit.

Fig. 4.9(c) shows the effect of using different types of HBES on VI, and it can be seen that the percentage of buses experiencing VI increases when HBES is charged and decreases during discharging. Because the parameters of the rated power and BC of Tesla/Powerwall 2, as labelled by Scenario 12, are higher than Tesla/Powerwall 1 and LG/RESU6.5, it makes HBES keeps charging between 10 A.M. and 11 A.M. compared to the other two types, which results in increasing the percentage of buses violating VI. During discharging HBES after 4 P.M., it is observed that, between 4 P.M. and 8 P.M., all HBES types bring the same percentage of buses experiencing VI. After 8 P.M., it is found that using Tesla/Powerwall 1 and LG/RESU6.5, as labelled by Scenarios 15 and 16, increased the percentage to 90% and lasted until midnight. In contrast, using Tesla/Powerwall 2 decreased the percentage to 70% and was only between 8 P.M. and 10 P.M.

4.2.6 Impact of PV and Load Data Clustering

Table 3.2 data provides a more realistic representation of the load and PV yearly profiles. The k-mean clustering approach was developed in Section 3.1.1.3 for the entire year's data (solar irradiation, temperature, and conventional load), and eight clusters were obtained. Each cluster is represented with the corresponding number of days and the probability of occurrence. In order to show the importance of this representation on the obtained results, two deterministic scenarios (i.e., Scenarios 17 and 18) are considered. To investigate the impact of PV and load representative clusters on DT overload and aging, and VI, these deterministic scenarios are evaluated and compared against Scenario 8, in which the PV and conventional load profiles are assigned based on a random selection of any of the eight clusters. In Scenario 17, cluster-1 with the highest number of corresponding days is used, while Scenario 18 was considered using cluster-5 which has the lowest number of

corresponding days.

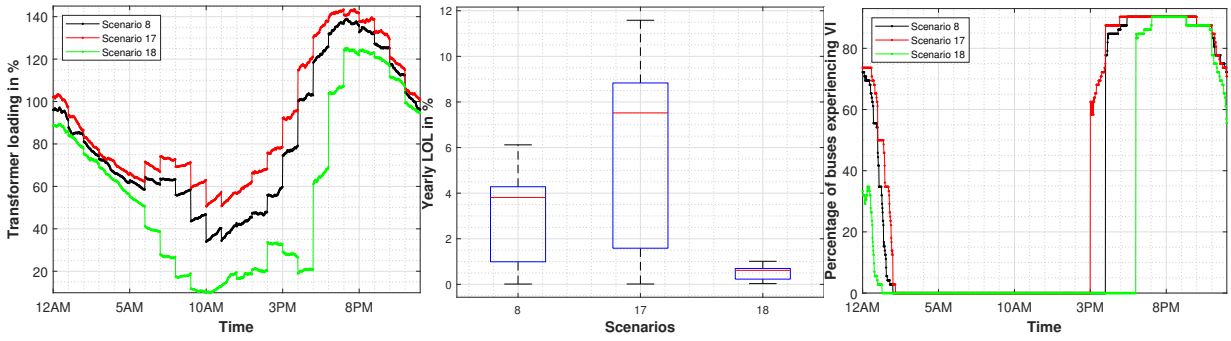

(a) (b) (c)

Figure 4.10: Impact of PV and load clusters on DT overload and aging, and VI. (a) DT daily overload. (b) DT aging. (c) Percentage of buses experiencing VI.

The impact of these scenarios on DT daily overload is presented in Fig. 4.10(a). It can be observed that using cluster-1, as labelled by Scenario 17, provided the worst DT overload, while in the case of using cluster-1 (Scenario 18), the loading was the least. It is also observed that having diversity in selecting the PV and load profiles, as labelled by Scenario 8, has brought the DT loading to the middle between cluster-1 and cluster-5.

Fig. 4.10(b) shows the impact on DT aging, and the results have shown that the median of DT yearly LOL in the case of Scenario 18 (cluster-5) was 0.62%, while it was increased to 3.81% and 7.52% in the case of Scenario 8 and Scenario 17, respectively. It is noticed that in the case of Scenario 18, all DT LOLs are within the normal limit (i.e., 5%), while in the case of Scenario 8 and Scenario 17, the LOLs are increased beyond the normal limit. It was only a tiny number of DTs that violated the LOL normal limit in Scenario 8, while it was greater than 50% in the case of Scenario 17.

The same observation is repeated when studying the impact on VI, as depicted in Fig. 4.10(c). It can be seen that using cluster-1, as labelled by Scenario 17, impacted more on the percentage of the buses experiencing VI followed by Scenarios 8 and 18, respectively.

4.2.7 Comparison With Previous Research

The results obtained using the proposed SAT-based approach of the PEV driver model are compared to those obtained in the previous research in [45] and [32]. The proposed SAT approach has the advantage of considering the realistic driving behavior, including the number and sequence of trips per day, into PEV charging demand profiles. These multiple trips in the proposed SAT approach are modeled considering different PDFs, including the start time of the daily trip chain, the parking duration (PDT), the driven distance (TDM), the driving duration (DDT), and the transition probability matrix of the driver movement among different trips in a day. In contrast, the simplified model, as denoted by ATDD, in the literature considers one trip per day and represents the driving behavior by only two PDFs (i.e., arrival time and daily distance). At the same PEV penetration level (i.e.,80%), the impact of the proposed SAT approach versus a simplified ATDD model is presented in Table 4.6. The DT overload, VI, and UV are evaluated using the probability of violating the accepted limits, while DT aging was assessed based on the percentage of yearly LOLs and remaining life in years. It can be observed from the table that the proposed framework has negatively impacted the overall results compared to the previous works. Using the proposed SAT approach has increased the probabilities from 0.44, 0.47,

Table 4.6: A summary of result evaluation - comparing the proposed framework with previous works (Scenario 4 vs. Scenario 5).

Case study	Probability of violating limits			Yearly DT LOL%	DT remaining life (Years)
	DT overload	VI	UV		
Proposed SAT approach	0.48	0.53	0.09	15.86	6.30
Simplified ATDD approach	0.44	0.47	0.07	12.61	7.92

and 0.07 to 0.48, 0.53, and 0.09 for DT overload, VI, and UV. In the case of DT aging, the yearly LOL was increased by 3.25% when the proposed SAT is used, and the transformer lifetime expectancy is reduced to a more realistic figure, from 7.92 to 6.30 years.

4.3 Summary

This chapter developed a new framework for assessing and enhancing voltage quality, DT overload and aging when residential prosumer ownership of PEVs is considered. The framework includes the behavior of PEV drivers using a SAT-based approach, which considers complete daily PEV driving cycle activities, into existing assessment models. A probabilistic PF using MCMC was developed to estimate the effect of different PEV and PV penetration levels on DT overload and aging, VI, and over and under voltage issues in the EDS. A control strategy for HBES units at the residential premises was also proposed for use by utility companies in order to alleviate DT overload and extend transformer lifetime. The results showed that using the proposed SAT-approach at the same PEV penetration level (i.e., 80%) degrades DT lifetime faster than the simplified model in the literature, and that the the remaining DTs lifetime was degraded from 7.9 to 6.5 years.

Chapter 5

Community Battery ESS Planning to Accommodate PEV Loads in a Three-Phase Active Distribution System[1]

In the previous chapter, the impact of residential prosumer ownership of PEVs on DT overload and aging, as well as VI and voltage levels, is discussed. Chapter 3 also proposes a solution to mitigate DT overload by implementing a control strategy using the HBES, which may be used by utility companies to enhance transformer lifetime expectancy. This chapter presents a heuristic methodology to plan for siting and sizing the community battery ESS while considering DT' LOL and VI. In addition to considering the conventional load (residential and commercial), the framework considers a PEV charging demand-based SAT approach, as well as PV options. Based on a backward-propagation algorithm, this chapter proposes to determine CBESS sites and sizes over the planning horizon while minimizing the total capital and operation costs.

[1]The present work is under review and will be submitted for publication in:
Y. O. Assolami, A. Gaouda and R. El-shatshat, "Community Battery ESS Planning to Accommodate PEV Loads in a Three-Phase Active Distribution System," in *IEEE Transactions on Transportation Electrification*.

5.1 Nomenclature

EDS Operations and CBESS Planning Model for the Horizon Year

Indices and Sets

j, k	Index of buses in distribution system, $(j,k) \in \mathcal{N}$
t	Index of time, $t \in \mathcal{T}$
a, b, c	Phases,
p	Phases, $p = a, b, c$, $p \in \mathcal{R}$

Parameters

C_P^{F}	Fixed installation cost of CBESS, \$
$C_P^{\mathrm{V}}, C_E^{\mathrm{V}}$	Variable installation cost of CBESS associated with power (\$/kW) and energy (\$/kWh), respectively
$C^{\mathrm{OM_F}}$	Fixed operation and maintenance cost of ESS, \$/kW-year
Ω_j	Phases group at bus j
$C^{\mathrm{OM_V}}$	Variable operation and maintenance cost of ESS, \$/kWh
R_m	Minimum allowable reserve of CBESS, %
$P^d_{j,p,t}$	Averaged Residential and commercial active load, kW
$Q^d_{j,p,t}$	Averaged Residential and commercial reactive load, $kvar$
$PEV^d_{j,p,t}$	Averaged PEV load demand, kW
PV_t	PV generation profile, kW
$P^{\min}, P^{\max}$	Power limits of distribution substation, kW
$V^{\min}, V^{\max}$	Voltage limits, kW
η^{CH}/η^{DCH}	Charging and discharging efficiency of CBESS, %
Υ_t	Electricity price, \$/kWh

$\text{VI}^{\max}\%$	Maximum allowable limit of VI violation, %
$\text{PV}^{\max}$	Maximum allowable PV penetration level at each bus, unitless
m_j	The number of phases at bus j.
h_j	The number of houses at bus j.

Variables

$E_{j,p,t}$	Actual energy capacity of CBESS, kW
$X_{PV\,j,t}$	PV penetration level, Unitless
J_1, J_2	CBESS installation and operation costs, \$.
$\overline{J}$	CBESS installation and operation cost with Penalty Function Approach (PFA), \$.
$P^{SS}_{j,p,t}, Q^{SS}_{j,p,t}$	Active/reactive power drawn from substation, kW
$P^{INST}_{j,p}, E^{INST}_{j,p}$	Installed power/energy capacity of CBESS, kW/kWh
$P^{INST}_{y}, E^{INST}_{y}$	Total installed power/energy capacity of CBESSs at Year y, kW/kWh
$P^{Rate}_{j,p}, E^{Rate}_{j,p}$	Rated power/energy capacity of CBESS, kW
$P^{CH}_{j,,p,t}, P^{DCH}_{j,p,t}$	Active power to be charged/discharged to/from CBESS, kW
$SoC_{j,p,t}$	State of charge of CBESS, kW
$V_{j,p,t}$	Voltage at bus, V
$V_{AVG,j,t}$	Average of the three phases voltages, V
$\delta_{j,p,t}$	Voltage angle at bus, *radian*
$S_{j\to kp,t}$	Power flow from bus j to k, $(j,k) \in \mathcal{N}$

5.2 Proposed Backward Propagation Approach For Multi-year Planning Considering CBESS Siting and Sizing

The necessary required procedures to achieve the proposed framework outcomes are presented in Fig 5.1. The proposed framework develops a multi year planning methodology for siting and sizing the CBESSs, to accommodate high penetration levels of a PEV load-based SAT approach. The framework uses two main stages as described in

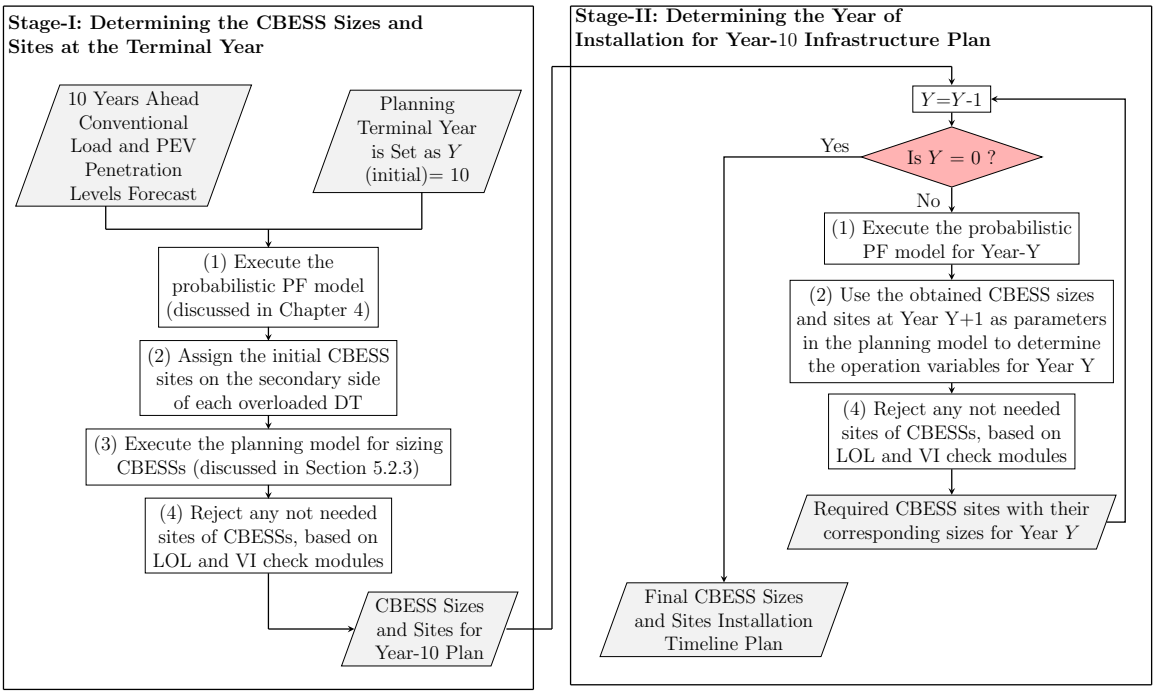

Figure 5.1: Proposed framework.

the following. In Stage-I, the CBESS locations and optimal power and capacities, as well as PV penetration level, which need to be in place at the plan of the terminal year, are determined, while Stage-II determines the optimal year of commissioning the obtained decisions in Stage-I. The backward propagation starts from the plan of the terminal year Y and ends at the first year. For each year, a post-processing evaluation based on an

LOL and VI check module is introduced to determine the required installed units of CBESSs, with the previous year decision plan as a reference.

5.2.1 Stage-I: Optimal Sizing of CBESSs for the Terminal Year

In this stage, the CBESS power and capacities are optimally determined for the terminal year. The detailed step-by-step procedure is explained as follows.

Step 1: Read the PEV penetration level and the conventional peak load at Year 10.

Step 2: Read the EDS information data (i.e., configuration, lines, transformers, and peak loads) from [98] (details in Appendix A).

Step 3: Read the obtained PDFs for the PEV load model based SAT-approach (discussed in Section 3.1.1.1 of Chapter 3).

Step 4: Read the conventional daily load profile clusters with their corresponding probabilities (discussed in Section 3.1.1.3 of Chapter 3).

Step 5: Select cluster-1 data (i.e., temperature and irradiation) for constructing PV generation profiles. In the planning model, cluster-1 is selected to be used for PVs in order to reduce the level of complexity.

Step 6: Execute the probabilistic PF based on the MCMC model using the above input data (described in Fig. 4.2 of Chapter 4).

Step 7: Use the output of Step 6 and create an evaluation for the DT overload and aging, VI and voltage level, as discussed in Section 4.2 of Chapter 4 based on [108].

Step 8: Allocate the initial CBESS sites on secondary side of the DTs that experience overload.

Step 9: Run the planning model (discussed in Section 5.2.3) to determine the optimal CBESS power ($P_{j,p}^{INST}$) and energy ($E_{j,p}^{INST}$) sizes, the required PV penetration level and other system operation variables.

Step 10: Start the process of revising the selected initial CBESS sites. The CBESS at each site is re-evaluated using PF with/without being installed. The CBESS

units are removed one at time and the effect of each site removal on DT LOLs and VI is studied and checked with standards.

Step 11: Use the output from the previous step to determine if a particular CBESS is rejected or included in the solution. If removing a CBESS at bus j leads to violating LOL and VI normal limits, it cannot be removed and will be selected for the solution. Otherwise, it can be rejected and removed from the optimal solution.

Step 12: Validate the impact of the revised CBESS sites, after removing the unnecessary CBESS units, using PF, and check if it satisfies system operation constraints. If YES, go to the next step, otherwise go back and return the removed CBESS units one-by-one until all constraints are met.

Step 13: Obtain the final plan decisions for the terminal year (Y), which satisfy the DT LOL normal limit and planning model constraints. The final plan infrastructure includes CBESS sites and sizes.

5.2.2 Stage-II: Year of Installation for CBESS Sizes and Sites

After determining the optimal CBESS sizes, along with their locations for the terminal year Y in Stage-I, Stage-II is developed to determine the installation year of CBESS sizes and sites at the terminal year.

The obtained $E_{j,p}^{INST}$ and $P_{j,p}^{INST}$ at the terminal year Y from Stage-I are used as inputs to Stage-II. In this stage, the CBESS sizes and sites obtained from Stage-I are used during the backward propagation to the initial year in order to identify when these sizes and sites need to be installed.

In the earliest years, the CBESS $E_{j,p}^{INST}$ and $P_{j,p}^{INST}$, along with their locations from the previous year, are used as parameters for the planning model to obtain operation variables that include variables such as CBESS charging and discharging profiles as well as the required PV. Once the operation variables are obtained, the CBESS sites are re-evaluated using Steps 10-12 in Stage-I to determine the needed CBESS sites for the current year.

The final obtained solution over all years satisfies the DT' LOL and VI normal limits and meets the targeted plan at the terminal year. The step-wise detailed procedures for executing Stage-II are outlined in Fig. 5.2.

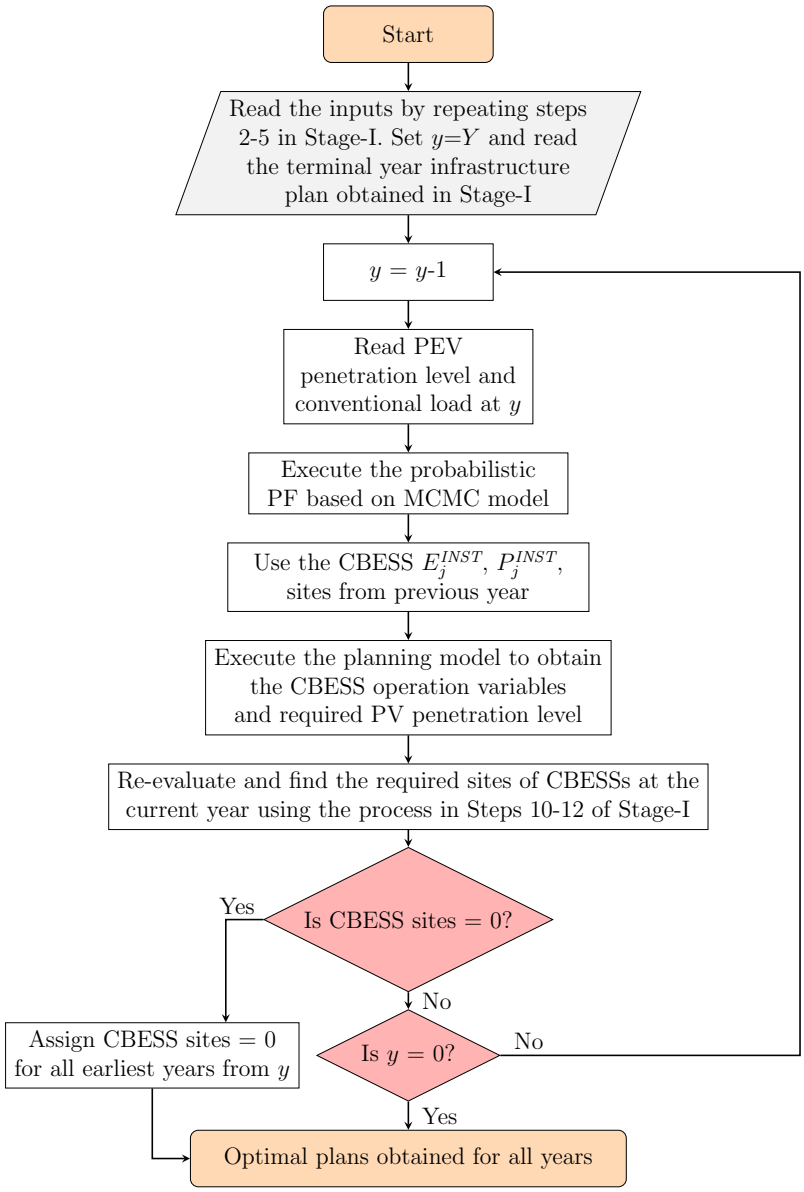

Figure 5.2: Flowchart for Stage-II

5.2.3 Planning Model for Sizing CBESSs in a Three-Phase Distribution System for the Horizon Year

The planning model seeks to optimally size the CBESSs in a three-phase EDS, considering the minimization of the annualized investment and operation costs during the horizon year. The locations are determined in a preliminary step using the probabilistic PF outputs previously described in Stage-I and Stage-II. The planning model is solved as an optimization problem wherein the mathematical model, including the objective function and constraints, is given as follows:

Objective Function

The objective function J of the planning model minimizes the total installation and operation costs at the horizon year and is given as follows:

$$J = J_1 + J_2 \tag{5.1}$$

The first term, J_1, represents the CBESS initial installation cost while the total operation cost is denoted by J_2.

CBESS Initial Installation Cost: comprises the CBESS power and energy unit costs, denoted by C_P^{V} and C_E^{V}, in $\$/kW$ and $\$/kWh$, respectively, as given below:

$$J_1 = \sum_{j}^{\mathcal{N}} \left[C_P^{\mathrm{V}} P_j^{INST} + C_E^{\mathrm{V}} E_j^{INST} + C_P^{\mathrm{F}} \right] \tag{5.2}$$

Operation Cost: includes the annual fixed operation and maintenance cost (O&M), the annual variable O&M cost associated with CBESS charging and discharging, and the cost of imported power from the external grid, as given below:

$$J_2 = \sum_{j}^{\mathcal{N}} \left[C^{\mathrm{OM_F}} P_j^{Rate} + 365. \sum_{t}^{T} \left(C^{\mathrm{OM_V}} (P_{j,t}^{CH} + P_{j,t}^{DCH}) + \Upsilon_t P_{j=1,t}^{SS} \right) \right] \tag{5.3}$$

The objective function in (5.1) is subjected to the following constraints:

Load Flow Equations

The injected power at each bus includes the imported power from the substation and PV, CBESS discharging and charging power, and PEV and conventional net load.

$$\sum_{p=1}^{\psi}(P_{j,t,p}^{SS} + X_{PVj,t}.h_j.PV_t + P_{j,t,p}^{DCH} - P_{j,t,p}^{CH} - P_{j,t,p}^{d} - \mathrm{PEV}_{j,p,t}^{d}) = \Re\Big(\sum_{k=1}^{N} S_{j\to k_{t,p}}\Big) \\ , \ \forall t \in \mathcal{T};\ \forall (j,k) \in \mathcal{N} \quad (5.4)$$

$$\sum_{p=1}^{\psi}\Big(Q_{j,t,p}^{SS} - Q_{j,t,p}^{d}\Big) = \Im\Big(\sum_{k=1}^{N} S_{j\to k_{t,p}}\Big) \quad , \quad \forall t \in \mathcal{T}; \quad \forall (j,k) \in \mathcal{N} \quad (5.5)$$

The operation of an EDS requires setting a limit on the main substation and bus voltages. These limits, which are included in our planning model as inequality constraints, are given below:

$$V_j^{min} \le V_{j,p,t} \le V_j^{max}, \quad \forall t \in \mathcal{T};\ \forall j \in \mathcal{N} \quad (5.6)$$

$$P_j^{min} \le \sum_{p=1}^{N} P_{j,p,t}^{SS} \le P_j^{max}, \quad \forall t \in \mathcal{T};\ \forall j \in \mathcal{N} \quad (5.7)$$

In order to maintain the deviation in voltage between the three phases within acceptable limits, a constraint for VI is introduced, as given below:

$$\%\mathrm{VI}_{j,t} = \frac{max[V - V_{AVG,j,t}]}{V_{AVG,j,t}} \cdot 100 \quad (5.8)$$

Equation (5.8) is computed to evaluate the imbalance in the voltage at buses, the average of the three-phase to phase voltage that is computed in (5.9), along with the maximum deviation from the averages, is used.

$$V_{AVG,j,t} = \frac{|V_{j,a,t}| + |V_{j,b,t}| + |V_{j,c,t}|}{m_j} \quad (5.9)$$

The ANSI C84.1 standard [105] recommends that the %VI does not exceed 3%, as stated in constraint (5.10).

$$\%\mathrm{VI}_{j,t} \leq \mathrm{VI}^{\max}\% \tag{5.10}$$

PV Generation Constraint

The amount of imported PV generation at each bus is limited to a maximum penetration level, as given in constraint (5.11). The penetration level of PV has to be equal to or less than 100%. The h at bus j is multiplied by the PV penetration level and PV_t in order to determine the PV generation at each bus.

$$X_{PV\,j,t} \leq \mathrm{PV}^{\max} \tag{5.11}$$

CBESS Sizing Constraints

• Once the CBESS unit is installed, its energy capacity is determined based on the energy to power ratio, as given below:

$$P_{j,p}^{INST} \leq E_{j,p}^{INST} \tag{5.12}$$

The $P_{j,p}^{INST}$ and $E_{j,p}^{INST}$ are assumed to be integer variables following the ESS available market.

Also, the rated CBESS power and energy sizes must remain constant through the planning horizon using constraints (5.13) and (5.14).

$$P_{j,p}^{Rate} = P_{j,p}^{INST} \tag{5.13}$$

$$E_{j,p}^{Rate} = E_{j,p}^{INST} \tag{5.14}$$

• CBESS Operation Constraints: When CBESS units are installed, the discharging and charging process and battery energy balance is defined in the following constraints:

$$SoC_{j,p,t} = SoC_{j,p,t-1} + \eta^{CH} P_{j,p,t}^{CH} - \frac{P_{j,p,t}^{DCH}}{\eta^{DCH}} \tag{5.15}$$

In (5.15), the SoC of each CBESS unit keeps the energy balance during the day. It increases/decreases with CBESS charging and discharging, respectively. The CBESS physical capacity imposes a limit on its SoC, as given in (5.16).

$$R_m \; E_{j,p}^{INST} \leq SoC_{j,p,t} \leq E_{j,p}^{INST} \tag{5.16}$$

To have a fair daily operation of CBESS, it is assumed that the SoC at the beginning and end of the day is equal, as stated in (5.17). This constraint will help to prevent the optimization model from choosing a very high SoC value at the beginning of the day and from fully discharging all the energy at the end of the day.

$$SoC_{j,p,t=1} = SoC_{j,p,t=24} = 0.5 \; E_{j,p,t} \tag{5.17}$$

Furthermore, the discharging and charging capability from/to CBESSs is limited to the rated power of CBESS, as given in (5.18) and (5.19).

$$P_{j,p,t}^{CH} \leq P_{j,p}^{Rate} \tag{5.18}$$

$$P_{j,p,t}^{DCH} \leq P_{j,p}^{Rate} \tag{5.19}$$

5.2.4 Solution Methodology

Since the planning model discussed in the previous section involves continuous and integer variables, the problem is then defined as Mixed Integer Non-linear Programming (MINLP) [109]. The nature of the Optimum Power Flow (OPF) is always non-convex and therefore the original form of the model in this work cannot be solved using the classical optimization approaches (e.g., Branch and Bound) [109]. This work suggests using population-based stochastic meta-heuristic algorithms to solve the three-phase OPF problem. A matlab Genetic Algorithm (GA) toolbox [110] is used to optimally determine the values of the decision variables previously mentioned in the planning model. The backward-forward sweep PF is implemented to study the behavior of the three-phase EDS and validate the obtained variables from the optimization.

5.2.4.1 Constraints Processing

GA algorithms are more commonly used to solve unconstrained optimization problems. They encounter difficulty in managing the imposed constraints and this becomes more complicated when the decision variables are integers [111]. The injected power equality constraints are managed through a power flow calculation, as they must be satisfied once PF is converged. The inequality constraints, which are dependant on the variables inside the PF calculation, are modeled using the PFA. The PFA transforms the constrained optimization problems to unconstrained problems by introducing a penalty factor on the constraints in order to avoid violating their own acceptable range [112]. A new objective function is formulated by adding the penalty function terms on the inequality constraints and combining them with the original objective function. When the PFA is implemented in our model, the model is converted to a group of unconstrained optimization problems that have to converge to the same solution of the original constrained problem. Based on the quadratic penalty factor approach introduced in [113] and [114], quadratic penalty terms are augmented to the original objective function in (5.1) in order to avoid any violation, which results in the following modified objective function:

$$\overline{J} = J + Penalty \tag{5.20}$$

$$\begin{aligned} Penalty = K_{V1}.\sum_{j=1}^{N}\sum_{t=1}^{T}\sum_{p\in\Omega_j}(V_{j,p,t} - V_j^{max})^2 + K_{V2}.\sum_{j=1}^{N}\sum_{t=1}^{T}\sum_{p\in\Omega_j}(V_j^{min} - V_{j,p,t})^2 + \\ K_{V3}.\sum_{j=1}^{N}\sum_{t=1}^{T}(\%\mathrm{VI}_{j,t} - \mathrm{VI}^{\max}\%)^2 + K_{V4}.\sum_{j=1}^{N}\sum_{t=1}^{T}(P_j^{min} - \sum_{p\in\Omega_j}P_{j,p,t}^{SS})^2 + \\ K_{V5}.\sum_{j=1}^{N}\sum_{t=1}^{T}(\sum_{p\in\Omega_j}P_{j,p,t}^{SS} - P_j^{max})^2 \end{aligned} \tag{5.21}$$

where K_{V1}, K_{V2}, K_{V3}, and K_{V5} are the penalty factors for lower and upper voltage limits, VI, and the main substation power minimum and maximum allowable limit. The added quadratic terms in (5.21) introduce a high penalty to constraint violation by

driving constraint variables to their closest acceptable limits.

5.3 Results and Discussion

In this work, a modified IEEE 123 node PDS feeder is used to examine the proposed planning framework. A testbed system is the primary feeder with 4.16 kV and includes single and three-phase loads and feeders. In the proposed assessment framework discussed in Chapter 4, the primary system was modified to include a detailed SDS when studying the impact of using a SAT approach with a PEV load while considering residential prosumers. The process of implementing the proposed framework in this chapter reveals the complexity of adding the SDS to our planning optimization problem. The SDS increases the optimization problem dimensions, hence the performance of the computational burden is reduced. Therefore, the research presented in this chapter uses the output from the probabilistic PF (discussed in Chapter 4) to represent the behavior of the SDS as a lumped load at the secondary side of the DTs. The apparent power of the existing single-phase loads in the primary system is either 44.72 kVA, 22.36 kVA, or 82.76 kVA. These loads are replaced by center tape DTs and the size is selected based on the apparent power of loads: 50 kVA DT rating replaced 44.72 kVA loads; 25 kVA DT rating replaced 22.36 kVA loads; and 75 kVA DT rating replaced 82.76 kVA loads. The number of added DTs is 47 with 50 kVA, 31 with 25 kVA, and 2 with 75 kVA, respectively.

In the planning model, the 24 demand profiles at each node in the system are taken from the probabilistic PF averaged results. It is assumed that the conventional load and PEV penetration levels increase by 1% and 10% annually over a 10-year planning horizon [87]. A probabilistic PF is performed for each year to include the variation in weather and residential consumption for the 365 days. When it is converged, the average of PF results is computed and used to represent the year. Thus, the average of the 24 demand profiles at each node is used as parameter to the planning model in order to size and site CBESSs. For the 10 year planning period, one simulation is executed per year wherein the averaged demand represents the whole year. For PV generation, a k-mean clustering approach is developed in Section 3.1.1.3 of Chapter 3 to find the most representative clusters of PV

annual data. In order to reduce the level of complexity, cluster-1 was selected for use in the planning model as it represents the highest number of corresponding days.

The CBESS installation and operation cost parameters are given in Table 5.1 [67].

Table 5.1: CBESS Cost Parameters

	C_P^{V}	C_E^{V}	$C^{\mathrm{OM_F}}$	$C^{\mathrm{OM_V}}$	C_P^{F}
	$\$/kW$	$\$/kWh$	$\$/kW$	$\$/kWh$	$\$$
CBESS	287.5	338	26.8	0.002	20,000

The proposed planning framework is also examined using different PEV models, as follows:

Case-1 **(Proposed SAT-based approach)**: In this case, the impact of the daily driving cycle parameter (i.e., PDT, TDM, DDT, and driver movement) model (discussed in Chapter 3) on PEV demand is considered into the proposed CBESS planning problem.

Case-2 **(Simplified PEV model)**: This case considers the oversimplified model of PEV daily driving behavior parameters (i.e., only the destination arrival time and daily distance) and includes their effect on the proposed CBESS planning model.

Stage-I is used to optimally determine the power and energy sizes of CBESS units for the terminal year. It should be noted that the sites of CBESSs are initially allocated to the secondary sides of any overloaded DTs. Once the planning model is executed to determine the sizes, heuristic procedures are developed to determine the accepted/rejected CBESS sites. Hence, the accepted sites are now included only in the final solution, along with their optimal CBESS sizes. For the case study in this chapter, the initial CBESS sites are determined to be 78 units, distributed on the secondary sides of 25 and 50 kVA DTs. Table 5.2 shows the results of determining the sizes and sitings of CBESS for the terminal year. At the initial stage, the probabilistic PF results are used to determine the sites for CBESS units. It was found that 78 DTs were overloaded and therefore were assigned as preliminary locations for CBESSs. For the selected sites of CBESSs, the planning model was executed and the initial optimal solution was $21,394$ kWh and $2,394$ kW, for energy and power sizes, respectively. After carefully investigating the impact of individual CBESS site removal on DT LOLs, as previously explained in Steps 9-12 of Stage-I, the LOL check

Table 5.2: Stage-I CBESS Sizing and Sitings Using LOL and VI Check Module Considering Case-1.

	Energy/power total sizing kWh/kW	Number of CBESS sites	Number of rejected CBESS	Number of DT violated LOL	Probability of violating VI
Initial solution	$21,394/2,393$	78	-	0	0
LOL check module	$16,132/1,514$	47	31	0	0.1441
Final accepted solution after VI check module	$18,404/1,866$	60	18	0	0

module was used to reject 31 sites of CBESSs. The LOL check module selects only the CBESSs that do not contribute to increasing the LOL beyond the normal limit and removes them from the CBESS list. As noted in the second row of Table 5.2, these rejected sites did not lead to any violation of LOL values, but the probability of violating VI was brought to 0.1441. Because there was a violation to VI standards, the VI check module was used to revise the 31 reject/accept decisions and to reinstate the units that make a contribution to VI. In order to meet the required VI standards, it was determined that 13 out of 31 units needed to be reinstated back to service. The final solution to satisfying the LOL and VI standards is highlighted in the third row of Table 5.2. The total optimal energy and power capacity is $18,404$ kWh and $1,866$ kW, which are distributed over 60 CBESS units. The terminal year plan, which includes 60 CBESS sites along with their power and energy sizes, is used as input to Stage-II in order to determine the year of installation.

In Stage-II, the obtained CBESS $P_{j,p}^{INST}$ and $E_{j,p}^{INST}$ sizes from Stage-I are maintained fixed for the earliest years, but the required CBESS units that must be installed at each Year y are determined.

Table 5.3 shows the results of the total sizing and siting of the CBESSs using the proposed backward propagation approach, as labelled by Stage-II. The process starts from year Y-1 and ends at the initial year. The highlighted rows denote the total required CBESS sizes for the given year, presenting the cumulative presence of the units that are in service. For example, in Year-7, the total required cumulative CBESS size for the EDS is $16,132$ kWh/$1,514$ kW and this capacity will be distributed over 47 units, whose individual

Table 5.3: Stage-II CBESSs Total Sizes Using Backward Propagation Approach Based LOL and VI Check Modules: Case-1 (Proposed SAT-Based Approach)

	Energy/power total sizing kWh/kW	Number of CBESS sites	Number of rejected CBESSs	Number of DT violated LOL	Probability of violating VI
Year-10 (obtained from Stage-I)					
Final accepted solution after VI check module	$18,404/1,866$	60	18	0	0
Year-9 (number of rejected CBESSs is out of 60)					
LOL check module	$16,132/1,514$	47	13	0	0.0735
Final accepted solution after VI check module	$17,357/1,708$	54	6	0	0
Year-8 (number of rejected CBESS is out of 54)					
LOL check module	$16,132/1,514$	47	7	0	0.0087
Final accepted solution after VI check module	$16,998/1,648$	52	2	0	0
Year-7 (number of rejected CBESS is out of 52)					
LOL check module	$16,132/1,514$	47	5	0	0
Final accepted solution after VI check module	$16,132/1,514$	47	5	0	0
Year-6 (number of rejected CBESS is out of 47)					
LOL check module	$16,132/1,514$	47	0	0	0
Final accepted solution after VI check module	$16,132/1,514$	47	0	0	0
Year-5 (number of rejected CBESS is out of 47)					
LOL check module	0	0	47	0	0.1059
Final accepted solution after VI check module	$7,489/704$	22	25	0	0
Year-4 (number of rejected CBESS is out of 22)					
LOL check module	0	0	22	0	0.0567
Final accepted solution after VI check module	$3,104/287$	9	13	0	0
Year-3 (number of rejected CBESS is out of 9)					
LOL check module	0	0	9	0	0.0307
Final accepted solution after VI check module	$1,680/150$	5	4	0	0
Year-2, **Year-**1, **and Year-**0					
No required installations for any CBESSs, LOL and VI standards are not violated					

sizes are the corresponding energy and power obtained at the terminal year.

At Year-9, CBESS sizings, along with their sites for the terminal year, are used as parameters for the planning model in order to determine the operation variables and required PV penetration level. It is noted that having 60 CBESSs at Year 9 is not economical and that only 54 of the units are sufficient to meet LOL and VI standards as well as operation constraints. Use of the LOL check module has resulted in the rejection of 13 CBESS units out of 60, but the probability of violating the VI index was increased to 0.0735. In order to satisfy both LOL and VI, the rejected 13 units needed to be revised using the VI check module. It was found that 7 units of the rejected 13 must be returned to service in order to meet both LOL and VI. The final solution for Year 9 was $17,357$ kWh and $1,708$ kW for total energy and power, respectively. Since 54 units need to be in service at Year 9, 6 CBESS units need to be installed at Year-10.

At Year-8, it was found that the LOL standards are met with 47 CBESS units in place while, in the case of satisfying both LOL and VI, there was a need to have 52 in service. The total CBESS energy and power, which must be in place at Year-8, is $16,998$ kWh and $1,648$ kW, respectively.

In the case of Year-6 and Year-7, only 47 CBESS sites were needed. When the LOL check module was initially used, the obtained solution was within VI and all other constraints. The obtained total capacity and power of CBESS installations at the two years are $16,132$ kWh and $1,514$ kW, respectively.

For Year-5, there was no need to install any CBESS in order to meet the LOL, but the VI was violated with 0.1059 probability. It is observed that there is a need to install 22 units of CBESS to keep VI within the standard, with a total of $7,489$ kWh and 704 kW for energy and power, respectively.

It was noted that the LOL has never been violated at Year-4 and Year-3, even with no CBESS. For keeping the VI within standards, the CBESS contributed by installing 9 and 5 units, with total sizes of $3,104$ kWh/287 kW and $1,680$ kWh/150 kW, respectively. For Year-2 and the earliest years, no CBESS installation was required. It was found that the LOL, VI, and system operation constraints were satisfied without the need of CBESS infrastructure.

After the cumulative total CBESS sizes, the number of units in place and the corresponding years were determined in Table 5.3 using Stage-I and Stage-II. The exact actual number of CBESS sites to be installed in each year of the plan horizon, along with their total sizes, are presented in Table 5.4.

Table 5.4: Stage-II: Infrastructure Plan for CBESS Installations Over the Plan Horizon

Case-1 (Proposed SAT-based approach)				Case-2 (Simplified PEV model)		
Year	E_y^{INST} (kWh)	P_y^{INST} (kW)	No. of installed CBESS units	E_y^{INST} (kWh)	P_y^{INST} (kW)	No. of installed CBESS units
0	0	0	0	0	0	0
1	0	0	0	0	0	0
2	0	0	0	0	0	0
3	1,680	150	5	1,359	127	4
4	1,424	137	4	2,367	238	7
5	4,385	417	13	7,876	747	24
6	8,643	810	25	2,299	223	7
7	0	0	0	1,598	154	5
8	866	134	5	0	0	0
9	359	60	2	450	79	3
10	1,047	158	6	1,119	188	7
Total	18,404	1,866	60	17,068	1,756	57

As depicted in Table 5.4, it can be noted that the total number of installed CBESSs was 60 units for Case-1, which decreases to 57 when Case-2 is considered. This observation indicates that using the proposed SAT-based approach for modeling PEV demand increases CBESS installations compared to the PEV simplified model. It is also noted that the proposed SAT based-approach increases the required total sizes of CBESSs by 1,336 kWh and 110 kW for energy and power, respectively, compared to the simplified model.

In both cases, there was no CBESS installation at Year-0, Year-1, and Year-2, respectively. The majority of CBESS units were installed at Year-6 for Case-1 and Year-5 when Case-2 is used. It was also found that no installation was required at Year-7 when the proposed PEV SAT-based approach is considered while, in the case of using the simplified PEV model, no installation was marked at Year-8. Although the demand at

the terminal year was significantly high, the exact number of installed units at the same year was only 6 and 7 for Case-1 and Case-2, respectively, while the remaining units in service were installed gradually through the previous years.

Table 5.5: Capital and Operation Costs of Optimal CBESS Plan Decisions

	Case-1 (Proposed SAT-Based Approach)		Case-2 (Simplified PEV Model)	
	Installation	Operation	Installation	Operation
	J_1,\$	J_2,\$	J_1,\$	J_2,\$
Year 0	-	1,836,852	-	1,836,852
Year 1	-	1,937,542	-	1,902,905
Year 2	-	2,038,466	-	1,977,744
Year 3	610,965	2,136,552	495,854	2,056,021
Year 4	520,699	2,236,380	868,471	2,123,877
Year 5	1,602,017	2,308,020	2,876,850	2,174,811
Year 6	3,154,209	2,372,261	841,174	2,237,504
Year 7	-	2,418,118	584,399	2,270,605
Year 8	331,233	2,488,749	-	2,251,139
Year 9	138,592	2,546,761	174,812	2,330,181
Year 10	399,311	2,559,979	432,272	2,269,108
Total,\$	6,757,027	24,879,686	6,273,834	23,430,751

Table 5.5 examines the impact of the proposed SAT-based approach versus the simplified PEV model on the capital and operation costs of the 10 year proposed planning framework. The operation and installation costs are presented for Case-1 and Case-2, starting from the initial year and ending at the terminal year. It is observed that the operation cost of the EDS increases over the plan horizon, and includes the fixed and variable annual costs of CBESS as well as the cost of imported power from the main substation. At both cases, although there was no CBESS installations during Year-2 and earliest years, the local distribution company (LDC) still need to pay for the purchased imported power from the external grid. As the demand increases over the plan horizon, more CBESS installations are added, hence there are associated O&M costs. In Case-1, the installation cost in Year-6 is the highest because of the installed sizes of $P_{j,p}^{INST}$ and $E_{j,p}^{INST}$ and the highest number of installed units, while the highest installation cost in

Case-2 was in Year-5.

It is seen from Table 5.5 that, in Case-1, the LDC needs to invest in CBESS installation over the plan horizon with a total budget of M$6.7 compared to M$6.3 for Case-2, which is lower than 7.2% of Case-1. This is because of the oversimplified assumptions in the PEV model that are considered in Case-2 while Case-1 has taken the realistic SAT characteristic of the PEV model.

5.4 Summary

This chapter introduced a novel backward-propagation approach to developing a CBESS planning framework in order to accommodate a high penetration level of PEV loads, taking into consideration DT' LOL and VI aspects. Two sequential stages were developed to determine the CBESS sizes and sites, starting from the terminal year and ending at the initial year. The obtained CBESS sizes, with their corresponding sites from Stage-I, are re-evaluated at each year using the planning model as well as LOL and VI check modules in order to determine the required CBESS units that meet LOL and VI standards. The proposed planning framework is examined using a realistic proposed PEV SAT-based approach versus the simplified PEV model presented in the literature, and evaluates CBESS sizes, siting, and installation and operation costs. The case studies and scenarios demonstrate the impact of neglecting PEV realistic driver behavior parameters on CBESS planning decisions while the results indicate that the realistic proposed SAT-based approach increases the required total CBESS investment budget from M$6.3 to M$6.7.

Chapter 6

Conclusions

6.1 Summary

The research presented in this thesis focuses on investigating the stochastic models of residential prosumer ownership of PEV loads, and these models are then integrated into the assessment and planning of an EDS.

Chapter-1 lays out the motivation to the research that is introduced in the subsequent chapters, emphasising the urgent need for modeling the realistic behavior of PEV drivers and the importance of including these elements into EDS assessment and planning models. A literature review of recent related works, particularly on PEV models, including their integration with residential prosumers on EDS assets as well as ESS assessment and planning, is presented. This chapter also presents the main research objectives and an overall layout of the thesis.

Chapter-2 presents a brief background on the topics related to the research objectives. PEV demand characteristics are discussed, including load nature, model, and basic definitions, followed by a definition of a trip chain and an overview of applications. Three-phase electrical distribution system models and components, including PF solution algorithm, are also discussed. Finally, an overview of PV and ESS technology, including definitions of important concepts, is presented.

Chapter-3 presents a comprehensive statistical analysis that considers different datasets (i.e., NHTS global, NY State, and City of Buffalo data) based on an updated version of NHTS. The aim of this chapter is to study the behavior of PEV SAT characteristics (i.e., PDTs, DDT, TDM, and driver movement from one location to another) and evaluate their effect on conventional loads when PVs are included. The MCMC, in conjunction with a trip chain methodology, is used to probabilistically estimate the uncertainty with a PEV charging load profile (e.g, home, work, and FCSs), conventional loads, and PV generation. Charging levels of 3.7, 6.6, and 50 kW are used as available sources of power at home, work, and FCSs, respectively. The impact of the location of each charging facility on the time taken to recharge is studied while considering different PEV battery specifications. The results reveal that the majority of charging activities take place at home, followed by at FCSs and work. The proposed framework shows an accurate estimation of the total daily load profile considering the stochastic nature of distributed PV resources on the SAT characteristics of PEV loads.

Chapter-4 proposes a new framework for assessing and enhancing voltage quality, DT overload and aging when residential prosumer ownership of PEVs is considered. The framework integrates the behavior of PEV drivers using a SAT-based approach, which considers complete daily PEV driving cycle activities, into existing assessment models. A probabilistic PF using MCMC was developed to estimate the effect of different PEV and PV penetration levels on DT overload and aging, VI, and over and under voltage issues in the EDS. A control strategy for HBES units at residential premises is also proposed for use by utility companies in order to alleviate DT overload and extend transformer lifetime. The proposed assessment framework, which uses a SAT-based approach, provides a more realistic evaluation for DT overload and aging, VI, and under and over voltages. The results show that the use of the proposed SAT-based approach has reduced DT lifetime to 6.30 years from 7.92 years for the same PEV penetration level.

Chapter-5 demonstrates a new backward-propagation approach to developing a CBESS planning framework in order to accommodate a high penetration level of a PEV load- based SAT approach, considering DT' LOL and VI aspects. Two sequential stages are developed to determine the CBESS sizes and sites, starting from the terminal year and ending at the initial year. The obtained CBESS sizes, with their corresponding sites from Stage-I, are

conducted and re-evaluated at each year. In Stage-II, the planning model is solved for Year Y to determine the operation variables for CBESS sites and sizes obtained at Year Y+1. The LOL and VI check modules are then introduced to determine the needed CBESS units that meet LOL and VI standards. The proposed planning framework is examined using the realistic proposed PEV SAT-based approach versus the simplified PEV model in the literature wherein CBESS sizes, siting, and installation and operation costs are evaluated. The effects of neglecting PEV realistic driver behavior parameters on CBESS planning decisions are discussed, the results of which indicate that the realistic proposed SAT-based approach increases the required total CBESS investment budget from M$6.3 to M$6.7.

The following key findings are the main conclusions that can be drawn from the research:

- The inclusion of SAT characteristics of driver behavior into a PEV profile model gives a more realistic representation of a PEV SOC model that depends on a previous state during the day. A SAT-based approach accurately addresses the daily driving cycles and includes PEV charging location, SOC, and time. The impact of the location of each charging facility on the time taken to recharge is studied, the results of which reveal that the majority of charging activities take place at home, followed by at FCSs and work.

- Integrating PEV demand using a SAT-based approach into the EDS affects the assessment and planning of DT overload and aging, VI and under and over voltage. This helps the utility to avoid an unrealistic estimation of the EDS assets condition that may lead to inappropriate decisions during the operation or planning phase.

- Including SAT features in the assessment model shows that the DT lifetime has reduced from 7.92 years to 6.30 years. If SAT parameters are ignored, the operation of DT is expected to fail and consequently be reflected in the provided quality of services.

- Neglecting SAT characteristics in the CBESS planning model affects the optimal planning decisions over the planning horizon and is reflected in a reduction in the total number of CBESS installations. This has resulted in a considerable number of changes to the investment timelines, as well as total operation and installation costs.

6.2 Contributions

The main contributions of the research presented in this thesis can be summarized as follows:

- The PEV stochastic model, as previously reported in the literature, is extensively improved by taking into account a realistic pattern of PEV daily driving cycles. The improved model includes the SAT characteristics of driver behavior that consequently impact the PEV charging demand.
- A new PEV SAT model is integrated while considering the uncertainty of PV generation (i.e., temperature and irradiation) and conventional loads. The integration of these components further enhances and improves the existing tools that take care of modeling the uncertainty of active distribution network components.
- A new assessment framework is developed using the above models in order to evaluate distribution transformer (DT) overload and aging, voltage imbalance (VI), and under and over voltage, considering a complete and more realistic EDS model.
- A realistic estimation for the remaining lifetime of the DTs is quantified while considering SAT models of PEV charging with residential prosumers in different scenarios and case studies.
- A new control strategy is developed using different generations of home battery energy storage (HBES) units with PVs at residential premises while considering a SAT approach based on different levels of PEV demand. The proposed strategy is developed to avoid DT overload as well as to enhance and extend DT lifetime.
- A new multi-year planning framework is proposed to size and site the CBESSs while considering a PEV demand-based SAT approach as well as PV options. A heuristic planning algorithm is developed using the backward propagation approach in order to determine the CBESS sizes and sites over the planning horizon while maintaining LOL and VI within standards.

The main contents of Chapter-3 have been published in the 2019 IEEE Electrical Power and Energy Conference [115] and the IEEE Canadian Journal of Electrical and Computer Engineering [99]. The main contents of Chapter 4 have been accepted for publication in IEEE Transactions on Transportation Electrification [108]. The main content of Chapter-5 is under review and will be submitted for possible publication in IEEE Transactions on Transportation Electrification.

6.3 Future Work

The work presented in this thesis can be further extended to address the following research considerations:

- The proposed PEV model in this thesis is implemented using the updated NHTS survey data, which simulates driver behavior based on gasoline vehicles. There is value in extending the SAT approach in this work by investigating the impact of real data simulating PEV behavior with non-conventional vehicles.
- The PEV amd CBESS models can be extended to include battery degradation that may consequently affect the assessment and planning of an EDS.
- Further improvements can be applied to the optimization model for the CBESS planning framework in order to provide a more global solution using convex optimization numerical techniques such as semidefinite or second order cone programming.
- Machine learning algorithms can be applied to estimate mathematical expressions of a PEV load-based SAT approach and incorporate their variables into the optimization model of the CBESS planning framework.

References

[1] C. Canizares and J. Nathwani, "Towards an ontario action plan for plug-in-electric vehicles (pevs)," Waterloo Institute for Sustainable Energy, University of Waterloo, Tech. Rep., 2010.

[2] Monthly plug-in ev sales scorecard: Historical charts. [Online]. Available: https://insideevs.com/news/344007/monthly-plug-in-ev-sales-scorecard-historical-charts/.[Accessed:28-August-2020].

[3] International energy agency (IEA), global ev outlook 2019. IEA. [Online]. Available: https://www.iea.org/reports/global-ev-outlook-2019

[4] I. S. Association *et al.*, "Ieee guide for loading mineral-oil-immersed transformers and step-voltage regulators," 2012.

[5] Annual solar pv capacity installations in the u.s. residential sector from 2005 to 2019. statista. [Online]. Available: https://www.statista.com/statistics/185694/us-residential-annual-pv-installed-capacity-since-2005/

[6] Tesla energy storage. [Online]. Available: https://www.tesla.com/en_CA/energy.

[7] (2020, October) U.S. Home Energy Storage Market Achieves Record Growth in Third Quarter 2019. [Online]. Available: https://www.globenewswire.com/.

[8] T. Gonen, *Electric power distribution engineering*. CRC press, 2015.

[9] A. D. Hilshey, P. D. H. Hines, P. Rezaei, and J. R. Dowds, "Estimating the impact of electric vehicle smart charging on distribution transformer aging," *IEEE Trans. on Smart Grid*, vol. 4, no. 2, pp. 905–913, June 2013.

[10] K. Yunus, M. Reza, H. Zelaya-De La Parra, and K. Srivastava, "Impacts of stochastic residential plug-in electric vehicle charging on distribution grid," in *2012 IEEE PES Innov. Smart Grid Technologies (ISGT)*. IEEE, 2012, pp. 1–8.

[11] L. P. Fernandez, T. G. San Román, R. Cossent, C. M. Domingo, and P. Frias, "Assessment of the impact of plug-in electric vehicles on distribution networks," *IEEE Trans. on power systems*, vol. 26, no. 1, pp. 206–213, 2010.

[12] P. Papadopoulos, S. Skarvelis-Kazakos, I. Grau, L. M. Cipcigan, and N. Jenkins, "Electric vehicles' impact on british distribution networks," *IET Electrical Systems in Transportation*, vol. 2, no. 3, pp. 91–102, 2012.

[13] K. Yunus, H. Z. De La Parra, and M. Reza, "Distribution grid impact of plug-in electric vehicles charging at fast charging stations using stochastic charging model," in *Proceedings of the 2011 14th European Conference on Power Electronics and Applications*. IEEE, 2011, pp. 1–11.

[14] O. Hafez and K. Bhattacharya, "Queuing analysis based pev load modeling considering battery charging behavior and their impact on distribution system operation," *IEEE Trans. on Smart Grid*, vol. 9, no. 1, pp. 261–273, 2016.

[15] S. M. Alshareef and W. G. Morsi, "Impact of fast charging stations on the voltage flicker in the electric power distribution systems," in *2017 IEEE Electrical Power and Energy Conference (EPEC)*. IEEE, 2017, pp. 1–6.

[16] A. Almutairi and M. M. Salama, "Assessment and enhancement frameworks for system reliability performance using different pev charging models," *IEEE Transactions on Sustainable Energy*, vol. 9, no. 4, pp. 1969–1984, 2018.

[17] A. Almutairi, M. Alotaibi, and M. Salama, "Goodness of fit statistical analysis for different variables of pev driver behaviour," in *2018 IEEE Canadian Conference on Electrical & Computer Engineering (CCECE)*. IEEE, 2018, pp. 1–4.

[18] A. Almutairi, A. B. Humayd, and M. Salama, "Quantifying the impact of pev charging loads on the reliability performance of generation systems," in *2016 IEEE Power and Energy Society General Meeting (PESGM)*. IEEE, 2016, pp. 1–5.

[19] A. Almutairi and S. Alyami, "Load profile modeling of plug-in electric vehicles: Realistic and ready-to-use benchmark test data," *IEEE Access*, vol. 9, pp. 59 637–59 648, 2021.

[20] A. S. B. Humayd and K. Bhattacharya, "A novel framework for evaluating maximum pev penetration into distribution systems," *IEEE Transactions on Smart Grid*, vol. 9, no. 4, pp. 2741–2751, 2016.

[21] Y. H. Febriwijaya, A. Purwadi, A. Rizqiawan, and N. Heryana, "A study on the impacts of dc fast charging stations on power distribution system," in *2014 International Conference on Electrical Engineering and Computer Science (ICEECS)*. IEEE, 2014, pp. 136–140.

[22] C. Jiang, R. Torquato, D. Salles, and W. Xu, "Method to assess the power-quality impact of plug-in electric vehicles," *IEEE Transactions on Power Delivery*, vol. 29, no. 2, pp. 958–965, 2013.

[23] D. Wang, X. Guan, J. Wu, and J. Gao, "Analysis of multi-location pev charging behaviors based on trip chain generation," in *2014 IEEE International Conference on Automation Science and Engineering (CASE)*. IEEE, 2014, pp. 151–156.

[24] D. Tang and P. Wang, "Probabilistic modeling of nodal charging demand based on spatial-temporal dynamics of moving electric vehicles," *IEEE Trans. on Smart Grid*, vol. 7, no. 2, pp. 627–636, 2015.

[25] S. Sun, Q. Yang, and W. Yan, "A novel markov-based temporal-soc analysis for characterizing pev charging demand," *IEEE Trans. on Industrial Informatics*, vol. 14, no. 1, pp. 156–166, 2017.

[26] H. Lin, K. Fu, Y. Liu, Q. Sun, and R. Wennersten, "Modeling charging demand of electric vehicles in multi-locations using agent-based method," *Energy Procedia*, vol. 152, pp. 599–605, 2018.

[27] T. Shun, L. Kunyu, X. Xiangning, W. Jianfeng, Y. Yang, and Z. Jian, "Charging demand for electric vehicle based on stochastic analysis of trip chain," *IET Generation, Transmission & Distribution*, vol. 10, no. 11, pp. 2689–2698, 2016.

[28] H. Pezeshki and P. Wolfs, "Impact of high pv penetration on distribution transformer life time," in *2013 IEEE Power & Energy Society General Meeting*. IEEE, 2013, pp. 1–5.

[29] D. Martin, S. Goodwin, O. Krause, and T. Saha, "The effect of pv on transformer ageing: University of queensland's experience," in *2014 Australasian Universities Power Engineering Conference (AUPEC)*. IEEE, 2014, pp. 1–6.

[30] M. Gray and W. Morsi, "On the role of prosumers owning rooftop solar photovoltaic in reducing the impact on transformer's aging due to plug-in electric vehicles charging," *Electric Power Systems Research*, vol. 143, pp. 563–572, 2017.

[31] S. F. Abdelsamad, W. G. Morsi, and T. S. Sidhu, "Probabilistic impact of transportation electrification on the loss-of-life of distribution transformers in the presence of rooftop solar photovoltaic," *IEEE Transactions on Sustainable Energy*, vol. 6, no. 4, pp. 1565–1573, 2015.

[32] M. ElNozahy and M. M. Salama, "Studying the feasibility of charging plug-in hybrid electric vehicles using photovoltaic electricity in residential distribution systems," *Electric Power Systems Research*, vol. 110, pp. 133–143, 2014.

[33] F. Giordano, A. Ciocia, P. Di Leo, A. Mazza, F. Spertino, A. Tenconi, and S. Vaschetto, "Vehicle-to-home usage scenarios for self-consumption improvement of a residential prosumer with photovoltaic roof," *IEEE Transactions on Industry Applications*, vol. 56, no. 3, pp. 2945–2956, 2020.

[34] L. Cheng, Y. Chang, and R. Huang, "Mitigating voltage problem in distribution system with distributed solar generation using electric vehicles," *IEEE Transactions on sustainable energy*, vol. 6, no. 4, pp. 1475–1484, 2015.

[35] N. Jabalameli and A. Ghosh, "Online centralized coordination of charging and phase switching of pevs in unbalanced lv networks with high pv penetrations," *IEEE Systems Journal*, 2020.

[36] M. Zeraati, M. E. H. Golshan, and J. M. Guerrero, "A consensus-based cooperative control of pev battery and pv active power curtailment for voltage regulation in distribution networks," *IEEE Transactions on Smart Grid*, vol. 10, no. 1, pp. 670–680, 2017.

[37] U. Datta, A. Kalam, and J. Shi, "Smart control of bess in pv integrated ev charging station for reducing transformer overloading and providing battery-to-grid service," *Journal of Energy Storage*, vol. 28, p. 101224, 2020.

[38] J. R. Agüero, P. Chongfuangprinya, S. Shao, L. Xu, F. Jahanbakhsh, and H. L. Willis, "Integration of plug-in electric vehicles and distributed energy resources on power distribution systems," in *2012 IEEE International Electric Vehicle Conference*. IEEE, 2012, pp. 1–7.

[39] S. Hashemi, G. Yang, J. Østergaard, S. You, and S.-T. Cha, "Storage application in smart grid with high pv and ev penetration," in *IEEE PES ISGT Europe 2013*. IEEE, 2013, pp. 1–5.

[40] Y. Yang, Q. Ye, L. J. Tung, M. Greenleaf, and H. Li, "Integrated size and energy management design of battery storage to enhance grid integration of large-scale pv power plants," *IEEE Transactions on industrial electronics*, vol. 65, no. 1, pp. 394–402, 2017.

[41] M. ElNozahy, T. K. Abdel-Galil, and M. Salama, "Probabilistic ess sizing and scheduling for improved integration of phevs and pv systems in residential distribution systems," *Electric Power Systems Research*, vol. 125, pp. 55–66, 2015.

[42] M. Gray and W. Morsi, "On the impact of single-phase plug-in electric vehicles charging and rooftop solar photovoltaic on distribution transformer aging," *Electric Power Systems Research*, vol. 148, pp. 202–209, 2017.

[43] T. J. Geiles and S. Islam, "Impact of pev charging and rooftop pv penetration on distribution transformer life," in *2013 IEEE Power & Energy Society General Meeting*. IEEE, 2013, pp. 1–5.

[44] M. H. Mobarak, R. N. Kleiman, and J. Bauman, "Solar-charged electric vehicles: A comprehensive analysis of grid, driver, and environmental benefits," *IEEE Transactions on Transportation Electrification*, 2020.

[45] S. A. El-Bataway and W. G. Morsi, "Distribution transformer's loss of life considering residential prosumers owning solar shingles, high-power fast chargers and second-generation battery energy storage," *IEEE Transactions on Industrial Informatics*, vol. 15, no. 3, pp. 1287–1297, 2018.

[46] C. de Mattos Affonso and M. Kezunovic, "Technical and economic impact of pv-bess charging station on transformer life: A case study," *IEEE Transactions on Smart Grid*, vol. 10, no. 4, pp. 4683–4692, 2018.

[47] V. C. Cunha, R. Torquato, T. R. Ricciardi, W. Freitas, and B. Venkatesh, "Assessing energy storage potential to facilitate the increased penetration of photovoltaic generators and electric vehicles in distribution networks," in *2017 IEEE Power & Energy Society General Meeting*. IEEE, 2017, pp. 1–5.

[48] S. A. El-Battawy, B. Basta, and W. G. Morsi, "Impact of integrating electric vehicles and rooftop solar photovoltaic on transformer's aging considering the effect of ambient temperature," in *2018 IEEE Electrical Power and Energy Conference (EPEC)*. IEEE, 2018, pp. 1–6.

[49] Y. Xiang, Z. Jiang, C. Gu, F. Teng, X. Wei, and Y. Wang, "Electric vehicle charging in smart grid: A spatial-temporal simulation method," *Energy*, vol. 189, p. 116221, 2019.

[50] Y. Xia, B. Hu, K. Xie, J. Tang, and H.-M. Tai, "An ev charging demand model for the distribution system using traffic property," *IEEE Access*, vol. 7, pp. 28 089–28 099, 2019.

[51] S. Cheng, Z. Wei, D. Shang, Z. Zhao, and H. Chen, "Charging load prediction and distribution network reliability evaluation considering electric vehicles' spatial-temporal transfer randomness," *IEEE Access*, vol. 8, pp. 124 084–124 096, 2020.

[52] Y. Mu, J. Wu, N. Jenkins, H. Jia, and C. Wang, "A spatial–temporal model for grid impact analysis of plug-in electric vehicles," *Applied Energy*, vol. 114, pp. 456–465, 2014.

[53] R. Li, W. Wang, and M. Xia, "Cooperative planning of active distribution system with renewable energy sources and energy storage systems," *IEEE access*, vol. 6, pp. 5916–5926, 2017.

[54] S. Wen, H. Lan, Q. Fu, C. Y. David, and L. Zhang, "Economic allocation for energy storage system considering wind power distribution," *IEEE Transactions on power Systems*, vol. 30, no. 2, pp. 644–652, 2014.

[55] M. Sedghi, A. Ahmadian, and M. Aliakbar-Golkar, "Optimal storage planning in active distribution network considering uncertainty of wind power distributed generation," *IEEE Transactions on Power Systems*, vol. 31, no. 1, pp. 304–316, 2015.

[56] A. S. Awad, T. H. El-Fouly, and M. M. Salama, "Optimal ess allocation for load management application," *IEEE Transactions on Power systems*, vol. 30, no. 1, pp. 327–336, 2014.

[57] F. Luo, K. Meng, Z. Y. Dong, Y. Zheng, Y. Chen, and K. P. Wong, "Coordinated operational planning for wind farm with battery energy storage system," *IEEE Transactions on Sustainable Energy*, vol. 6, no. 1, pp. 253–262, 2015.

[58] H. Alharbi and K. Bhattacharya, "Stochastic optimal planning of battery energy storage systems for isolated microgrids," *IEEE Transactions on Sustainable Energy*, vol. 9, no. 1, pp. 211–227, 2017.

[59] I. Alsaidan, A. Khodaei, and W. Gao, "A comprehensive battery energy storage optimal sizing model for microgrid applications," *IEEE Transactions on Power Systems*, vol. 33, no. 4, pp. 3968–3980, 2017.

[60] O. Alrumayh, S. Wong, and K. Bhattacharya, "Inclusion of battery soh estimation in smart distribution planning with energy storage systems," *IEEE Transactions on Power Systems*, vol. 36, no. 3, pp. 2323–2333, 2020.

[61] T. Qiu, B. Xu, Y. Wang, Y. Dvorkin, and D. S. Kirschen, "Stochastic multistage coplanning of transmission expansion and energy storage," *IEEE Transactions on Power Systems*, vol. 32, no. 1, pp. 643–651, 2016.

[62] T. Alharbi, K. Bhattacharya, and M. Kazerani, "Planning and operation of isolated microgrids based on repurposed electric vehicle batteries," *IEEE Transactions on Industrial Informatics*, vol. 15, no. 7, pp. 4319–4331, 2019.

[63] D.-J. Kim, K.-S. Ryu, H.-S. Ko, and B. Kim, "Optimal operation strategy of ess for ev charging infrastructure for voltage stabilization in a secondary feeder of a distribution system," *Energies*, vol. 13, no. 1, p. 179, 2020.

[64] S. Elbatawy and W. G. Morsi, "Integration of prosumers with battery storage and electric vehicles via transactive energy," *IEEE Transactions on Power Delivery*, 2021.

[65] M. K. Gray and W. G. Morsi, "A novel transactive energy framework for prosumers with battery storage and electric vehicles," in *2018 IEEE Electrical Power and Energy Conference (EPEC)*. IEEE, 2018, pp. 1–6.

[66] S. Shao, F. Jahanbakhsh, J. R. Agüero, and L. Xu, "Integration of pevs and pv-dg in power distribution systems using distributed energy storage—dynamic analyses," in *2013 IEEE PES Innovative Smart Grid Technologies Conference (ISGT)*. IEEE, 2013, pp. 1–6.

[67] S. A. El-Batawy and W. G. Morsi, "Optimal design of community battery energy storage systems with prosumers owning electric vehicles," *IEEE Transactions on Industrial Informatics*, vol. 14, no. 5, pp. 1920–1931, 2017.

[68] W. El-Khattam, K. Bhattacharya, Y. Hegazy, and M. Salama, "Optimal investment planning for distributed generation in a competitive electricity market," *IEEE Transactions on power systems*, vol. 19, no. 3, pp. 1674–1684, 2004.

[69] A. S. B. Humayd and K. Bhattacharya, "Distribution system planning to accommodate distributed energy resources and pevs," *Electric Power Systems Research*, vol. 145, pp. 1–11, 2017.

[70] S. Onori, L. Serrao, and G. Rizzoni, "Hybrid electric vehicles: Energy management strategies," 2016.

[71] R. C. Green II, L. Wang, and M. Alam, "The impact of plug-in hybrid electric vehicles on distribution networks: A review and outlook," *Renewable and sustainable energy reviews*, vol. 15, no. 1, pp. 544–553, 2011.

[72] C. Toepfer, "Sae electric vehicle conductive charge coupler, sae j1772," *Society of Automotive Engineers*, 2009.

[73] D. Wu, *Integrating plug-in electric vehicles into the electric power system.* Iowa State University, 2012.

[74] M. González Vayá, "Optimizing the electricity demand of electric vehicles: creating value through flexibility," Ph.D. dissertation, ETH Zurich, 2015.

[75] U.S. Department of Energy, "Hybrid and plug-in electric vehicles all-electric vehicles, clean cities," Tech. Rep., 2014.

[76] F. Primerano, M. A. Taylor, L. Pitaksringkarn, and P. Tisato, "Defining and understanding trip chaining behaviour," *Transportation*, vol. 35, no. 1, pp. 55–72, 2008.

[77] (2020, November) National Household Travel Survey. [Online]. Available: https://nhts.ornl.gov/

[78] W. H. Kersting, *Distribution system modeling and analysis.* CRC press, 2017.

[79] *IEEE Recommended Practice for Utility Interface of Photovoltaic (PV) Systems.* IEEE Std 929-2000.

[80] F. A. Farret and M. G. Simoes, *Integration of alternative sources of energy.* John Wiley & Sons, 2006.

[81] A. Goetzberger and V. U. Hoffmann, *Photovoltaic solar energy generation*. Springer Science & Business Media, 2005, vol. 112.

[82] I. Hadjipaschalis, A. Poullikkas, and V. Efthimiou, "Overview of current and future energy storage technologies for electric power applications," *Renewable and sustainable energy reviews*, vol. 13, no. 6-7, pp. 1513–1522, 2009.

[83] W. Alharbi, "Flexibility provisions from energy hubs for sustainable energy systems," 2018.

[84] S. Choi, K.-J. Tseng, D. Vilathgamuwa, and T. D. Nguyen, "Energy storage systems in distributed generation schemes," in *2008 IEEE Power and Energy Society General Meeting-Conversion and Delivery of Electrical Energy in the 21st Century*. IEEE, 2008, pp. 1–8.

[85] A. Nourai, R. Sastry, and T. Walker, "A vision & strategy for deployment of energy storage in electric utilities," in *IEEE PES General Meeting*. IEEE, 2010, pp. 1–4.

[86] DTE Energy, "DTE energy advanced implementation of energy storage technologies," DTE Energy, Detroit,MI, Tech. Rep., 2015.

[87] D. E. Olivares, C. A. Cañizares, and M. Kazerani, "A centralized energy management system for isolated microgrids," *IEEE Transactions on smart grid*, vol. 5, no. 4, pp. 1864–1875, 2014.

[88] (2020, November) National Household Travel Survey (NHTS) Codebook. [Online]. Available: https://nhts.ornl.gov/2009/pub/Codebook.pdf

[89] (2020, November) United States Guide: Work environment, Salaries, working hours and vacations. [Online]. Available: https://www.justlanded.com/english/United-States/USA-Guide/Jobs/Work-environment

[90] (2020, November) Canadian EV sales. [Online]. Available: https://docs.google.com/spreadsheets/d/1dLFJwZVdvNLRpmZqPznlzz6PB9eHMe5b-bai_ddRsNg/edit#gid=1383542355

[91] (2020, November) U.S. Department of Energy, Energy Efficiency and Renewable Energy. [Online]. Available: https://www.fueleconomy.gov/feg/Find.do?action=sbsSelect&id=39836&id=39842&id=39839

[92] (2020, November) Canadian weather energy and engineering datasets (cweeds). [Online]. Available: http://reports.ieso.ca/public/DemandZonal/

[93] A. Sankarakrishnan and R. Billinton, "Sequential monte carlo simulation for composite power system reliability analysis with time varying loads," *IEEE Trans. on power Systems*, vol. 10, no. 3, pp. 1540–1545, 1995.

[94] J. Han, J. Pei, and M. Kamber, *Data mining: concepts and techniques*. Elsevier, 2011.

[95] Q. Zhao, V. Hautamaki, and P. Fränti, "Knee point detection in bic for detecting the number of clusters," in *International conference on advanced concepts for intelligent vision systems*. Springer, 2008, pp. 664–673.

[96] J. Smith, R. Dugan, and W. Sunderman, "Distribution modeling and analysis of high penetration pv," in *2011 IEEE Power and Energy Society General Meeting*. IEEE, 2011, pp. 1–7.

[97] (2019, May) National Household Travel Survey. [Online]. Available: https://nhts.ornl.gov/

[98] Ieee distribution system analysis subcommittee, distribution test feeders. [Online]. Available: https://site.ieee.org/pes-testfeeders/resources/.[Accessed:8-August-2020].

[99] Y. O. Assolami, A. Gaouda, and R. El-Shatshat, "A new framework for plug-in electric vehicle charging models supported by solar photovoltaic energy resources," *IEEE Canadian Journal of Electrical and Computer Engineering*, vol. 44, no. 2, pp. 118–129, 2021.

[100] C. A. Burk, J. L. Bala, and J. Z. Gibson, "Electric secondary distribution system design," in *2007 39th North American Power Symposium*. IEEE, 2007, pp. 582–588.

[101] R. Vicini, O. Micheloud, H. Kumar, and A. Kwasinski, "Transformer and home energy management systems to lessen electrical vehicle impact on the grid," *IET Generation, Transmission & Distribution*, vol. 6, no. 12, pp. 1202–1208, 2012.

[102] M. Gray, "Analysis and evaluation of transactive energy control in active distribution systems," Ph.D. dissertation, 2016.

[103] D. Said, K. Nor, and M. Majid, "Analysis of distribution transformer losses and life expectancy using measured harmonic data," in *Proceedings of 14th International Conference on Harmonics and Quality of Power-ICHQP 2010*. IEEE, 2010, pp. 1–6.

[104] S. Bahramirad, W. Reder, and A. Khodaei, "Reliability-constrained optimal sizing of energy storage system in a microgrid," *IEEE Transactions on Smart Grid*, vol. 3, no. 4, pp. 2056–2062, 2012.

[105] N. E. M. Association *et al.*, "American national standard for electric power systems and equipment-voltage ratings (60 hertz)," Tech. Rep.

[106] C. Grigg, P. Wong, P. Albrecht, R. Allan, M. Bhavaraju, R. Billinton, Q. Chen, C. Fong, S. Haddad, S. Kuruganty *et al.*, "The ieee reliability test system-1996. a report prepared by the reliability test system task force of the application of probability methods subcommittee," *IEEE Transactions on power systems*, vol. 14, no. 3, pp. 1010–1020, 1999.

[107] J. Bishop, "Profiles on residential power consumption," *The Fire Protection Research Foundation*, 2010.

[108] Y. O. Assolami, A. Gaouda, and R. El-shatshat, "Impact on voltage quality and transformer aging of residential prosumer ownership of plug-in electric vehicles: Assessment and solutions," *IEEE Transactions on Transportation Electrification*, pp. 1–1, 2021.

[109] J. A. Taylor, *Convex optimization of power systems*. Cambridge University Press, 2015.

[110] (2021, August) Genetic algorithm matlab toolbox. [Online]. Available: https://www.mathworks.com/help/gads/ga.html

[111] D. J. Reid, "Genetic algorithms in constrained optimization," *Mathematical and computer modelling*, vol. 23, no. 5, pp. 87–111, 1996.

[112] G. Chen, X. Yi, Z. Zhang, and H. Lei, "Solving the multi-objective optimal power flow problem using the multi-objective firefly algorithm with a constraints-prior pareto-domination approach," *Energies*, vol. 11, no. 12, p. 3438, 2018.

[113] M. Liu, C. A. Canizares, and W. Huang, "Reactive power and voltage control in distribution systems with limited switching operations," *IEEE Transactions on Power Systems*, vol. 24, no. 2, pp. 889–899, 2009.

[114] M. Liu, S. Tso, and Y. Cheng, "An extended nonlinear primal-dual interior-point algorithm for reactive-power optimization of large-scale power systems with discrete control variables," *IEEE Transactions on Power Systems*, vol. 17, no. 4, pp. 982–991, 2002.

[115] Y. O. Assolami, A. Gaouda, and R. El-Shatshat, "Impact of spatial-temporal driver's behaviours on pev charging demand," in *2019 IEEE Electrical Power and Energy Conference (EPEC)*. IEEE, 2019, pp. 1–6.

Appendices

Appendix A: The IEEE 123 Node Distribution System Primary Feeder Data

Table A.1: Line segment data

Node A	Node B	Length (ft.)	Config.
1	2	175	10
1	3	250	11
1	7	300	1
3	4	200	11
3	5	325	11
5	6	250	11
7	8	200	1
8	12	225	10
8	9	225	9
8	13	300	1
9	14	425	9
13	34	150	11
13	18	825	2
14	11	250	9
14	10	250	9

15	16	375	11
15	17	350	11
18	19	250	9
18	21	300	2
19	20	325	9
21	22	525	10
21	23	250	2
23	24	550	11
23	25	275	2
25	26	350	7
25	28	200	2
26	27	275	7
26	31	225	11
27	33	500	9
28	29	300	2
29	30	350	2
30	250	200	2
31	32	300	11
34	15	100	11
35	36	650	8
35	40	250	1
36	37	300	9
36	38	250	10
38	39	325	10
40	41	325	11
40	42	250	1
42	43	500	10
42	44	200	1
44	45	200	9
44	47	250	1

45	46	300	9
47	48	150	4
47	49	250	4
49	50	250	4
50	51	250	4
52	53	200	1
53	54	125	1
54	55	275	1
54	57	350	3
55	56	275	1
57	58	250	10
57	60	750	3
58	59	250	10
60	61	550	5
60	62	250	12
62	63	175	12
63	64	350	12
64	65	425	12
65	66	325	12
67	68	200	9
67	72	275	3
67	97	250	3
68	69	275	9
69	70	325	9
70	71	275	9
72	73	275	11
72	76	200	3
73	74	350	11
74	75	400	11
76	77	400	6

76	86	700	3
77	78	100	6
78	79	225	6
78	80	475	6
80	81	475	6
81	82	250	6
81	84	675	11
82	83	250	6
84	85	475	11
86	87	450	6
87	88	175	9
87	89	275	6
89	90	225	10
89	91	225	6
91	92	300	11
91	93	225	6
93	94	275	9
93	95	300	6
95	96	200	10
97	98	275	3
98	99	550	3
99	100	300	3
100	450	800	3
101	102	225	11
101	105	275	3
102	103	325	11
103	104	700	11
105	106	225	10
105	108	325	3
106	107	575	10

108	109	450	9
108	300	1000	3
109	110	300	9
110	111	575	9
110	112	125	9
112	113	525	9
113	114	325	9
135	35	375	4
149	1	400	1
152	52	400	1
160	67	350	6
197	101	250	3

Table A.2: Overhead line configurations (Config.)

Config.	Phasing	Phase Cond.	Neutral Cond.	Spacing
		ACSR	ACSR	ID
1	A B C N	336,400 26/7	4/0 6/1	500
2	C A B N	336,400 26/7	4/0 6/1	500
3	B C A N	336,400 26/7	4/0 6/1	500
4	C B A N	336,400 26/7	4/0 6/1	500
5	B A C N	336,400 26/7	4/0 6/1	500
6	A C B N	336,400 26/7	4/0 6/1	500
7	A C N	336,400 26/7	4/0 6/1	505
8	A B N	336,400 26/7	4/0 6/1	505
9	A N	1/0	1/0	510
10	B N	1/0	1/0	510
11	C N	1/0	1/0	510

Table A.3: Underground line configuration (Config.)

Config.	Phasing	Cable	Spacing ID
12	A B C	1/0 AA, CN	515

Table A.4: Transformer data

	kVA	kV-high	kV-low	R - %	X - %
Substation	5,000	115 - D	4.16 Gr-W	1	8
XFM - 1	150	4.16 - D	.480 - D	1.27	2.72

Table A.5: Shunt capacitors

Node	Ph-A	Ph-B	Ph-C
	kVAr	kVAr	kVAr
83	200	200	200
88	50	0	0
90	0	50	0
92	0	0	50
Total	250	250	250

Table A.6: Three-phases switches

Node A	Node B	Normal
13	152	closed
18	135	closed
60	160	closed
61	610	closed
97	197	closed
150	149	closed
250	251	open
450	451	open
54	94	open
151	300	open
300	350	open

Table A.7: Spot loads

Node	Load	Ph-1	Ph-1	Ph-2	Ph-2	Ph-3	Ph-4
	Model	kW	kVAr	kW	kVAr	kW	kVAr
1	Y-PQ	40	20	0	0	0	0
2	Y-PQ	0	0	20	10	0	0
4	Y-PR	0	0	0	0	40	20
5	Y-I	0	0	0	0	20	10
6	Y-Z	0	0	0	0	40	20
7	Y-PQ	20	10	0	0	0	0
9	Y-PQ	40	20	0	0	0	0
10	Y-I	20	10	0	0	0	0

11	Y-Z	40	20	0	0	0	0
12	Y-PQ	0	0	20	10	0	0
16	Y-PQ	0	0	0	0	40	20
17	Y-PQ	0	0	0	0	20	10
19	Y-PQ	40	20	0	0	0	0
20	Y-I	40	20	0	0	0	0
22	Y-Z	0	0	40	20	0	0
24	Y-PQ	0	0	0	0	40	20
28	Y-I	40	20	0	0	0	0
29	Y-Z	40	20	0	0	0	0
30	Y-PQ	0	0	0	0	40	20
31	Y-PQ	0	0	0	0	20	10
32	Y-PQ	0	0	0	0	20	10
33	Y-I	40	20	0	0	0	0
34	Y-Z	0	0	0	0	40	20
35	D-PQ	40	20	0	0	0	0
37	Y-Z	40	20	0	0	0	0
38	Y-I	0	0	20	10	0	0
39	Y-PQ	0	0	20	10	0	0
41	Y-PQ	0	0	0	0	20	10
42	Y-PQ	20	10	0	0	0	0
43	Y-Z	0	0	40	20	0	0
45	Y-I	20	10	0	0	0	0

46	Y-PQ	20	10	0	0	0	0
47	Y-I	35	25	35	25	35	25
48	Y-Z	70	50	70	50	70	50
49	Y-PQ	35	25	70	50	35	20
50	Y-PQ	0	0	0	0	40	20
51	Y-PQ	20	10	0	0	0	0
52	Y-PQ	40	20	0	0	0	0
53	Y-PQ	40	20	0	0	0	0
55	Y-Z	20	10	0	0	0	0
56	Y-PQ	0	0	20	10	0	0
58	Y-I	0	0	20	10	0	0
59	Y-PQ	0	0	20	10	0	0
60	Y-PQ	20	10	0	0	0	0
62	Y-Z	0	0	0	0	40	20
63	Y-PQ	40	20	0	0	0	0
64	Y-I	0	0	75	35	0	0
65	D-Z	35	25	35	25	70	50
66	Y-PQ	0	0	0	0	75	35
68	Y-PQ	20	10	0	0	0	0
69	Y-PQ	40	20	0	0	0	0
70	Y-PQ	20	10	0	0	0	0
71	Y-PQ	40	20	0	0	0	0
73	Y-PQ	0	0	0	0	40	20

74	Y-Z	0	0	0	0	40	20
75	Y-PQ	0	0	0	0	40	20
76	D-I	105	80	70	50	70	50
77	Y-PQ	0	0	40	20	0	0
79	Y-Z	40	20	0	0	0	0
80	Y-PQ	0	0	40	20	0	0
82	Y-PQ	40	20	0	0	0	0
83	Y-PQ	0	0	0	0	20	10
84	Y-PQ	0	0	0	0	20	10
85	Y-PQ	0	0	0	0	40	20
86	Y-PQ	0	0	20	10	0	0
87	Y-PQ	0	0	40	20	0	0
88	Y-PQ	40	20	0	0	0	0
90	Y-I	0	0	40	20	0	0
92	Y-PQ	0	0	0	0	40	20
94	Y-PQ	40	20	0	0	0	0
95	Y-PQ	0	0	20	10	0	0
96	Y-PQ	0	0	20	10	0	0
98	Y-PQ	40	20	0	0	0	0
99	Y-PQ	0	0	40	20	0	0
100	Y-Z	0	0	0	0	40	20
102	Y-PQ	0	0	0	0	20	10
103	Y-PQ	0	0	0	0	40	20

104	Y-PQ	0	0	0	0	40	20
106	Y-PQ	0	0	40	20	0	0
107	Y-PQ	0	0	40	20	0	0
109	Y-PQ	40	20	0	0	0	0
111	Y-PQ	20	10	0	0	0	0
112	Y-I	20	10	0	0	0	0
113	Y-Z	40	20	0	0	0	0
114	Y-PQ	20	10	0	0	0	0

Appendix B: Secondary Distribution System Data

Table B.1: Winding resistance and reactance data for considered DTs

Ratings	$R_A\%$	$X_A\%$
75 kVA	0.8	0.96
50 kVA	1.014	1.37912
25 kVA	0.5367	0.8586

Table B.2: Type and length of used SL and SD

	Type	Length (ft)
SL	4/0 AA	125
SD	1/0 AA	90